PROCEEDINGS OF THE **SOUTH AFRICAN BALLISTICS ORGANISATION**

SYMPOSIUM 2023 | 9—11 MAY 2023

CSIR ICC, Pretoria, South Africa

EDITED BY: Prof Thanyani Pandelani

Proceedings of the South African Ballistics Organisation Symposium 2023

Council for Scientific and Industrial Research

Defence and Security Cluster

International Convention Centre, Pretoria

South Africa

9 -11 May 2023

Edited by

Prof Thanyani Pandelani – CSIR/UNISA

Many thanks to the organising committee who helped to ensure the quality of the papers.

Further copies of the proceedings can be obtained from D&S, CSIR.

ISBN: 978-0-6397-6256-2

Proceedings of the South African Ballistics Organisation Symposium 2023

Defence and Security Cluster

Council for Scientific and Industrial Research

www.csir.co.za

Symposium Scope and Objectives

The SABO 2023 symposium is jointly organised and supported by the Council for Scientific and Industrial Research (CSIR), in conjunction with the South African Ballistics Organisation Symposium.

The objective of the SABO symposium is to focus on the field of ballistics in the general areas of:

Internal Ballistics,
External Ballistics;
Terminal Ballistics
Vulnerability and Survivability

Scientific committee

Prof Thanyani Pandelani – Chair – CSIR/ Unisa
Dr Steeve Chung Kim Yuen - UCT
Mr Kassie Karsten - RDM
Dr Rene Heise - RDM
Ms Corlia Muller - RDM
Mr Kurt Strydom - RDM

South African Ballistics Organisation

Executive Committee

Dr Tleyane Jonas Sono – Chairman – CSIR
Mrs Bronwyn van Tonder - Rheinmetall Denel Munition
Mrs Roxanne Taylor - Rheinmetall Denel Munition
Mr Rudolf Gouws - Rheinmetall Denel Munition
Mr Cedric Brijraj - Armscor

Preface

One of the aims of the South African Ballistic Organisation (SABO) is to organise and host a local ballistic symposium every second year. This year SABO is hosting the 2023 symposium. The SABO 2023 Organising Committee has been overwhelmed by the response to the call for abstracts and would like to thank all the authors for their efforts.

We have a full program with participation from multiple organisations working in the field of ballistics including the Council for Scientific and Industrial Research (CSIR), Armscor, Rheinmetall Denel Munition (RDM), North West University (NWU), Delta V, Flamengro and Aballistic.

The oral papers provide insight into the research, development and innovation activities in areas of ballistics taking place within the country. The organisation continues to encourage a wide range of papers including works in progress and the involvement of the youth to sustain and improve the technical innovation to better the future of our country. We look forward to fruitful debate and engagement with the authors and delegates to stimulate new ideas to enhance the output of the research efforts. For the first time, the symposium will be hosting a poster session.

We are privileged to have two guest speakers, Mr Louis du Plessis from Aballistics and Brig Gen Andre Barends from SANDF. Mr Louis will give a keynote address on the Artillery regarding challenges of Future Warfare. Brig Gen Andre Barends will provide strategic direction on technology development needs for the SANDF.

We are thankful for the sponsorships received from our Diamond (TANDM, ARMSCOR, Horne Technologies) and Gold (DCD, QFINSOFT and CSIR) sponsors.

We hope you will enjoy all the presentations covering a variety on the spectrum of ballistics.

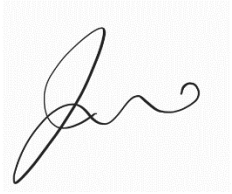

Dr TJ Sono
SABO Chairman

Content

Artillery in the Challenges of Future Warfare

J.L. du Plessis[1]

[1]*ABallistics – 44 Geelhout Avenue, Potchefstroom, 2531*

Email: Aballistics2017@gmail.com

Tell: (+27) 76 206 6508

***Abstract*—"If you want peace, prepare for war", apparently from Vash Chen. The question however is how to prepare for war. The conventional war machine is loaded with inertia and changes are not easily implemented, despite convincing evidence of its benefits. Weapon and ammunition developers must look into a crystal ball to decide on where to invest to be ready for emerging market opportunities. While military strategists must do the same to be prepared with what is available and wherever possible provide guidelines from their wish list to guide weapon and ammunition development. The present conflict between Russia and Ukraine becomes a laboratory where strategies are tested, and the effect of systems demonstrated. A "well-prepared first world war machine" starting marching orders at its own beat and apparent fast progress, more than 6 months later forced to reconsider its "preparedness" both in terms of strategy and capability. In a situation where: Wars are started by politicians, fought by soldiers, suffered by the population, and judged by the media, both the weapon developer and the military strategist must decide what is the best way "To prepare for war – in order to maintain peace".**

The paper speculates on how artillery systems might fit into the perceived future war and tries to table physical capabilities for consideration. The objective is to link these capabilities to what is considered the optimum system: "Maximize Enemy Vulnerability at Minimum Cost". This, however, would remain some mystery considering that cost is not only the investment to acquire a certain capability, but also the perceived cost of not having that capability.

In progressing from this philosophical viewpoint towards nuts-and-bolts, the paper tries to table emerging capabilities for artillery regarding means to extend range, improve accuracy and maintain mobility within the perceived battle scenario. In conclusion, the paper reiterates the focus areas for system developers in relation to the system life cycle phases taking cognizance of the fact that business opportunities lie in both legacy and futuristic concepts. As a final contribution, the paper ends with the belief that the best way to eliminate an enemy is still to make him your friend with special reference to the work of Dorothie and Martin Hellman [1], challenging us to peace on the planet.

Keywords—ABallistics, Artillery, Future, Warfare

Introduction

Since the "fall", conflicts and war have been an inevitable part of humanity. One would be arrogant to think that the causes for war can simply be unravelled into an empirical model that can be used to predict the occurrence and character of a future war and then use it to derive guidelines for Artillery within such a war. That would be an unrealistic objective for one paper and amount to the underestimation of the complexity of such an endeavour.

Therefore, if the honest reader is under the impression that the author does not fully comprehend the topic, due to the complex nature thereof, the reader is likely correct in their observation. Nevertheless, this paper is tabled to stimulate discussion, with the intent to mould ideas on the "Future War" and the possible role of Artillery in such a war. This paper approaches this by both reflecting on history and, observing what is currently transpiring with respect to maturing technologies and the use thereof. From the above stance, this paper aims to table the expected trends for Artillery weapons and ammunition, and their role in the "Future War".

In Anticipation of the Future War

To anticipate the evolution of the "Future War", we can only consider the following three states. Historical events, (as lessons from the past), the current ever-evolving technologies, and some measure of predictive imagination to envisage a concept of the future. The best vantage point from which to consider the "Future War" would be from the shoulders of giants. One of which is R.J. Rummel [2+3] who published his 5-volume endeavour on "UNDERSTANDING CONFLICT AND WAR". He summarizes the complexity of war in the following quote at the start of chapter 16 from volume 4: "Causes and Conditions of International Conflict and War".

"*War arises because of the changing relations of numerous variables--technological, psychic, social, and intellectual. There is no single cause of war. Peace is an equilibrium among many forces. Change in any particular force, trend, movement, or policy may at one time make for war, but under other conditions, a similar change may make for peace. A state may at one time promote peace by armament, at another time by disarmament, at one time by insistence on its rights, at another time by a spirit conciliation. To estimate the probability of war at any time involves, therefore, an appraisal of the effect of current changes upon the complex of intergroup relationships throughout the world. – Wright*"

Browsing the internet provides enough one-liner wisdom on the topic of war to fill a couple of papers, appealing to the whole spectrum from cynical to motivational emotions. Here are two representatives of these two poles: Apparently, Salvador Dali said, "A war does not show who is right, afterwards it only shows what is left". And George Washington said, "To be prepared for war is one of the most effective means of preserving peace". Discussing the role of Artillery in a future war encompasses more than a compilation of emotional one-liners.

Literature provides some insight into the origin of wars. History indicates that war is often deemed as the only remaining means to achieve the desired outcome. This is based on both an elevated perception of power and, (often), a misconception of capabilities. The author is indebted to an essay of Immerse [4] that provides an overview of the causes of war from a historic point of view, as illustrated in Fig. 1. See also Matthew [5] for valuable insight into wars and the causes thereof.

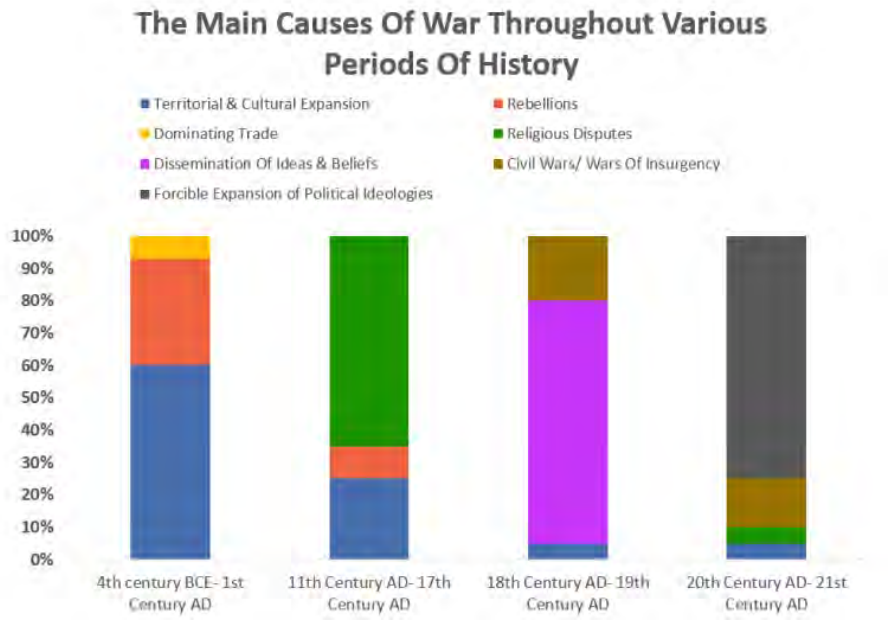

Fig. 1. Historic perspective on causes of war – Immerse [4]

One can ponder on this graph, with focus on the 20th-21st century. The conclusion could easily be derived that "forcible expansion of political ideologies" is most likely the cause of any future war. But the information displayed in Fig. 1, does not clearly reveal the influence of financial motives and control of valuable/scarce resources. The role of arms traders, as vividly addressed by Feinstein [6], and the

economics surrounding the arms industry must also be considered. Closer to home, Bowd [7], provides valuable insight in Africa's conflicts and possible means to avoid unnecessary bloodshed.

Contemplating the present conflict between Russia and Ukraine, "Forcible Expansion" both from Russia and indirectly from NATO, can be identified as triggers for the conflict. This was pointed out by Hellman [1] in 2016 as imminent cause for a (then) future conflict in Ukraine. Nevertheless, a premature evaluation of this current conflict indicates that three major elements play a role in how the engagement unfolds:

- The use and effect of unmanned drones.
- The benefit of long-range precision engagement using the Hi Mobility Artillery Systems.
- Training and morale of soldiers.

It is generally accepted that if 30% incapacitation is inflicted, the outcome of the battle is assumed to be sealed. Wainstein [8] however, clearly illustrated that with low morale, the outcome of the battle is achieved at significantly lower levels of incapacitation. While high morale might require incapacitation approaching 80% before a battle is won. This is presently evident in the Ukraine conflict. Another point emphasized by Wainstein is that high troop turnover, irrespective of the quantity, does not improve morale if the troops are not well-trained and equipped.

Through the media, we are exposed to the "irrationality" of the Russian attack on Ukraine in February 2022. But Hellman [1] pointed out in 2016, that the disrespect from the NATO alliance towards the Russian need for security and a reasonable buffer zone, could likely lead to dire consequences in Ukraine. His warnings were not unfounded considering how the events unfolded. The following abstract is taken from a report of the UK secretary of state security [9] in 2021.

"Ukraine has suffered significant territorial loss as a result of Russian aggression. Together with NATO Allies, we will help to build Ukraine's resilience to the continued aggressive tactics – conventional and sub-threshold – used by its neighbour. Our capacity-building mission, which includes both land and maritime training, will support the development of the Ukrainian Armed Forces and their interoperability with NATO. We will work with other partners in the Black Sea region, notably Bulgaria, Greece, Romania, and Turkey, to ensure freedom of navigation and security. As part of this we will continue to exercise our freedom to operate in the Black Sea"

Lessons from conflicts since World War II

Both World Wars I and II started regionally but developed into global involvement. In the aftermath of the wars, significant effort was put towards the prevention of any "Future War". Despite these noble efforts, the Second World War was followed by the "Cold War". This set about an unprecedented nuclear race, forcing some balance of fear, but not preventing regional expansion both by the USSR as well as the Western Alliances.

After this balance of power, various conflicts occurred, most of which can be defined as asymmetric. Larger conventional forces engaged less well-defined enemies. The preparation for these asymmetric conflicts, hinged largely on mobility, and weapons and equipment were developed accordingly. Considering the conflicts in Vietnam, Iraq, and Afghanistan, the success of the outcome in these conflicts is still up for speculation. Evidence is also clear that influx of weapons from non-direct involved sources, very often directly from arms dealers, prolonged most of these conflicts, way beyond the initial expected duration. This despite international sanctions and arms control efforts. The concept of "Blitz Krieg" often did not materialize due to unexpected buy-ins on the war. In the present Ukraine-Russia conflict the idea of "a crowd funded war", emerged.

Literature reveals quotes like: "Six months or eternity". One wonders how the current conflict in Ukraine, and will unfold, considering that it has already passed this "six-month" boundary. The importance of the "time value of military" is the topic of Givhan's thesis [10]. He opens in chapter 1 with the following quote from the 1936 Command and General Staff School Manual:

"In most of the great wars of history, there can be found military exploits calculated to feed the press rather than to beat the enemy. Statesmen at times become unduly impatient regarding the inevitable slowness with which the obstacles to success are overcome in the field".

Emerging Technologies

The miniaturization of electronic components and the explosion of communication capabilities combined with global navigational options have reach a level of maturity that vastly influence not only the battlefield, but also the options for Artillery systems. The following abstract from Watling [11], illustrates how the integration of some of these technologies in 2014 affected the outcome of a battle:

"In the early hours of 11 July 2014, the Ukrainian 24th Mechanised Brigade was manoeuvring near Zelenopillya, about 10km from the Russian border. Shortly after taking up positions, the Ukrainians found that their communications and navigation equipment was being interfered with. At around 4:20am they noticed unmanned aerial vehicles (UAVs) apparently observing the column. Then the firing started. Approximately 40 salvos of Russian rockets struck the Ukrainians within a five-minute period. The equipment of two understrength battalions was destroyed. This incident, though far from isolated, sent a shiver of alarm through Western militaries, for good reason."

The role of Artillery in a future war will still be to "shape the battlefield" for the occupation of territory. And to optimize its effectiveness, it would exploit new technologies for, amongst other, guidance to improved accuracy, communication for improved situational awareness, warheads for improved (and probably selectable) effect on target, explosives, and propellants to reduce vulnerability, (IM).

Performance Parameters for Artillery

Throughout history, technology often provided the upper hand in conflicts when it (1) increases the number of dimensions controlled and then (2) extend the range and (3) accuracy in each dimension. That is why air superiority was such an advantage when most systems were still Earth bound. Weapon systems have been developed to supply reasonable performance in the three spatial dimensions. Future improvement would then come through extension of range and improvement of accuracy. Optimisation of effect on target could also be linked to control of the three special dimensions. The fourth dimension that is now being occupied is time. This is linked to the data available regarding situational awareness and the time necessary to react. Both these concepts are addressed in so-called Network Centric Warfare [12]. Design drivers for future Artillery and ammunition can therefore be summarised as:

- Increase range – standoff.
- Improve accuracy.
- Optimise effect on target.
- Improved situational awareness and reduced response time.
- Improve mobility, i.e., air transportable to the battle as well as mobility on the battlefield.

Developing new weapons and ammunitions does not occur overnight. It is a time-consuming process and typically take ten or more years. Changing military doctrine to field these capabilities is just as time consuming. Nisser [13] proposed a theoretical model to guide the successful implementation of new military doctrine. In future "change" would probably one of the few constants to deal with. To prepare for the future war, the process to implement doctrines should be capable to accommodate change and implement/exploit the capabilities of emerging technologies. It is expected that smaller dynamic "special operation" groups might be the way to accommodate the rather slow crunching of the existing conventional warfare strategies. Sun Tsu [14] in his ancient classic work on warfare is an ardent believer in situational awareness and being equipped with the wisdom to adapt for the battle on hand, as reflected in the following quotes:

"Do not repeat the tactics which gained you one victory, but let your methods be regulated by the infinite variety of circumstances. He who can modify his tactics in relation to his opponent and thereby succeed in winning, may be called a heaven-born captain".

Besides these physical performance parameters and the organisational makeup to exploit the future capability, developing future Artillery systems and operating it should aways be guided by a cost optimisation of the war effort. And it is suggested that the optimum be defined by:

- $Maximise$: $F = \frac{Enemy\ Vulnerability}{Cost\ to\ procure\ and\ use\ of\ a\ system}$

An element of cost that is of paramount importance, but very difficult to quantify, is the cost for not having a certain capability. When driven back against the wall to obtain a certain capability "at all costs", means that you would be exploited by friend and foe, usually via arms traders. Plan to avoid this situation.

The cost element regarding Artillery in the Future War, inevitably drive the business opportunities for Artillery System and Ammunition development during the preparation for such a war. When considering these business opportunities, it is important find the optimum match between present capabilities and perceived opportunities. Ground-breaking developments often comes from subsidized research and end in patents, and not always as a game changer in the marketplace. The better business opportunity often lies with the innovative application of some more matured technologies. For the Artillery industry it is advised to snatch opportunities within existing capabilities focusing on the stages related to the life cycle of your technology and exploiting the opportunities within the total Time-System/Hierarchy Space illustrated in Fig. 2.

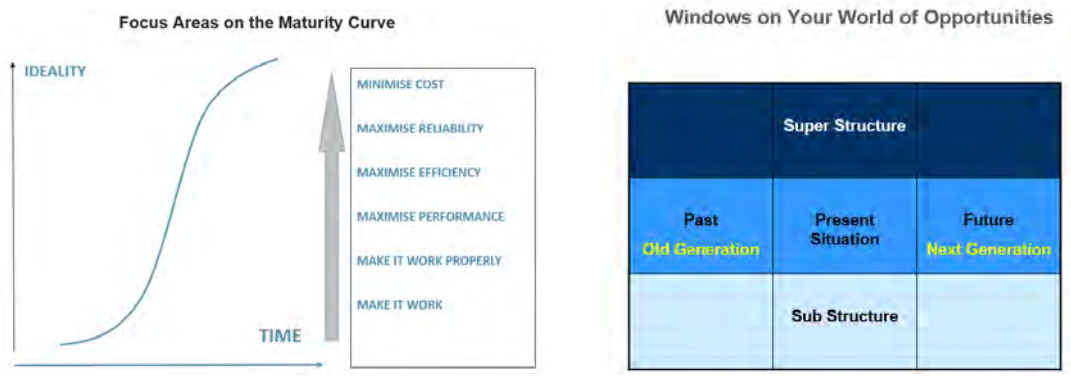

Fig. 2. Business Focus in product Lifecycle and Opportunity in Time-System Space

Range Extension and the Means to Achieve it

Artillery gun systems are asymptotically approaching a sweet spot compromise between the maximum impulse delivered to the projectile and the requirement for a light and mobile launch platform. In the Western world at least, the calibre of choice is presently 155mm and the projectile launch mass has stabilized at about 45kg. In 1990 the aim was to achieve 40km. During that time, Gunners [15], summarizes the means to increase range as illustrated in Fig. 3. The 40km boundary was reached using an optimized projectile shape, [ERFB], and introducing Base Bleed as the means to reduce base drag. By 1999 [16] a range of 60km for a 155mm artillery projectile fitted with a combination of base bleed and rocket assistance was tabled. There is still some regard for the lighter 105mm. With warhead optimisation and range extension, it is presently possible for the lighter 105mm artillery gun system to match the performance, both in range a lethality, that was up to 2000 only possible to achieve by the 155m. For the rest of this evaluation, the 155mm will be used to speculate on future performance.

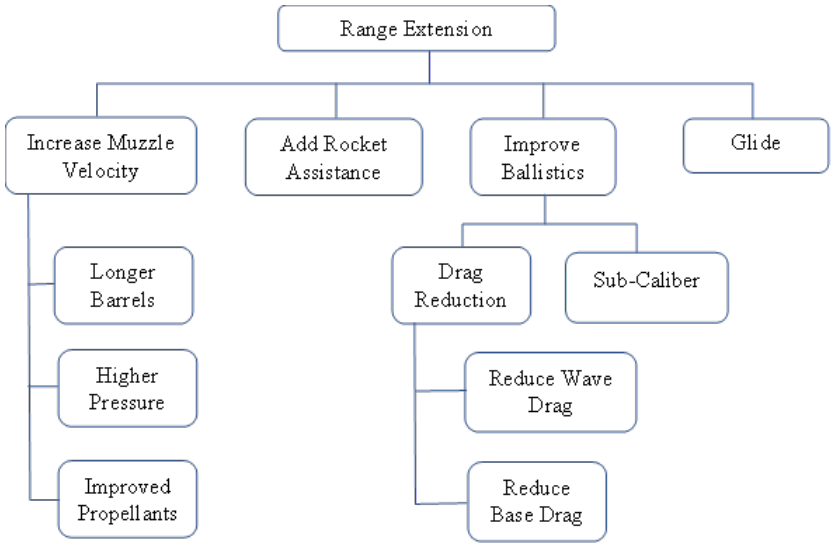

Fig. 3. Summary of means to extend the range for Artillery Projectiles – Gunners [16]

For the immediate future, the 155mm barrel length might increase from the present standard of 52 calibres [8m] to 62 calibres [9.6m] but increasing barrel length has a limited contribution towards range extension. Presently, improvement of the temperature sensitivity of artillery gun propellants allows to increase the typical maximum muzzle velocity for a 45kg projectile from 950m/s to 1000 – 1100 m/s. Fig. 4 illustrates how the range can be extended using:

- Base Bleed and or Rocket Assistance
- Exploit Gliding during the descending leg of the trajectory

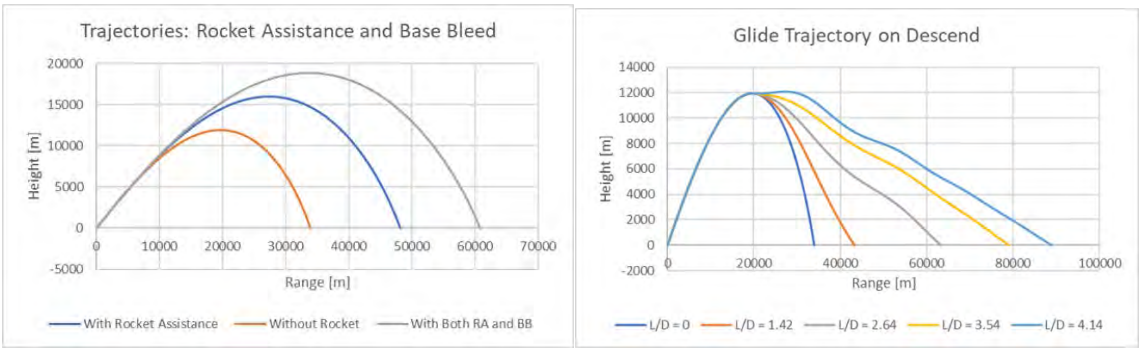

Fig. 4. Simulation results for range extension of a 155mm, 45kg projectile launched at 1000m/s.

Volcano [17] is a sub-calibre projectile launched from a 155mm weapon and demonstrated to reach beyond 70km exploiting gliding on the descending leg of the trajectory.

Accuracy and the Means to Achieve it

The typical impact dispersion of an unguided spin-stabilized Artillery projectile is:

- Probable Error in Range = 0.35% of Range
- Probable Error in Cross Range = 1mil = 0.1% Range

Both a reduction in impact dispersion and an improvement in accuracy would be required for long-range artillery. The difference between dispersion and accuracy is illustrated in Fig. 5.

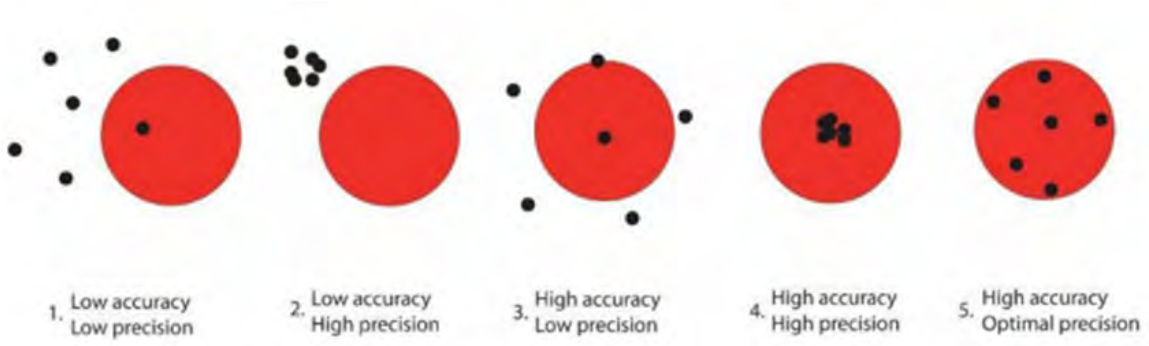

Fig. 5. Illustration of the difference between impact dispersion and accuracy – Dullum [18].

Optimum target coverage is achieved with an impact dispersion [i.e., the standard deviation in impact] equal to about 50% of the target radius as illustrated in Fig. 6, for an area target with a radius of 200m. The rationale behind an optimum dispersion is:

- If the impact dispersion is too small the lethal footprint of individual shots would overlap around the mean point of impact.
- If the impact dispersion is too large, many shots will impact beyond the target perimeter.

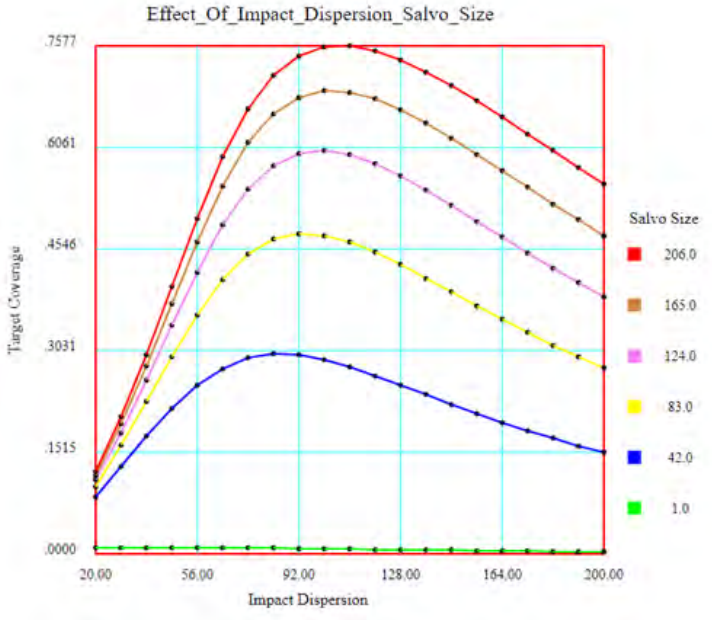

Fig. 6. Coverage of a target with a radius of 200m with shots having a lethal radius of 20m.

For Long-Range Artillery systems, impact correction or guidance become imperative to ensure that a reasonable effect on the target is achieved. Presently fuzes with guidance or impact error reduction capability are fielded, retrofittable to existing Artillery ammunitions. Then there are projectile concepts that are specifically designed for guidance. Some of the concepts found in the literature are shown in Table I.

TABLE I: SOME IMPACT CORRECTION AND GUIDANCE ARTILLERY PROJECTILES

Name	Country
One-Dimensional (Range) Correction	
SPACIDO	France
TFC	Germany
STAR	United Kingdom
LCCM	USA
ATOM	Turkey
Two-Dimensional (Range and Drift) Correction	
PGK ATK	USA
CCF	Europa
Terminal Guidance – Laser Target Designation	
COPPERHEAD M712	USA
KRASNOPOL	Russia
GP1/6	China
BASIR	Iran
KVITRYK	Ukraine
Autonomous Terminally Guided Projectiles	
EXCALIBUR	USA
VULCANO	Europa

Adding guidance to an Artillery projectile comes at a significant price tag. Geswender [19] presents average unit procurement cost, [AUPC], and expected impact dispersion for the various guidance options available for artillery projectiles as shown in Fig. 7. The different options considered are:

- 1D-PGK — Range correction only.
- 2D-PGK — Both range and cross-range corrections.
- 2D-CCf and GIF — Course correction fuze with controlled canards.
- 3D-ERM — Extended Range Munition (Naval).
- 6D-Excal — Excalibur.
- 2D-HAMR — Projectile with Thrust Impulse Control.

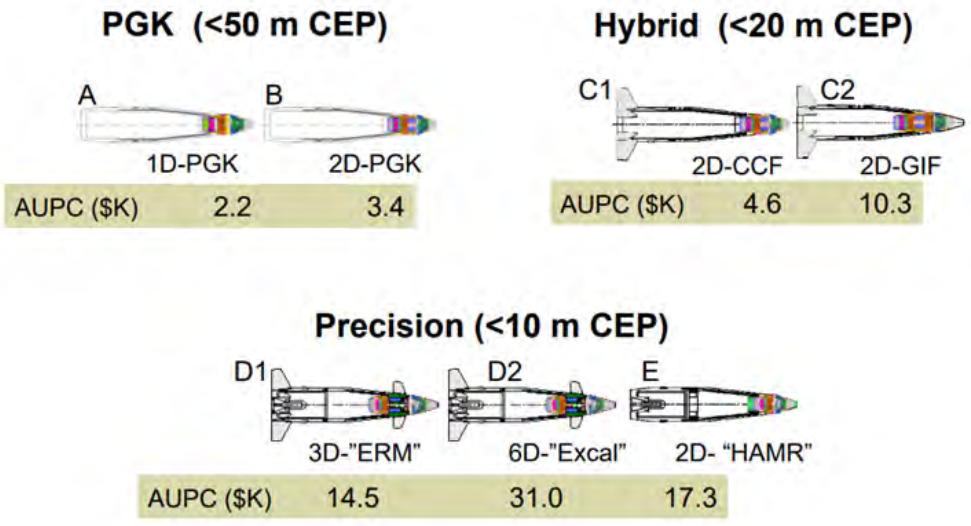

Fig. 7. Comparative costs and performance for various guidance options – Geswender [19].

The additional cost to add guidance for an artillery projectile should be evaluated in terms of the cost to achieve a required goal. Brady [20] present an analysis of contemporary 155mm artillery projectiles and his conclusion resonate with intuition that the guided projectile is best suited to engage point and small area targets, while the conventional projectiles without guidance might be the better option for larger area targets.

Artillery Rocket Systems not to be Neglected

Artillery rockets warrant its own evaluation. A comprehensive overview on Artillery Rocket systems and its performance is presented by Dullum [21]. The value of these systems to project a formidable force is battle proven. The present Russian-Ukraine conflict is no exception as proven by the impact of the High Mobility Artillery Rocket System [HIMARS]. The feedback through the Western media on the contribution of the HIMARS might not be a true reflection of the reality but suffice to say the introduction of it to the battle scenario coincide with what is presently paraded as a major shift in battle momentum. Surely there would have been numerous other contributing factors to acknowledge, but it should not downgrade the contribution of Artillery Rocket systems.

In line with the crystal ball gazing for Artillery Gun weapons and ammunition, one could summarize that Artillery Rocket Systems will be used to shape the battlefield of the future war at ranges of 70km and beyond. It will use guidance not only to reduce impact errors, but also use terminal guidance to engage designated targets. And any drive to exploit this capability should go hand in hand with a drive to develop the capability and doctrine to counter the same capability assuming the enemy will have access to the same capabilities.

Network-centric Approach to Warfare

Throughout history, situational awareness was of paramount importance for the effective utilization of Artillery. Forward observation is often seen as the real control of Artillery fire. This is now complemented with various means of remote sensing obtained from manned and unmanned platforms including satellite imaging. The explosion in available data and the communication thereof is blended into what has become known as Network Centric Warfare [12]. Together with the exponential growth in available information, grows the misinformation and means to interrupt healthy communication. That is why many systems developed with global navigation as prime source of spatial reference will also be equipped with independent inertial reference systems as backup when deprived from global reference systems.

Wisdom in Avoiding the Future War – a case for Peace

Being confronted with the reality that only 8% of documented history was without war, Immerse [4], it might feel impossible to avoid the future war. This is not a pessimistic, but quite realistic perspective, considering that at the time of preparing this paper [Oct 2022] there were more than 20 countries involved in armed conflict as illustrated in Fig. 8. This picture only indicates the countries directly involved in the conflicts and not the proxy alliances supplying support and fuelling the conflicts. This might be sufficient motivation for George Washington's quoted one-liner: "If you want peace, prepare for war". But through a realistic appraisal of history the reality should dawn that "Wars do not really solve conflicts, one of the warring parties might just loose more than the other" as illustrated in Fig. 9. And that resonate with the proposal tabled by Hellman [1] and endorsed by the late Gorbachev that humanity should start to respect the opinions of even our enemies if we hope to arrive at negotiated resolutions. Threatening from a point of confidence in your perceived power, might not be the best starting point. In line will Hellman's [1] plea one can at least start by investing some portion of the effort to prepare for war, to cultivate respect and understanding of diversity. This might be an elusive goal but at least worth considering, accepting the fact that wars will not bring a lasting solution.

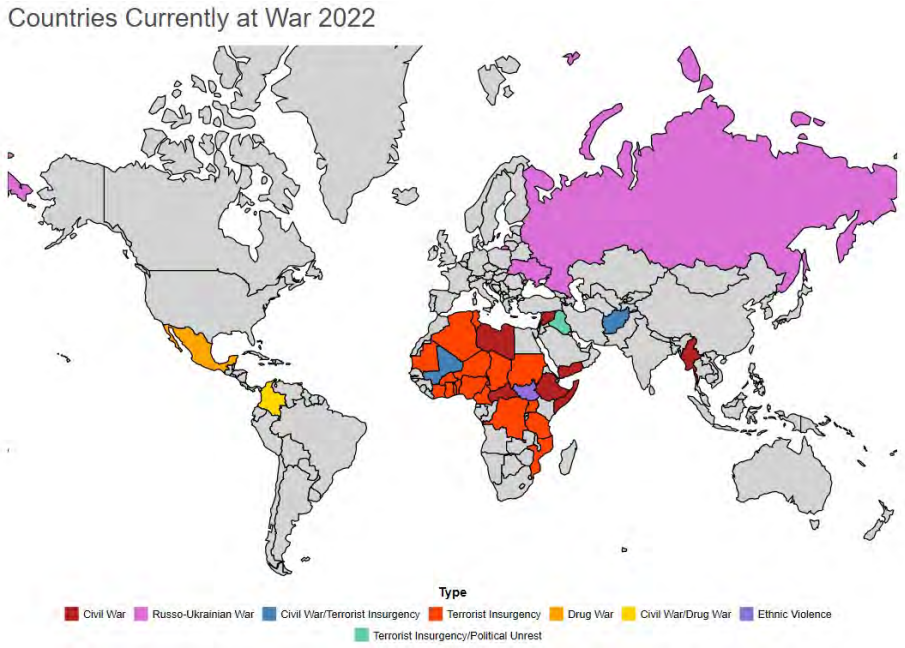

Fig. 8. Counties presently in armed conflicts [22].

"This has got to be one of the most powerful photographs I have ever seen. Above is a battalion of the Cameron Highlanders in 1914, prior to being despatched to the front line; below is the same battalion upon their return in 1918 after the armistice. "

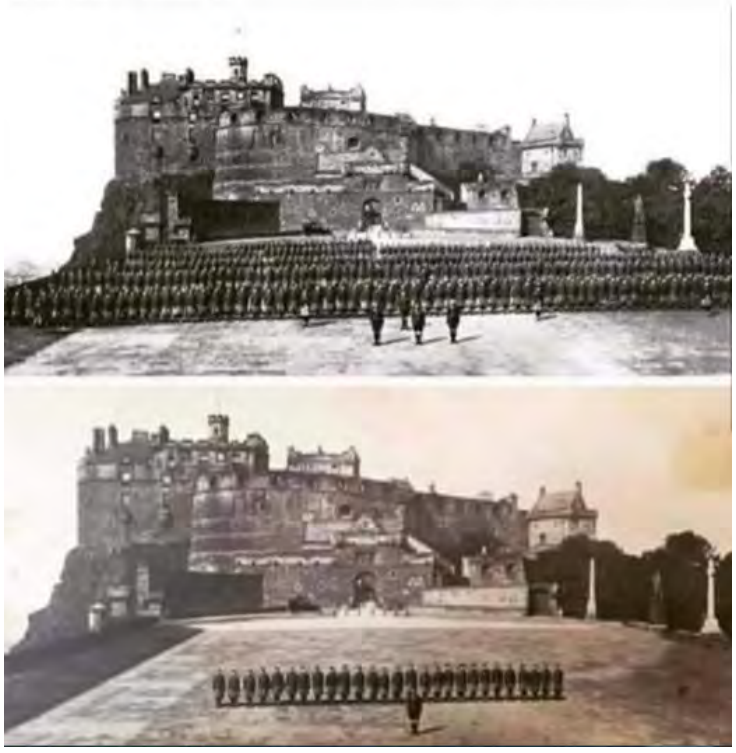

Fig. 9. The effect of war – source unknown.

Conclusion

The future war seems inevitable, and Artillery would be part of it and still applied to shape the battlefield in favour of the friendly forces. The performance of Artillery will be enhanced by (a) increasing the range, (b) improving the accuracy through guidance, (c) optimizing the effect on the target, and (d) being entrenched within a network-centric warfare concept with (e) high mobility and flexibility with regards to doctrine.

This future Artillery will consist of both Artillery Gun Systems and Artillery Rocket Systems working in synergy to execute attacks with surgical precision on high-value small targets on the one hand, as well as provide "heavy bombardment" for prolonged target coverage. The challenge will be to the provide these capabilities cost-effectively, without becoming a high value target yourself. Preparation for the future war should consider protection against the same idealized weapon just perceived.

There is fundamental research on the causes of wars, and proposals to improve mutual respect as well as an appreciation of diversity, including the enemy, to reduce and possibly avoid future wars. But this often does not meet the expectations of the popular vote from politicians and world leaders. Nevertheless, nothing is withholding any individual to start working on both (a) future Artillery systems as well as (b) future Peace, simultaneously. While contemplating the role of Artillery in a future war, and considering peace as an alternative, an old legend comes to mind: "The black dog and white dog within me is constantly fighting and the one I give the most food always wins". One should take cognisance of the fact that wars did not bring lasting solutions and the notion, (apparently coined by Einstein), that "stupidity is to do the same thing and expect different results".

References

[1] Dorothie and Martin Hellman, "A New Map for Relationships – Creating True Love at Home & Peace on the Planet", New MAP Publishing 2016.

[2] R.J. Rummel, "Understanding Conflict and War", Vol. 1-5, Published by Sage Publications, Beverly Hills, California, 1975-1981

[3] Nils Petter Gleditsch, "R.J. Rummel: An Assessment of His Many Contributions", SpringerBriefs on Pioneers in Science and Practice Volume 37

[4] Arwa Immerse, "What are the Main Causes of War?" https://resources.finalsite.net> dohacollegecom.

[5] Matthew O. Jackson and Massimo Morelli, The Reasons for Wars – an Updated Survey", Handbook on the Political Economy of War, edited by Chris Coyne, Elgar Publishing

[6] Andrew Feinstein, "The Shadow World Inside the Global Arms Trade", Published by Jonathan Ball Publishers, 2011.

[7] Richard Bowd and Annie Barbara Chikwanha, "Understanding Africa's contemporary conflicts", Select conference papers from the AHSI Conference on Peace and Security in Africa 'Beyond the African Union Charter, Peace, Security and Justice', Addis Ababa, Ethiopia, 21 – 22 February 2008.

[8] Leonard Wainstein, "The Relationship of Battle Damage to Unit Combat Performance", Institute for Defense Analysis Paper P-1903, 1986

[9] Ben Wallace, "Defence in a competitive age", CP411, Presented to Parliament by the Secretary of State for Defence by Command of Her Majesty March 2021

[10] Walter D. Givhan, "The Time Value of Military Force in Modern Warfare", Thesis presented to the Faculty of the School of Advance Airpower Studies, Alabama, 1996

[11] Jack Watling, "The Future of Fires: Maximizing the UK's Tactical and Operational Firepower", Royal United Services Institute for Defence and Security Studies, 2019

[12] David S. Alberts, John J. Garstka, Frederick P. Stein, "Network Centric Warfare: Developing and Leveraging Information Superiority",CCRP Publications.

[13] John Nisser, "Implementing military doctrine: A theoretical model", Comparative Strategy, https://doi.org/10.1080/01495933.2021.1912514 >

[14] Sun Tsu, "On the Art of War", Translated by Lionel Giles and published by Allandale Online Publishing, 2000.

[15] N.E. Gunners, "A study of base-bleed propellant and grain optimization", 13'th International Symposium on Ballistics, Stockholm, 1992.

[16] J.L. du Plessis, JdeB. Mare and F.A. Venter, "Some Trade-Offs for Understanding the Role of Artillery", 18th International Symposium on Ballistics, San Antonio, 1999.

[17] Diehl and Oto Melara (Now Leonardo) Brochure “VULCANO Guided Ammunition Family”

[18] O.S. Dullum, K. Fulmer, N.R. Jenzen-Jones, C. Lincoln-Jones, and D. Palacio, “A Technical Analysis of the Employment, Accuracy and Effects of Indirect-Fire Artillery Weapons”, ARES, 2017.

[19] Chris E Geswender and Stephen Bennett, “Alternatives for Architecturing Low-Cost Guided Projectiles”, 43rd Annual Gun & Missiles Conference, 2008.

[20] M.R. Brady and P. Goethals, “A comparative analysis of contemporary 155 mm artillery projectiles”, Journal of Defense Analytics and Logistics Vol. 3 No. 2, 2019 pp. 171-192.

[21] O. Dullum, “The Rocket Artillery Reference Book”, FFI-Rapport 2009/00179, Norwegian Defence Research Establishment (FFI), June 2010.

[22] https://worldpopulationreview.com > country-rankings “Countries Currently at War 2022 – World Population Review”

USING ANSYS AUTODYN TO NUMERICALLY INVESTIGATE THE FEASIBILITY OF FORWARD-FIRING MULTIPLE EFPs OFF A CYLINDRICAL CHARGE.

S. Kriek and F.J. Mostert[1]

[1]*DeltaV Aerospace (Pty) Ltd, 13 Cyclonite Street, Somerset West, 7130, South Africa*

shaun.kriek@deltav-aerospace.com

+27 21 851 3754

***Abstract*—ANSYS Autodyn® was used to investigate the feasibility of multiple explosively-formed projectiles (MEFPs) in the application of a forward-firing cylindrical explosive charge of fixed diameter and length. The MEFP payload configuration comprised a copper liner partitioned into hexagons forming an array around a centrally-located unit on the front face of a rear-detonated cylindrical explosive column. The hexagonal shape of the units was chosen due to its high packing density, and its potential to form favourable aerodynamic geometries when subjected to explosive loading. The formation of EFPs from hexagonal units was investigated numerically, with particular focus on the EFP length, shape, and velocity. Numerical simulations were performed of two MEFP configurations – one with a planar and another with a spherical explosive-liner interface – to predict the overall performance of the projectiles in terms of trajectory, stability, and kinetic energy. When configured on a planar explosive face, the EFPs were observed to occupy a small conical region with a high central concentration of projectiles. The distribution of the EFPs showed marked improvement, both in terms of uniformity and spread, by using an explosive with a spherical face, however, the velocity of the central EFPs was consequently reduced. Penetration analyses were performed by simulating the impact between a copper penetrator (with a shape matching that of the central EFP) and a 4340-steel target plate of varying thickness. With an initial kinetic energy of 4000 J, plate perforation was achieved at plate thicknesses up to 10 mm. The outcome of the numerical investigation of a forward-firing MEFP system, with hexagonal shaped units, has numerically demonstrated satisfactory projectile penetration and distribution performance.**

Keywords—MEFP, hexagonal EFP, forward-firing, projectile formation, penetration.

Introduction

Munitions countermeasures are crucial to close-proximity defence systems. Interceptors offer protection against incoming threats, by having the capability of successfully and reliably hitting, penetrating, and ultimately neutralising the targeted weapon. Typical ballistic threats include explosive payloads carried by mortars, rockets, missiles, and drones.

Explosively-formed projectiles (EFPs) have an initial geometry designed to focus the accelerating material into a concentrated zone along the longitudinal axis [1]. This implosion of material can produce compact projectiles with high kinetic energy and aerodynamic stability [2]. Single EFPs, which can be generated to have large kinetic energy, are mainly effective in high-precision applications, with limited suitability in applications where the target is either moving or does not have an exact known location. A system with multiple EFPs (MEFPs) [3] addresses this drawback by improving the hit probability with the target. While the MEFPs have reduced individual mass compared to a system with a single EFP, careful detonic design can ensure sufficient kinetic energy of the formed projectiles is achieved.

A forward-firing MEFP system is effective on the principle that, upon detonation, several individual EFPs are propelled along the munition flight vector toward an incoming target and occupy a conical domain that ensures a high probability of a hit on the target. The EFPs should be travelling with sufficient kinetic energy so that a successful hit would ensure target neutralisation. An advantage of this type of system is the addition of the dynamic payload velocity to the detonic velocity achieved by the EFPs.

Due to the complex nature of MEFP formation (being subject to the effects of the detonation wave, expansion of the detonation products, and the multiple explosive-metal interactions) an

analytical approach would not yield accurate results. The investigation into the feasibility of a forward-firing MEFP system therefore included numerical simulations to predict the shape, stability, velocity, and trajectory of the EFPs [4]. ANSYS Autodyn® was chosen as the explicit dynamics solver to execute the simulations. The investigation comprised three distinct stages: the explosion mechanics forming the units into projectiles, the exterior ballistics of the projectiles as the MEFPs accelerate and travel toward the target zone, and the terminal ballistics phase of the projectile penetrating a target. Two liner-explosive interface configurations were investigated; a planar face and a spherical interface were chosen to assess the effect of a planar and spherical detonation wave, res-pectively, on the formation and exterior ballistics of the projectiles.

MEFP Arrangement

Hexagonal-shaped units were selected because of their high packing density. This allowed several units to be economically arranged on the front face of the explosive. For the purposes of this investigation, the munitions calibre was fixed at 80 mm, so the size of each hexagonal unit was the only variable determining the number of units which could fit within the diameter of the explosive. The size of the hexagonal units would directly affect two opposing performance criteria: firstly, smaller hexagons would increase the number of the units which would improve the hit probability of the projectiles, and secondly, larger hexagons would produce projectiles with greater kinetic energy and greater penetration performance. A compromise was therefore required to achieve a layout which would yield both adequate hit probability and penetration results.

To determine the size of the hexagonal units, a study was performed assessing the minimum number of EFPs required for at least 90% hit probability, as well as an estimate of the minimum size required for the central projectile to achieve a velocity of 2500 m/s. A solution which satisfied both criteria was used as the basis of the MEFP study: the preliminary liner design was chosen to comprise a total of 61 hexagonal units, each with a side length of 5 mm, arranged against a planar explosive face. The second configuration required the same hexagonal units to be arranged against a spherical explosive face, which required greater spacing to prevent interference between the slightly rotated units. Consequently, there was not sufficient space to accommodate the six units at the furthermost corners of the arrangement, resulting in a total of 55 units present in the second configuration.

Due to the symmetrical arrangement of the hexagons (and the symmetry of the hexagons themselves), a quarter-symmetry model was used as a representation of the full configuration, particularly for the numerical analyses. As a result, 19 parts (comprising full and partial units) were included in the quarter model for the planar face configuration, as shown in Fig. 1. The spherical face configuration had a similar arrangement, with units 5 and 19 removed.

Geometric Definition of EFPs

The hexagonal unit was defined by a side length of 5 mm, corresponding to a circumscribing circle diameter of 10 mm. The unit was shaped to have a convex rear surface – in contact with the high explosive – and a concave front (free) surface to promote projectile formation during the explosive event. Both the rear and front surfaces were defined by spherical geometries. The shape of a hexagonal unit was governed by four major dimensions: the outer diameter, the centre and edge thicknesses, and the rear-face radius. Fig. 2 shows the 3D geometry of a hexagonal unit, as well as the

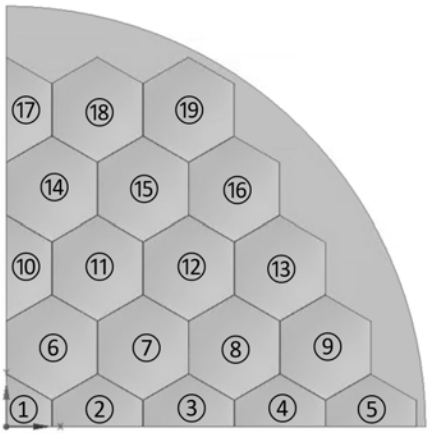

Fig. 1. MEFP arrangement and numbering convention for hexagonal liner in quarter-symmetry configuration.

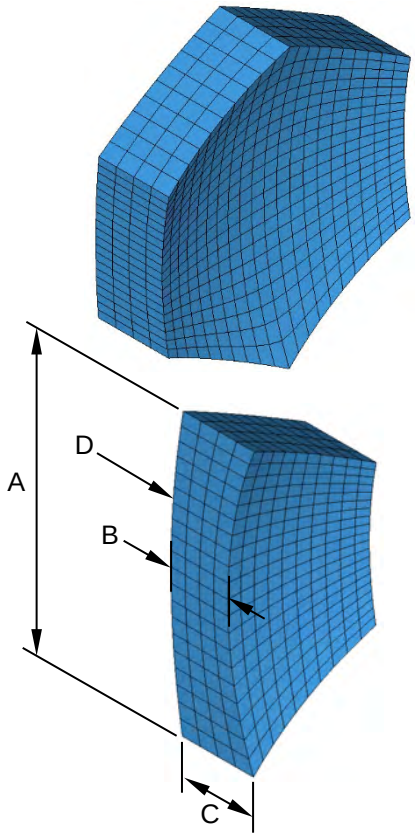

Fig. 2. 3D illustration of hexagon EFP (top) and a full section view showing the governing dimensions (bottom).

governing dimensions describing the shape; the values of the dimensions are listed in Table I. To maintain the required packing arrangement, the outer diameter was fixed. Only the centre thickness and rear-face radius were varied as these dimensions were observed to have the most effect on the initial EFP deformation and subsequent projectile formation. The outer diameter and edge thickness were fixed at 10 mm and 2.50 mm, respectively.

Development of Numerical Models

Individual EFP formation: The initial stage of the numerical investigation involved modelling and analysing the individual EFPs from hexagonally-shaped units. In leading up to a full

TABLE I. DIMENSIONS OF HEXAGON EFPS USED FOR PROJECTILE FORMATION SIMULATIONS.

Dimension	Minimum value (mm)	Maximum value (mm)
A: Outer diameter	10.0	10.0
B: Centre thickness	1.75	2.70
C: Edge thickness	2.50	2.50
D: Rear-face radius	20.0	30.0

MEFP analysis, a single hexagonal unit was investigated to determine which geometric parameters could be refined to produce an effective projectile.

Quarter symmetry models were utilised for the investigation. A cylindrical payload was simulated with a diameter of 80 mm and a length of 120 mm; a 3 mm casing surrounded the high explosive. A termination time of 30 µs was used for the simulations, allowing full detonation of the explosive and major projectile formation to be simulated.

The EFP material was selected to be oxygen-free high conductivity (OFHC) copper due to its proven track record as a suitable EFP material of relatively high density [1-3]. Composition B was assigned as the high explosive material and aluminium-2024 was chosen for the casing. Table II lists the material assignment, including strength and equation of state (EOS) models, for each of the parts used in the simulation.

The Jones-Wilkins-Lee (JWL) EOS was used to determine the pressure due to the expansion of the detonation products from the detonation of the high explosive, as described by (1) [5]:

$$P = A\left(1 - \frac{\omega}{R_1 V}\right) \cdot e^{-R_1 V} + \ldots \\ B\left(1 - \frac{\omega}{R_2 V}\right) \cdot e^{-R_2 V} + \frac{\omega E_0}{V} \qquad (1)$$

where A, B, R_1, R_2 and ω are material constants, V = relative volume, and E_0 = detonation energy per unit volume. The additional detonation constants required to accurately determine the detonation event included the detonation velocity (D), the Chapman-Jouguet pressure (P_{CJ}), and the initial density of the explosive (ρ_0). The EOS parameters and detonation constants of Composition B are listed in Table III.

TABLE II. MATERIAL ASSIGNMENT FOR PARTS USED IN EFP BLAST SIMULATION [6].

Part	Material	Density (kg/m^3)	Strength model	Equation of state
EFP	OFHC copper	8930	Steinberg-Guinan	Shock
High explosive	Composition B	1717	None	JWL
Casing	Aluminium 2024	2785	Steinberg-Guinan	Shock

TABLE III. EOS AND DETONATION PARAMETERS OF COMPOSTION B [6].

JWL EOS Parameters							
A (MPa)	B (MPa)	$R1$	R_2	ω	D (m/s)	E_0 (MJ/m^3)	P_{CJ} (MPa)
524230	7678	4.20	1.10	0.34	7980	8500	29500

Penetration analysis: The penetration capacity of the projectile was assessed by simulating the collision between a single projectile (OFHC copper, density = 8930 kg/m3) and a steel plate (S4340, density = 7830 kg/m3) of various thicknesses. The computation was done in ANSYS Autodyn® using 2D axial symmetry. The steel plate was modelled using a Lagrange mesh and assigned the Johnson-Cook parameters for both the strength and failure models. The Johnson-Cook models constitutively define the material flow stress (σ_f) and failure strain (ε_F) as a function of plastic strain (ε_p), strain rate ($\dot{\varepsilon}$), and temperature (T) [7]. Equation (2) and (3) describe the Johnson-Cook strength and failure models, respectively.

$$\sigma_f = [A + B\,(\varepsilon_p)^n] \cdot [1 + C\ln(\dot{\varepsilon}^*)] \cdot [1 - (T^*)^m] \quad (2)$$

$$\varepsilon_F = [D_1 + D_2 \cdot e^{D_3 \cdot \sigma^*}] \cdot [1 + D_4 \ln(\dot{\varepsilon}^*)] \cdot [1 + D_5 T^*] \quad (3)$$

where the homologous strain rate, temperature and stress are defined as $\dot{\varepsilon}^* = \dot{\varepsilon} / \dot{\varepsilon}_0$, $T^* = (T - T_r) / (T_m - T_r)$, and $\sigma^* = p / \sigma_{eff}$, respectively, and A = material yield stress, B = strain hardening coefficient, n = strain hardening exponent, C = strain-rate sensitivity coefficient, m = thermal sensitivity exponent, $D_1 \ldots D_5$ = damage parameters, $\dot{\varepsilon}_0$ = reference strain rate, T_r = reference temperature, T_m = material melt temperature, p = pressure and σ_{eff} = effective stress. The Johnson-Cook parameters are listed in Table IV.

The projectile was included in an Euler mesh to accommodate the extreme deformations thereof during impact with the target. The initial geometry of the projectile remained unchanged for each simulation. The shape was defined by a parabolic profile with an overall length of 10 mm, a cavity depth of 3 mm and an outer radius of 3.47 mm, such that the mass of the projectile matched that of the original hexagonal unit at 1.28 g. Since a 2D axial symmetry simulation was used in this investigation, the projectile was idealized as a paraboloid. The projectile was assigned an initial velocity of 2500 m/s; consequently, the projectile had an initial kinetic energy of 4000 J. Fig. 3 compares the shape used to define the projectile for the penetration analyses with the profile produced by the explosive formation simulations.

Full MEFP simulation: Due to the symmetry of the MEFP arrangement (and the symmetry of the hexagon units themselves), a quarter-symmetry model was used to represent the full configuration. The planar-faced MEFP configuration is shown in Fig. 4(a). A plane wave detonation was used to represent an ideal wave shaper, allowing for a uniform and simultaneous loading on each hexagonal unit. The arrival time of the explosive shock wave on the liner was approximately 15 µs, after which the blast pressure accelerated the liner and the individual hexagons. The projectiles formed within the next 15 µs and reached steady velocities within 40 µs of simulation time. The simulation termination time was set to 100 µs, allowing the projectiles to travel axially by approximately 200 mm.

The analysis of the planar-faced MEFP configuration indicated an inadequate projectile distribution; there was a lack of radial displacement exhibited by most of the EFPs, which was attributed to the planar face of the explosive. A

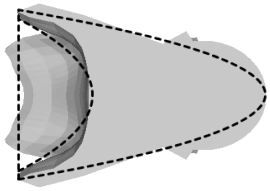

Fig. 3. Projectile shape for penetration analysis (dotted) vs projectile shape from projectile formation analysis.

TABLE IV. JOHNSON-COOK PARAMETERS FOR TARGET PLATE (S4304) USED IN EFP PENETRATION SIMULATION [6].

Johnson-Cook Strength Parameters							Johnson-Cook Damage Parameters				
A (MPa)	B (MPa)	n	C	m	$\dot{\varepsilon}_0$ (s^{-1})	T_{melt} (K)	D_1	D_2	D_3	D_4	D_5
792	510	0.26	0.014	1.03	1.00	1793	0.05	3.44	-2.12	0.002	0.61

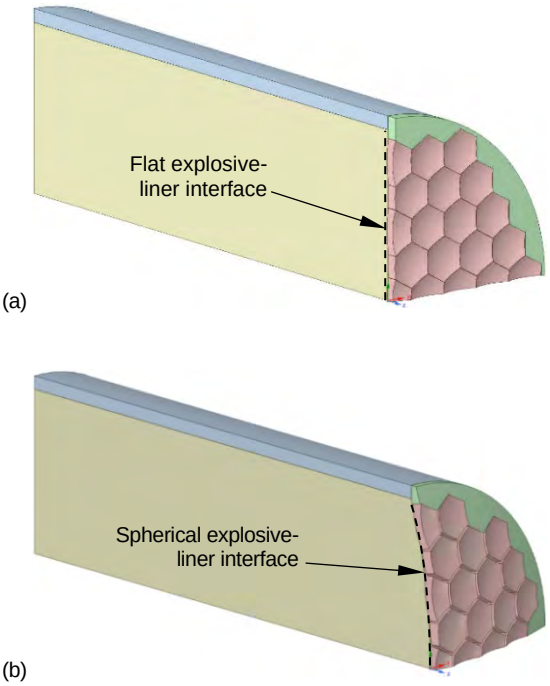

Fig. 4. MEFP quarter geometry of (a) planar and (b) spherical explosive configurations.

further implication of this design was the need for a planar detonation wave to ensure that the EFPs were simultaneously fired. Although a plane wave detonation was readily simulated in the numerical model, a wave shaper would be needed to form the required planar wavefront in practice, which would complicate the detonic design of this configuration. The advantage of this wavefront, however, was the greater energy flux associated with the plane wave (due to the reduced wavefront surface area compared to a spherical wave), which would result in a higher kinetic energy transfer to the EFPs, resulting in greater projectile velocities.

It was decided to introduce curvature to the end of the explosive interfacing with the MEFP liner to improve the projectile distribution by geometric means. The initial modification set the radius of the charge face to 120 mm, equal to the length of the explosive (or, more specifically, equal to the stand-off distance between the EFPs and the point of detonation). This geometry utilised the spherical nature with which the detonation wave travelled through the high explosive, such that the detonation wave reached each of the EFPs at the same time. Consequently, the design did not require a wave shaper to ensure simultaneous firing and formation of the projectiles.

Fig. 4(b) illustrates the MEFP payload geometry with the explosive-liner interface modified to form a spherical profile. All the hexagonal units, except the central hexagon, were transformed to adhere to the new surface profile. A separation gap was required to ensure there was no interference between the rear edges of adjacent hexagons. The payload diameter of 80 mm was large enough to allow most of the hexagons to have complete contact with the explosive; only the outermost units needed to be removed as there was insufficient space to allow complete contact with the explosive.

Projectile Formation

Numerical simulations were performed to determine the effect of the centre thickness and rear-face radius of the initial EFP geometry on the projectile formation. Suitable projectile formation was governed by three criteria: material distribution, velocity gradient (or elongation potential) and overall average velocity. The assessment of the material distribution was a means to infer the flight stability of the projectile. The development of fins, observed to be inherent to the initial hexagonal shape of the EFPs and ideal contributors to aerodynamic stability, was achieved by each of the formed projectiles. Short, compact projectiles with a forward centre of mass were favoured over longer projectiles which were tail-heavy. The velocity gradient (i.e., the change in velocity along the length of the projectile) was used as a measure of the expected elongation of the projectile. Differences above 300 m/s indicated the projectile was still undergoing significant elongation, while differences above 500 m/s indicated the possibility of projectile separation. Projectiles with velocity gradients

less than 150 m/s were deemed to have reached stable lengths quickly enough to be suitable EFP candidates. The overall average velocity was the primary measure used to assess the kinetic energy of the projectile. Higher overall velocities would result in a greater target penetration. For successful target neutralisation, hypersonic projectiles with velocities greater than 2000 m/s were required.

The centre thickness was varied from 1.75 mm to 2.70 mm with a fixed rear-face radius of 20.0 mm. The formation results of this study are shown in Table V. An increased centre thickness resulted in greater mass inertia of the EFPs. Consequently, the projectiles with greater centre thicknesses were observed to reach lower overall velocities, greater velocity gradients and a greater material distribution near the rear of the projectile – each being an undesirable trend. The effective length of the projectile (i.e., the length of

TABLE V. FORMATION OF EFPS WITH VARYING CENTRE THICKNESS (REAR-FACE RADIUS = 20.0 MM).

Centre thick-ness (mm)	Simulation time (µs)				
	18.0	21.0	24.0	27.0	30.0
1.75	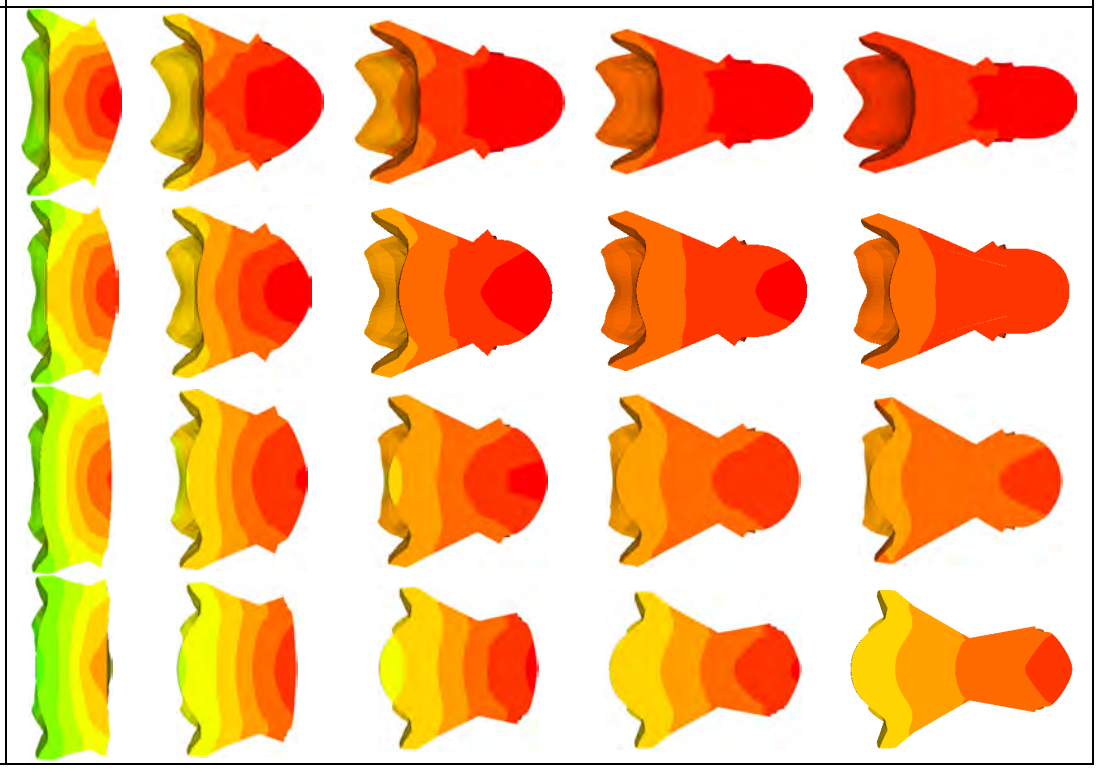				
2.00					
2.30					
2.70					

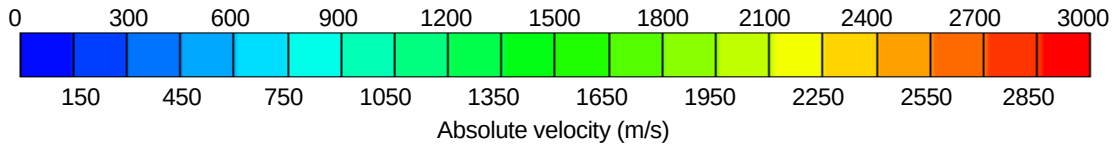

material along the projectile axis, excluding the fins) was observed to increase as the centre thickness increased. The EFP with a centre thickness of 2.00 mm was selected for further investigation since it remained compact, with an effective length of 8.95 mm, and had an average velocity of 2710 m/s. The rear-face radius of this configuration was varied to further reduce the effective length while maintaining the average velocity of the projectile.

The rear-face radius was varied from 20.0 mm to 30.0 mm, with a fixed centre thickness of 2.00 mm. The results of this investigation are shown in Table VI. The increased rear-face radius was observed to decrease the effective length of the projectile (with the overall length

only slightly increasing), and slightly increase the average velocity of the projectile.

With a rear-face radius of 30.0 mm, the effective length was 6.30 mm, and the overall length was 11.0 mm. The material distribution was improved by shifting more of the mass towards the front of the projectile. The slightly compact projectile was preferred as the EFPs positioned away from the centre of the explosive face were expected to undergo more extrusion than the centrally-located unit. The average velocity of the projectile was 2740 m/s, and the velocity gradient was approximately 100 m/s, indicating the formation was stable. Each of these qualities was favourable, hence the chosen dimensions for the initial EFP geometry were as follows: rear-face radius = 25.0 mm, centre thickness = 2.00 mm, edge thickness = 2.50 mm, and outer diameter = 10.0 mm.

Projectile External Ballistics

A snapshot of the simulation results of both MEFP configurations at a simulation time of 100 µs is shown in Fig. 5. The projectiles from

TABLE VI. FORMATION OF EFPS WITH VARYING REAR-FACE RADIUS (CENTRE THICKNESS = 2.00 MM).

Rear-face radius (mm)	Simulation time (µs)				
	18.0	21.0	24.0	27.0	30.0
20.0					
25.0					
30.0					

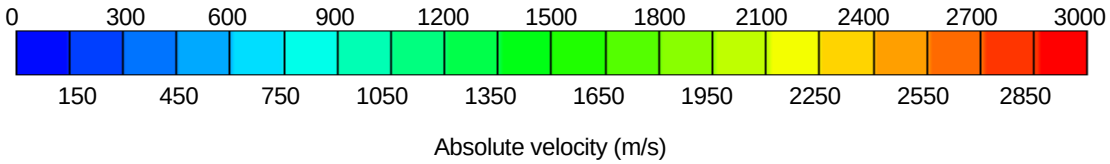

the planar-faced explosive, shown in Fig. 5(a) and (b), were observed to predominantly move along the central axis and sightly radially outward. The projectile velocity was greatest in the central EFP, with reducing velocities as the radial position of the EFPs increased. The projectile velocity ranged from 3080 m/s (for the central hexagon) to 1770 m/s (for the outermost hexagons). Generally, the extrusion of the hexagonal units produced acceptably-shaped projectiles; only the furthermost projectiles exhibited excessive extrusion and would likely tear apart. The absence of significant velocity gradients across the projectiles indicated that the projectiles were stable (in terms of elongation) and no longer deforming. The outer ring of projectiles exhibited excessive yaw at 100 µs (almost 90°) and it is expected that these projectiles will exhibit excessive tumbling behaviour.

The distribution of the EFPs resulting from a spherical explosive-liner interface was shown to

be more uniform and further radially dispersed than the distribution resulting from a planar interface. The distribution of the EFPs at 100 µs for the configuration with a spherical-faced explosive is shown in Fig. 5(c) and (d). Most of the projectiles exhibited near-zero velocity gradients at 100 µs, indicating that the projectiles were no longer elongating. Overall, the shape of the projectiles remained compact and similar amongst all the EFPs in this configuration – a particularly promising outcome for the outer ring of EFPs, which, in the case with a planar-faced explosive, already displayed large elongations at 100 µs. The outer ring of projectiles showed velocity gradients of approximately 300 m/s, which indicated continued elongation of these projectiles was still occurring. Furthermore, the orientation of these projectiles, along with their velocity gradients, indicated that tumbling remained a concern.

The projectiles were analysed individually to determine the velocity and trajectory distribution of the complete MEFP liner. To track the individual projectiles, the numbering convention shown in Fig. 1 was used. The velocity of the projectiles was measured as a check for the required kinetic energy to undergo adequate penetration. Fig. 6 shows the absolute velocity of each of the projectiles from both MEFP configurations. At approximately 15 µs the explosive blast wave reached the liner. Thereafter, an almost instantaneous rise in

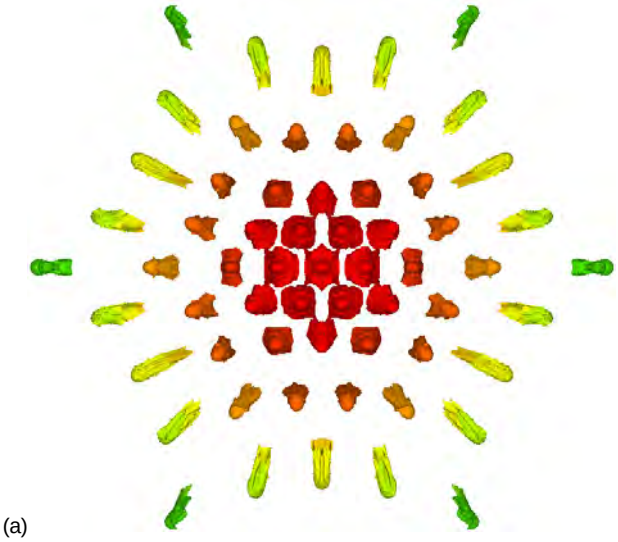

(a)

(b)

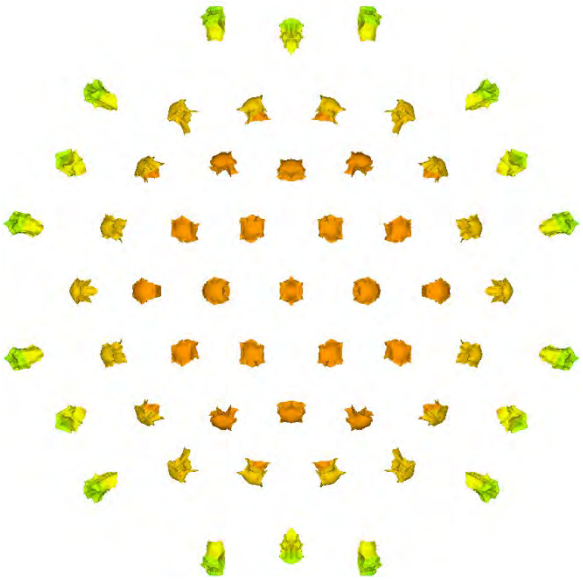

(c)

(d)

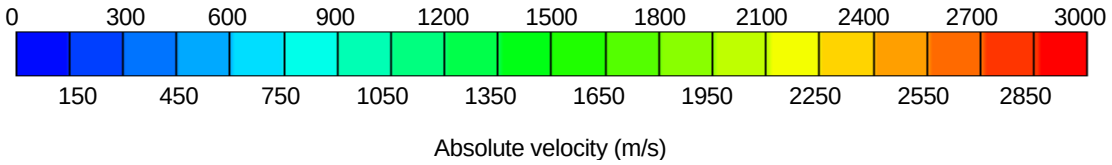

Fig. 5. Simulation results showing the distribution and velocity contours of projectiles at 100 µs, with (a) front and (b) side view of the full MEFP with the planar-faced explosive, and (c) front and (d) side view of the full MEFP with the spherical-faced explosive.

projectile velocity was observed. Following the initial acceleration of the projectiles, a steady velocity was achieved in each projectile. Higher velocities were observed in the projectiles near the centre of the liner than those positioned near the outer edge of the liner.

The maximum absolute velocity of the central EFPs of the spherical-faced explosive decreased by approximately 18% compared to the planar-faced explosive configuration (the centre EFP velocity dropped from 3080 m/s to 2520 m/s). The drop in velocity was anticipated since a plane-wave detonation (with comparatively higher energy flux than a spherical detonation wave) was used in the planar-face case, and a spherical (point) detonation was used in the spherical-face case. The effect was less

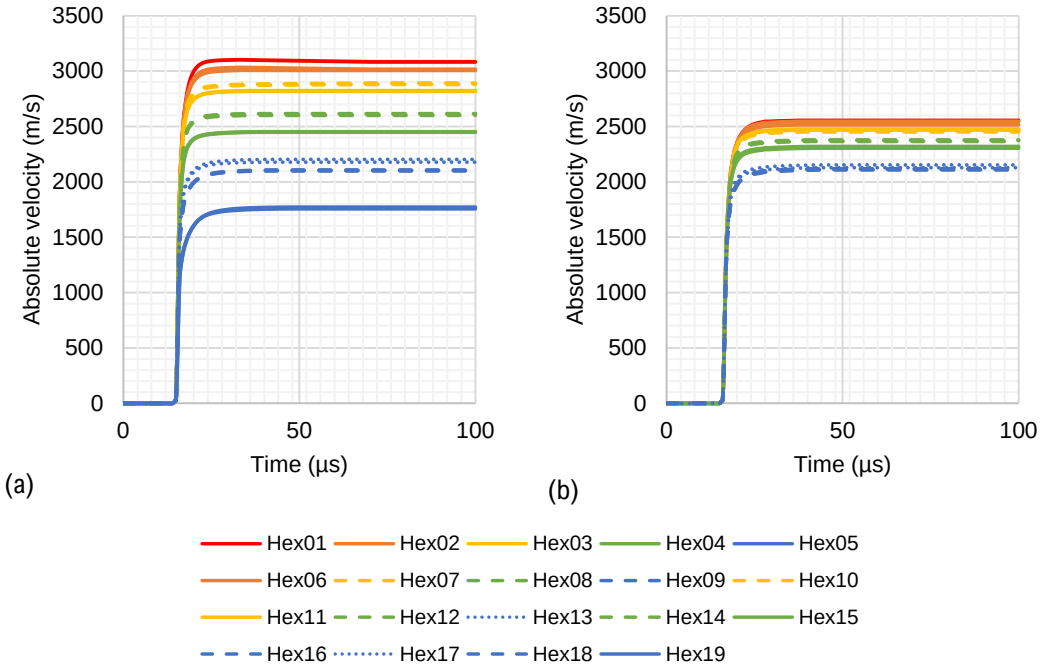

Fig. 6. Absolute velocity of MEFPs up to 100 µs for an explosive with (a) planar face and (b) spherical face.

significant on the outer EFPs, all of which (except for the furthermost hexagons) still exhibited velocities greater than 2000 m/s. The dominant factor affecting EFP velocity was attributed to the detonation wave shape of the explosive.

The displacement of each hexagon was analysed to determine the trajectory and distribution of the projectiles at a target zone. It was assumed that the projectiles would continue to move along straight-line trajectories. Shown in Fig. 7 are the distribution maps of the MEFPs at the same target distance for both explosive configurations. The region occupied by the projectiles was divided into 5 zones of equal area. For an ideal, uniform distribution, an equal number of projectiles should be present in each of the regions. The results from the planar explosive highlight the inadequate EFP distribution: the projectiles are concentrated near the centre of the target area, and only occupy a

small region within a 19° conical zone. The distribution of the MEFPs was greatly improved, both in terms of distribution and uniformity once the explosive was modified to have a spherical face. The results of the explosive with a spherical face yielded a distribution contained within an approximately 42° conical region.

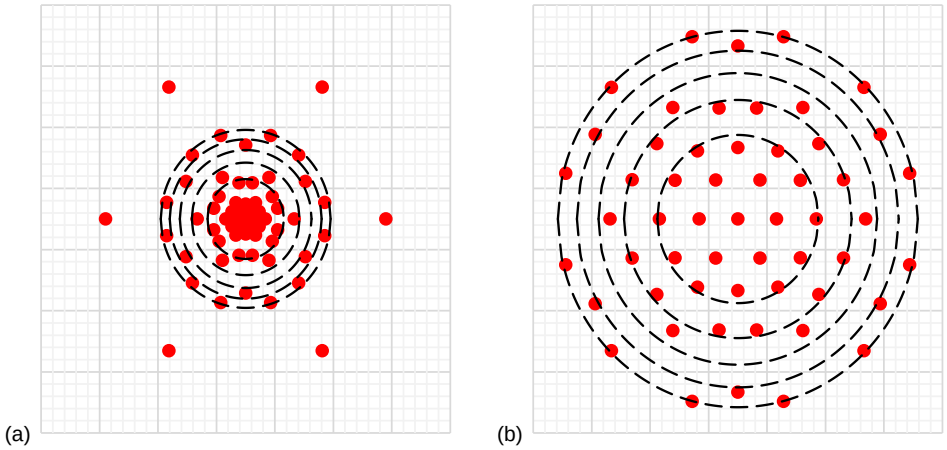

Fig. 7. Distribution map of MEFPs at the same target distance, for an explosive with (a) planar face resulting in a 19° conical angle, and (b) spherical face resulting in a 42° conical angle.

Projectile Terminal Ballistics

The penetration results were evaluated by two outcomes: the steel structure perforation and the residual kinetic energy of the projectile after the collision. Steel plates of thicknesses varying from 8 mm to 14 mm were analysed. Failure of the plate was controlled by element erosion, which was governed by the Johnson-Cook failure model. Fig. 8 illustrates the steel plate cross-section after the collision with the projectile. The projectile fully penetrated the steel plates with thicknesses 10 mm and less. For the thicker plates, the projectile was observed to embed itself within the steel; the projectile was on the verge of exiting the 12 mm plate, however, in the 14 mm plate there was no imminent perforation.

TABLE VII. RESIDUAL KINETIC ENERGY OF PROJECTILES AFTER COLLIDING WITH A STEEL PLATE.

Plate thickness (mm)	Residual kinetic energy (J)	Residual kinetic energy (%)
4.0	2480	62.0
6.0	1350	33.8
8.0	616	15.4
10	244	6.10
12	52.1	1.30
14	48.1	1.20

Table VII lists the kinetic energy of the projectile after penetrating the steel plate (with thicknesses 10 mm and less), and the relatively-low kinetic energy associated with the projectile embedded within the thicker steel plates.

Conclusions

Computational analyses were performed to develop the MEFP liner design comprising up to 61 hexagonal units on the front face of a cylindrical explosive column. Two explosive configurations were investigated: a planar and spherical explosive-liner interface. The spherical interface required greater spacing between the EFPs, resulting in an arrangement with total of 55 units on the explosive face. The dimensions of the centrally-positioned EFP were determined by a numerical investigation of the projectile formation, in terms of velocity, shape and stability.

The simulation of the projectile formation, velocity, and trajectory of the MEFP design with a planar explosive face yielded results which indicated that further improvement was required. The overall velocities of the projectiles showed promising results: more than half the projectiles yielded steady velocities of more than 2500 m/s (the baseline for the penetration analysis), while all the projectiles (besides those located at the

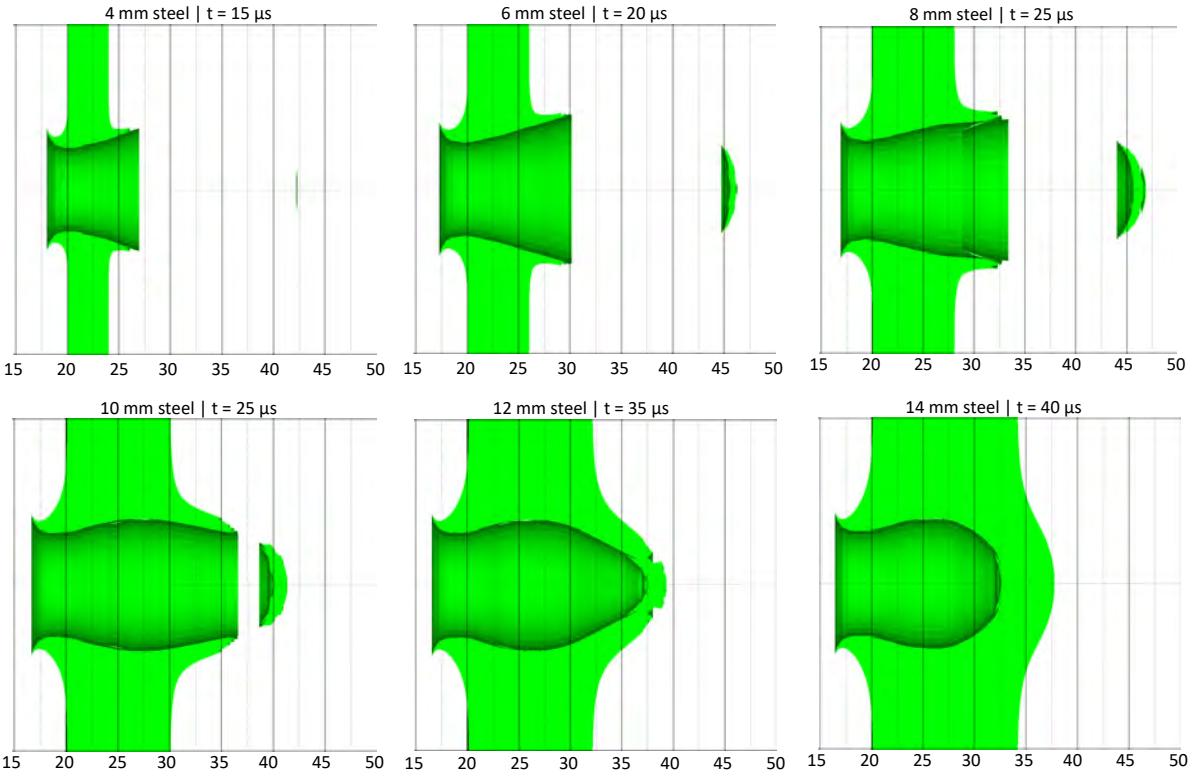

Fig. 8. Simulated penetration of steel plates after colliding with a 1.28 g copper projectile moving at 2500 m/s.

furthest corners of the MEFP arrangement) yielded velocities above 2000 m/s. The outer ring of projectiles exhibited excessive yaw at 100 µs and were expected to exhibit unstable tumbling behaviour. Furthermore, the trajectory of the projectiles indicated a dense distribution at the target zone, occupying a volume defined by a 19° conical angle. This region excluded six EFPs, located at the furthest corners of the MEFP arrangement, which were predicted to have unstable formations, low kinetic energies, and poor penetration potential.

The simulation with a spherical explosive face produced compact, stable EFPs, even for the outermost projectiles. Although the outer ring of EFPs was likely to also undergo tumbling action, the shortened length of these projectiles would make the tumbling effect less severe. Point detonation was used to develop a spherical wavefront to match the spherical explosive-liner interface; one drawback of this configuration was the reduced energy transfer associated with the spherical wavefront compared to the plane wave detonation simulated in the planar-face case. Consequently, the absolute velocity of the central EFPs was approximately 18% less than that of the corresponding EFPs in the planar-faced explosive simulation. The absolute velocity of all the EFPs, however, remained above 2000 m/s. Overall, introducing a spherical explosive-liner interface greatly improved the distribution of the MEFPs: the distribution angle (defining the conical region occupied by the projectiles) was increased to 42° and the dispersion uniformity was greatly improved. Although a further increase in radius could hone the projectile dispersion if a limited target zone was required, a wave shaper would then need to be introduced to ensure a suitably-shaped wavefront was produced for simultaneous arrival times at each of the EFPs.

The penetration analysis was performed by simulating the impact between a copper penetrator – with a representative geometry based on the outcome of the projectile formation study – and 4340-steel target plates of varying thicknesses. The projectile impacted the target plate with a kinetic energy of 4000 J, and perforation was achieved for plate thicknesses up to 10 mm. Penetration of 12 mm and 14 mm thick plates was also simulated, however, no complete perforation was observed.

The numerical investigation into the feasibility of a forward-firing MEFP system has yielded promising results. Projectiles with high kinetic energy, and stable, compact shapes were formed from an array of hexagonal-shaped units.

With a spherical-faced MEFP configuration, a wide and uniform distribution of the EFPs was achieved, indicating a good hit probability with the target. Furthermore, the penetration results indicated that there was sufficient kinetic energy to ensure a hit would successfully neutralise the target. The investigation into the feasibility of this type of MEFP configuration, in the application of an incoming ballistics threat interceptor, has demonstrated satisfactory results.

References

[1] Weiman K. Research and development in the area of explosively formed projectiles charge technology. Propellants, Explosives and Pyrotechnics. 1993; 18 (5): 294-298.

[2] Lui J, Gu W, Lu M, Xu H and Wu S. Formation of explosively formed penetrator with fins and its flight characteristics. Defence Technology. 2014; 10: 119-123.

[3] Fong R, Ng W, Rice B and Tang S. Multiple explosively formed penetrator (MEFP) warhead technology development. Proceedings of the 19th International Symposium on Ballistics, Interlaken. 2001; 563:568.

[4] Koch RP, Snyder J, Fong R, Redner P, Sadangi R and Kapoor D. Using nickel-tungsten alloys to produce multiple explosively formed penetrator (MEFP) warheads. Proceedings of the 30th International Symposium on Ballistics, Long Beach. 2017.

[5] B.M. Dobratz and P.C. Crawford. LLNL handbook of explosives: Properties of chemical explosives and explosive simulants, Technical Report UCRL-52997, Lawrence Livermore National Laboratory, University of California, California, U.S.A (1985).

[6] Ansys AUTODYN® Explicit Materials Engineering Data (2022).

[7] G.R. Johnson and W.H. Cook. A constitutive model and data for metals subjected to large strains, high strain rates and high temperatures. Proceedings of the 7th International Symposium on Ballistics, pp. 541–547, Netherlands (1983).

**2023 Symposium on Ballistics of the
South African Ballistic Organization
9-11 May, CSIR, ICC, Pretoria, Gauteng
South Africa**

Preliminary Simulation to Ascertain the Heat Distribution of an Artillery Shell inside a Shipping Container

Stefan van der Walt[1]

[1]*Rheinmetall-Denel Munition, Boskop, Potchefstroom, 2520, South Africa*

Email: stefan.vanderwalt@rheinmetall-DM.com

Tell: 018 299 8898

***Abstract*— The conditions and manufacturing circumstances of an artillery shell can be accounted for during manufacturing and storage, which is not necessarily the case during transport in containers. This poses an important question: Theoretically how hot does the artillery shell get inside a container during the worst of circumstances? This is an important question since ammunition is qualified for use at a certain upper temperature limit, and it is important to know if that temperature is exceeded during these circumstances.**

The theoretical worst of circumstances was defined as a container being in full sun all day with the highest irradiation value during summer in South Africa, standing on a concrete surface. A heat transfer simulation was done using SolidWorks Flow (which is the FloEFD solver embedded inside SolidWorks). Ideal air was used as the fluid inside the container, with a 12 hour cycle simulated between 6 am and 6 pm. A 6 m container was used with its long side facing north. Gravity was activated to ensure circulation, no cloud cover was modelled, and only a single shell was inserted into the container on a pallet. The outer surfaces of the container was modelled as black body walls to ensure maximum heat absorption from the sun.

The results indicated that even at worst conditions the outer temperature exceeded 100 °C but the temperature didn't exceed 60 °C at any point inside the shell during the cycle. The air temperature inside the container did indicate that it formed layers of decreasing temperatures as the distance from the roof and walls increased. The temperature of the concrete on which the container stood also influenced the temperature curve in both its maximum temperature and the rate of cooling when the solar radiation intensity decreased in the late afternoon.

Future studies will definitely need to focus on measurements inside containers during the summer to see if it correlates with the simulation data. More than one complete 24 hour cycle must be simulated to see if the minimum temperatures during the cycle increases after each cycle. A container filled with more than one shell must also be simulated to see its effect on the temperature profile. (*Abstract*)

Keywords*— *SABO, FloEFD, SolidWorks Flow, Artillery, Shipping, Thermal Radiation, Heat Transfer

Introduction

The manufacturing of an artillery shell is a controlled process, and an exact account can be given for the conditions and manufacturing circumstances during every specific process. After manufacturing, the artillery rounds are stored inside bunkers or ammunition stores with controlled temperatures. After this, it is prepared for shipping, put inside shipping containers after which it will wait for pick up and eventual delivery to the docks, and uploaded onto a ship headed for the client's destination. For the duration the artillery shell is inside the container, the temperature cannot be controlled. Therefore, the question arises as to how hot an artillery shell get inside a container. This is an important question since ammunition is guaranteed or qualified at a certain maximum temperature, and it is important to know if that temperature is exceeded

during these circumstances. This study will address this question by performing a first-order simulation that assess the temperature inside a container standing in full sun on concrete during summer, as it was deemed the worst case during the logistics process.

Simulation Setup

Geometry

Shipping containers intended for intercontinental traffic come in various sizes, but the container length typically used for cargo transport is the 10 ft (3 m) standard, 20 ft (6 m) standard and the 40 ft (12 m) standard containers. For this study, the 20 ft (6 m) container will be used. The internal dimensions [1] of this container is summarised in TABLE I.

Table I: Internal Dimensions for the 6 M Standard Shipping Container

Component	Dimension [mm]
Length	5 898
Width	2 350
Height	2 390
Plate thickness	2

Although the sides of the container are made from corrugated steel sheets [1], it was modeled as smooth sheets to simplify the simulation and reduce simulation time. It was also assumed to be airtight, with no air escaping the container during the simulation. The floor was also modeled as metal sheets instead of plywood which is more conservative. A single artillery shell with explosive filling was placed on top of a wooden pallet. The detail of the shell was greatly reduced in order to simplify the simulation. The geometry used in the simulation is shown in Fig. 1 and the sectioned geometry used for the shell is shown in Fig. 2.

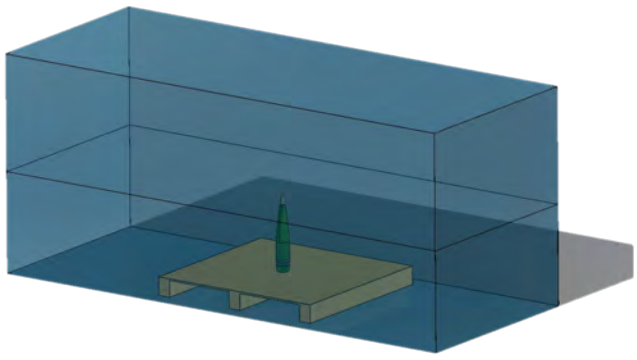

Fig. 1: Geometry as used in the simulation

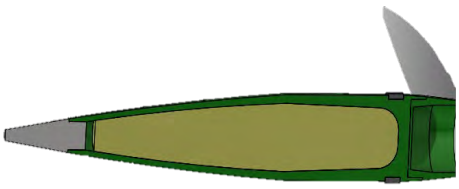

Fig. 2: Sectioned geometry of the artillery shell as used in the simulation

Setup and Assumptions

Various assumptions were made to simplify the simulation. The simulation was setup as an internal flow simulation (the flow occurring inside the container), which was filled with air with 0% relative humidity. Gravitational effects were activated to ensure circulation of the air inside the container due to convection. Heat conduction was also activated to accommodate heat transfer in the solids which included the container, pallet and shell assembly. Solar radiation was activated for the simulation for the actual time mentioned in the next point. The solar radiation followed the sun's trajectory in the sky, i.e. rising in the east and setting in the west.

The solution was time-dependent (i.e. a transient simulation) and started at 6:00 am and ended at 6:00 pm on 31 December with no cloud cover present. The long wall of the container faced north. The container stood on concrete with a constant temperature of 55 °C – this is a conservative assumption [2] and can expect slightly lower temperatures if more detailed models are used for the concrete heat transfer. One must also keep in mind that the container's inner floor would also not be in direct contact on the ground, but is elevated a bit and made of which will also insulate it somewhat from the hot concrete.

To minimise the solution time, only one shell was put on a pallet inside the container – this simulation still took roughly 14 hours to solve – the long solution time was mainly due to the presence of radiation. The calculation of the exchange areas needed to be done for each iteration and the resulting matrices are large and time consuming to solve. The outer surfaces of the container was seen as perfect blackbody walls i.e. it was perfect absorbers of the incoming solar radiation, which won't be the case in reality but is a conservative assumption. The inner walls of the container was assigned the radiative properties of sheet metal in order to more realistically radiate to the shell. The shell surfaces was set as perfect blackbody walls. The container was filled with air, with no ventilation. The initial temperature of the air and all solids were 23 °C.

Mesh

The mesh in SolidWorks Flow requires the definition of a global mesh containing zero level cells, indicating no refinement levels present on these cells. Cell refinement is a process that subdivides the rectangular computational mesh cell into eight smaller cells. Each level of subdivision is termed a level of refinement [3]. The cross-sectional area of the model (consisting of the container with the shell and pallet) consisted of a global mesh size of 10 cells per side. Along the length of the container, the global mesh consisted of 26 zero level cells. All the mesh refinement levels of the shell assembly was set to a maximum of level 4. These included the fluid and solid cells, as well as at the fluid-solid interface. The channel refinement for the flow passages contained 7 cells with a refinement level of 4. The refinement level for the pallet was set

to 2, with 5 channels of refinement. The mesh used for the simulation is given in Fig. 3, with the different levels of refinement indicated by the different colours.

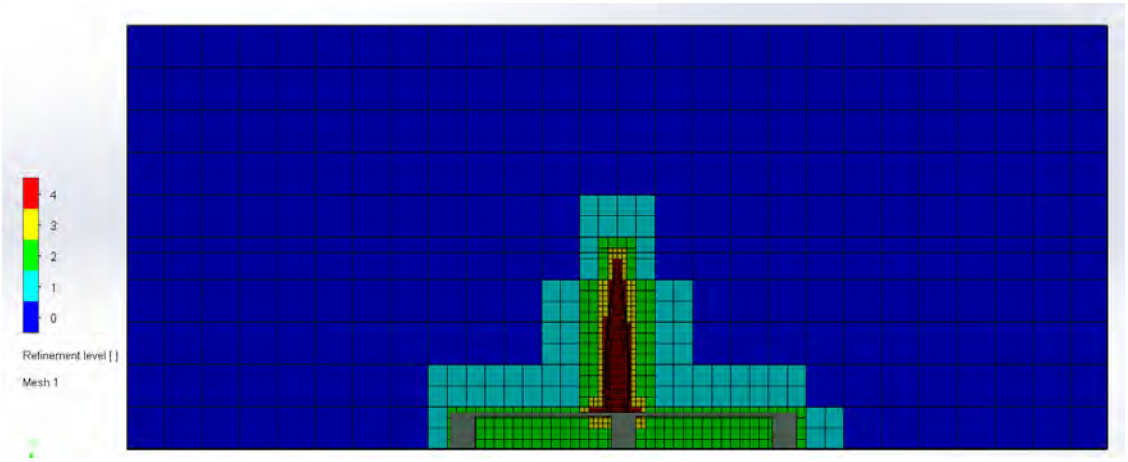

Fig. 3: Mesh as used for the simulation

Results

Container

Just to give an idea of the effect of direct solar radiation on metal, the temperatures at two distinct time frames were given: at 10:00 am (Fig. 4) and at 12:00 pm (Fig. 5). The maximum outer surface temperature at 10:00 am was 105 °C, while the maximum outer surface temperature at 12:00 pm was 112,5 °C. One can also see the sun rising over the container which is visible in Fig. 4 in the form of the outer temperature, where the radiation is hitting part of the eastern side of the container which is not present in Fig. 5 anymore (2 hours later) since the sun is now directly overhead.

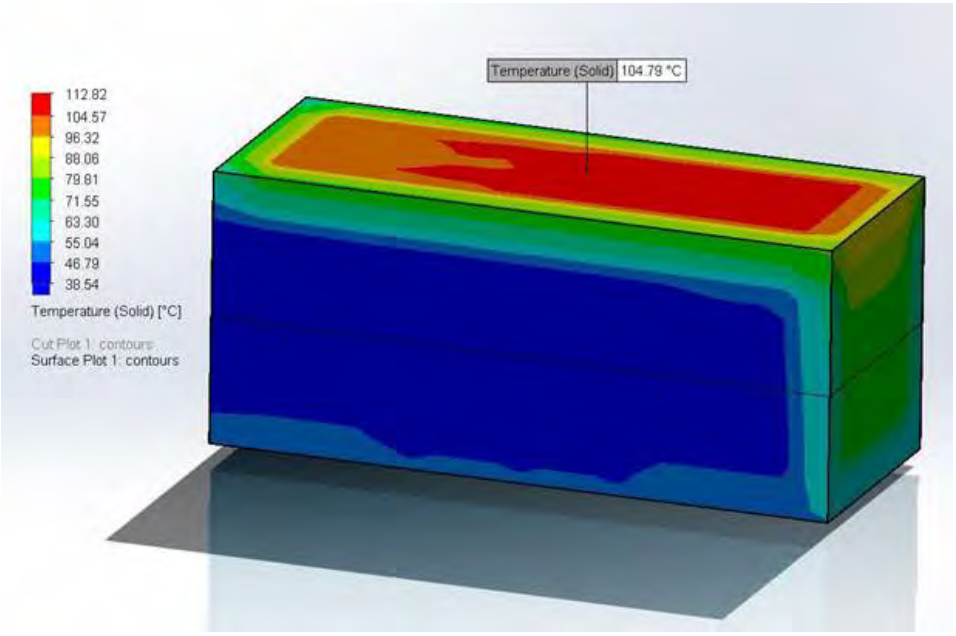

Fig. 4: Surface temperature plot of container outer surfaces at 10:00 am

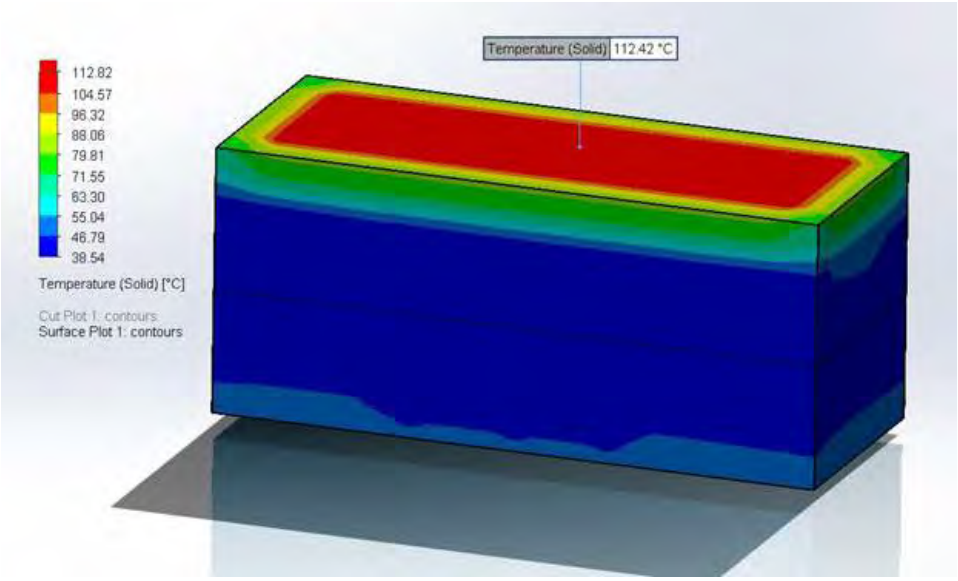

Fig. 5: Surface temperature plot of container outer surfaces at 12:00 pm

Air Inside the Container

The air inside the container was heated up due to the incoming radiation as well as due to the constant temperature boundary condition at its floor set at 55 °C. This heated floor caused the temperature curves to have a maximum for longer during the day, causing more heating. One can see that there is some oscillating of the air fluid temperature, which is due to the static air being heated up and then starting to circulate and mix with the colder air. The locations of the probe are shown in Fig. 6, which is done at 12:00 pm. Fig. 7 presents the temperature over time plots of all those probes.

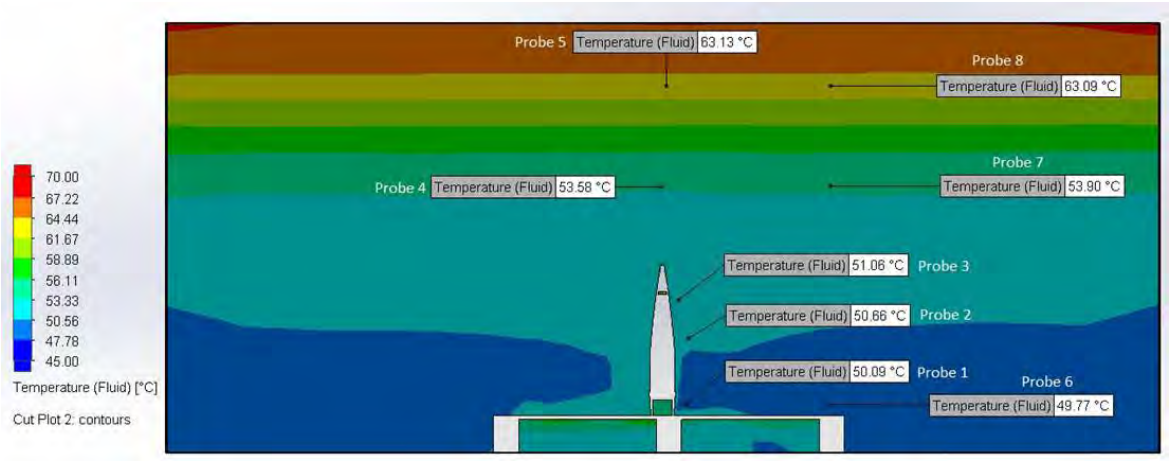

Fig. 6: Air temperature section view at 12:00 pm with probes defined

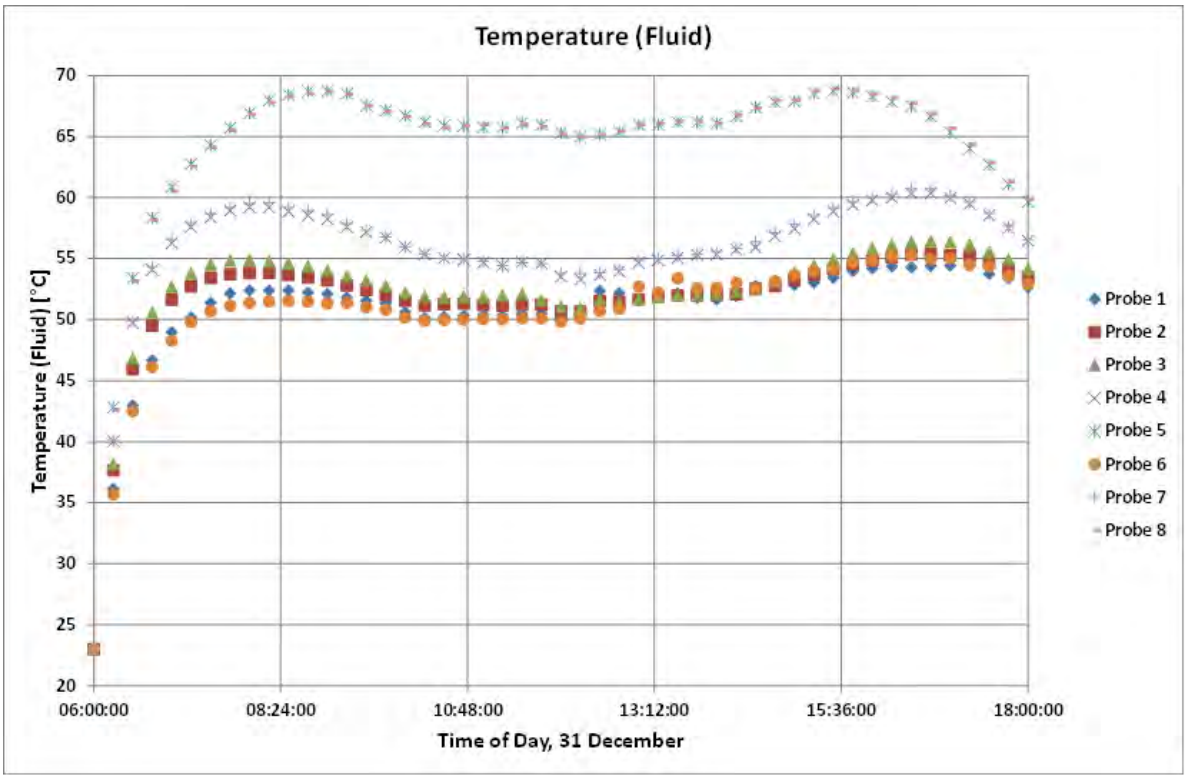

Fig. 7: Time plot for the different probes defined in Fig. 6

The Explosive Filling Temperature

10 probes were used to plot the results for the temperatures inside the explosive filling, whose location and reading is given in Fig. 8, taken at 13:30 during the cycle. The temperature versus time plot for these 10 probes are given in Fig. 9. The filling temperature of the explosives reached a maximum of 58 °C in the ogive at 13:45, with the bulk region of the filling being 1-2 °C lower. One expects to have a cyclical shaped curve (one that resembles more a sine curve than a power function), which would have been the case but the high constant floor temperature of 55 °C keeps the temperatures higher for longer and also causes the temperatures to fall at a slower rate.

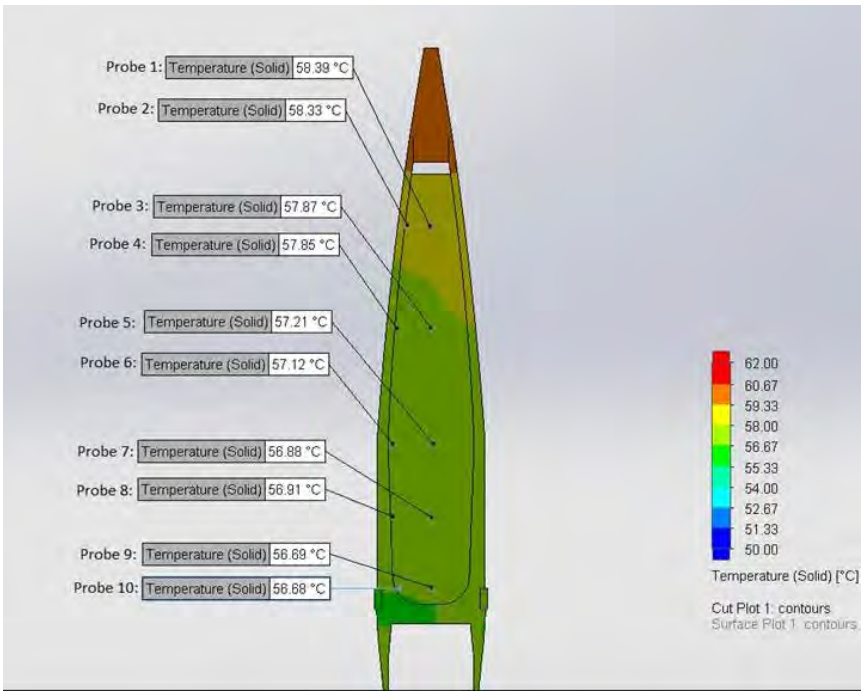

Fig. 8: Temperature section plot of shell at 13:30. Probe locations are defined

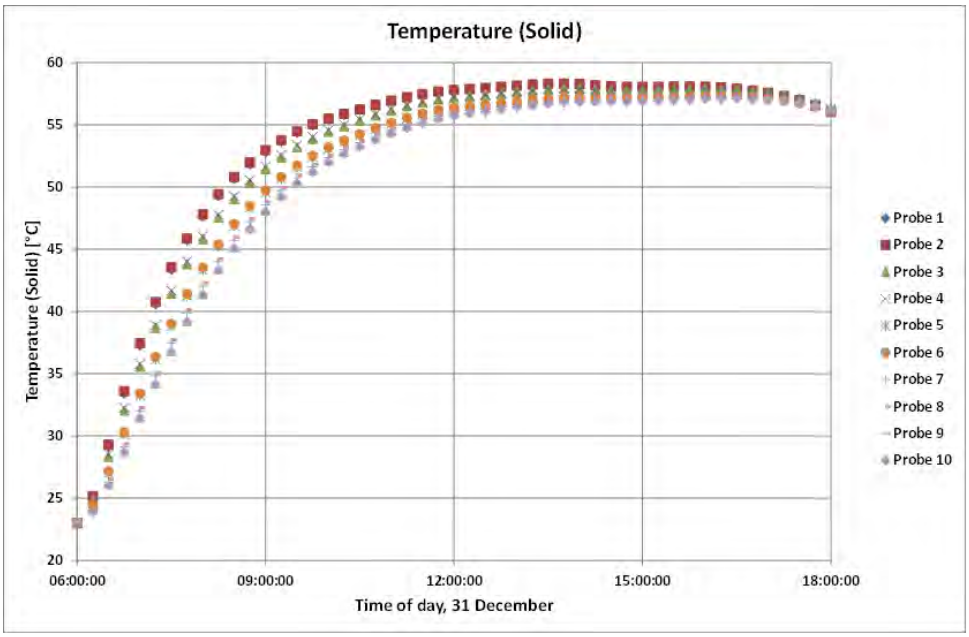

Fig. 9: Time plot for the shell for the different probes defined in Figure 8

Discussion and Conclusion

A first order simulation was done regarding the temperature inside a container during summer due to solar radiation and a warm cement floor. To save time, only one shell was inserted inside the container, and only one 12 hour cycle (between 6:00 am and 6:00 pm) was simulated during the summer with no clouds. The temperature plots from Fig. 9 showed that the air temperature closer to the roof of the container (probe 5

and 8) exceeded 63 °C during most of the cycle, while the air temperature in the centre of the container (probe 4) reached a peak of 60.7 °C only late in the day. The temperature lower in the container around the shell (probes 1, 2 and 3) reached a maximum of 56 °C late in the day, with its temperatures mostly below 55 °C.

The temperature inside the filling reached its highest temperature of 58 °C between 12:00 and 14:00 in the upper part of the filling (probe 1 and 2 in XP column), where the shell thickness is thinner, while the lower part of the explosive column was roughly 2 °C lower. There is also roughly a 1 °C difference in air temperature (between probe 1 and 3) between the higher and lower part of the shell. As already mentioned, the shape of the fillings temperature curve is flatter than expected, mainly due to the high temperature of the concrete floor keeping the temperature inside the container hotter for longer. It also seems to take over/become dominant after 15:00 in the afternoon (the slight second peak of the XP filling curve).

As mentioned this was a first order simulation, meaning that a lot of refinement can still be done over time, with some suggestions that follows. In order to see if the 63 °C is exceeded, one needs to refine the simulation by applying a more detailed function for the heat at the bottom of the container. The simulation must then be run for multiple continuous days to see if the minimum temperature (the container temperature and its contents) drops to the assumed initial temperature of 23 °C each time or if it gradually increases over each cycle, which might raise the overall temperature of the simulation. It is also recommended that one put data loggers in a container on-site, which is in full sun and standing on concrete and take measurements over several days during the summer in order to get a better idea of the trends involved, which could prove valuable.

References

[1] Technical Specification for a Typical Steel Dry Cargo Container 20' x 8' x 8'6" ISO 1CC Type "General Purpose", Steinecker Containerhandel, 2012.
[2] S. R. Abid, N. Taysi and M. Ozakca, “Temperature Records in Concrete Box-Girder Segment Subjected to Solar Radiation and Air Temperature Changes,” IOP Conf. Series: Materials Science and Engineering, vol. 870, 2020.
[3] Dassault Systemes, Technical Reference: Solidworks Flow Simulation 2021, 2020.

Evaluating the enhancing potential of metal hydride in high explosives using a simulation approach.

Lamla Thungatha[1], Nobuhle Nyembe[1], Conrad Mahlase[1], Lisa Ngcebesha[1], Simphiwe Ncwane[1]

[1]*Defence and security cluster, Landward sciences, Council for Scientific and Industrial Research (CSIR), Pretoria 0001, South Africa*

Email: LThungatha@csir.co.za

Tell: 0128414855t

Abstract

Modelling and simulation in energetic materials (EM) is a well-known field and it keeps on growing and improving. Being able to simulate the EM before doing synthesis or formulation in the laboratory is a safe route. By using the right simulation tools, the performance parameters such as enthalpy of formation, detonation pressure, detonation velocity and sensitivity can be estimated. Metals are known as enhancing additives to energetic materials and are used to make enhanced explosive composites. Metal hydrides are derived from pure metals or metalloids which can be covalently or ionically bonded to hydrogen. Metal hydrides have also been used to enhance the EM performance parameters such as specific impulses for solid propellant. In this work theoretical formulation optimization was done for 2,4,6-trinitrotoluene (TNT), 1,3,5-Trinitroperhydro-1,3,5-triazine (RDX), 2,2-Bis[(nitroxyl)methyl]propane-1,3-diyl dinitrate (PETN) and composition B with Alane (AlH_3), magnesium hydride (MgH_2), titanium hydride (TiH_2), Zirconium hydride (ZrH_2), lithium aluminium hydride ($LiAlH_4$) and sodium aluminium hydride (NaAlH4). The theoretical density and detonation properties of the formulations were estimated with EXPLO5. The densities of the formulations were observed to be affected by the addition of metal hydrides. Where the metal hydrides are made from heavy metals, formulation density increased with increasing metal hydride quantities and the lighter metal hydrides did the opposite. Despite the observed increase in density for some formulations, this did not translate into more increased detonation pressure except for the TNT formulation with ZrH_2. AlH_3 performed well for all the explosives, including PETN formulation.

Keywords—Metal hydrides, Simulation, Performance parameters, energetic materials, EXPLO5

Introduction

The use of energetic materials classified as explosives, propellants and pyrotechnics has been increasing over the years both in military and civilian applications. These materials are made from organic and inorganic molecules. When initiated these materials can either detonate or deflagrate, hence they are called energetic materials [1]. To achieve desired physical properties for these, energetic materials are formulated or blended with other molecules. Some of the important properties are detonation performance, thermal properties, water resistance processibility and shelf life. These properties are sometimes achieved through the synthesis and formulation of energetic materials [2]. To enhance the performance of energetic materials, energetic or fuel components are added as part of the formulation. Aluminium (Al) is an example of such a fuel component, and it has been introduced to improve energetic materials' performance [3]. The use of Al as a metal additive in energetic materials has been widely applied because of its high calorific value, which can increase reaction temperature, blast, and incendiary effects [4]. In explosives, Al has shown the ability to improve air blasts and raise reaction temperatures while in propellants it has shown the ability to increase the specific impulse and flame temperature [5]. Al supersedes other metals like Boron which have even higher calorific value, but its application is limited by difficulties in ignition due to high melting and boiling temperatures (2 177 and 3 658 °C respectively) [4]. Despite the enhanced performance obtained from using Al as an additive, the high density of Al (2.7 g/cm3) when compared to metal hydrides, e.g., AlH3 (1.477 g/cm3) results in increased volumetric loading of the resulting propellants [6].

Studies have shifted into exploring metal hydrides (MH) as additives in energetic materials. Metal hydrides are conventionally used in hydrogen (H_2) storage, H_2 generation, and fuel cells and recently have been studied for application in energetic materials [7-9]. Other metals like magnesium (Mg), Boron (B) and their alloys have also been explored as fuel sources for propellants [10]. However, metal hydrides seem to be a

more promising candidate as they possess higher combustion heat than the corresponding metals due to the introduction of "hydrogen energy" [11]. Besides the energy released from metal oxidation, the H_2 combustion also contributes to the overall released energy during the combustion processes [6]. Their chemical activity, high heat of combustion and generation of low molecular weight decomposition/combustion products also puts them in a better position to be used in energetic materials [12].

In this work, energetic materials formulated with metal hydrides were simulated to study the potential of these materials to enhance detonation performance.

Methods

EXPLO5

The use of EXPLO5, a thermochemical computer code, for the calculation of detonation parameters of energetic materials including high explosives has been demonstrated by several researchers [13-16]. This code is based on the chemical-equilibrium steady-state model of detonation [17]. It uses the Becker-Kistiakowsky-Wilson (BKW) equation of state (EOS) for gaseous detonation products, the ideal gas and the Murnaghan equation of states for condensed products [18-21]. The detonation product composition in the code is calculated by applying the Gibbs energy minimisation method and is designed so that the users can choose between the explosive types of constants in the BKW-EOS [22].

The simulation was done for the explosives containing TNT, RDX, PETN and Comp B. A similar initial temperature of 3 383 °C was used. BKW-EOS with Becker-Kistiakowsky-Wilson (BKWN) set of constants were used for the calculations. Shock adiabats of products at a maximum pressure of 41 GPa and density of 1.025 g/ml were calculated. Expansion isentropes of products using a density decrease ratio of 1.25 g/ml and freeze temperature of 1 527 °C were calculated.

Formulation of the metal hydride composite explosives

The formulations consist of the commonly used explosives with metal hydrides as listed in Table I. The percentage of the metal hydride in the formulation varies from 5 - 25 %. These were added to EXLO5 to determine the effect of metal hydrides on the performance of the explosive materials.

TABLE I: FORMULATION OPTIMISATION OF SOME EXPLOSIVES WITH METAL HYDRIDE

Explosive charge	**Percentage composition Explosive to AlH_3 (EX: AlH_3)**				
TNT	95:5	90:10	85:15	80:20	75:25
RDX	95:5	90:10	85:15	80:20	75:25
PETN	95:5	90:10	85:15	80:20	75:25
Composition B (RDX 60 %: TNT 40%)	57:38:5	54:36:10	51:34:15	48:32:20	45:30:25
Percentage composition Explosive to MgH_2 (EX: MgH_2)					
TNT	95:5	90:10	85:15	80:20	75:25
RDX	95:5	90:10	85:15	80:20	75:25
PETN	95:5	90:10	85:15	80:20	75:25
Composition B (RDX 60 %: TNT 40%)	57:38:5	54:36:10	51:34:15	48:32:20	45:30:25
Percentage composition Explosive to TiH2 (EX: TiH2)					

TNT	95:5	90:10	85:15	80:20	75:25
RDX	95:5	90:10	85:15	80:20	75:25
PETN	95:5	90:10	85:15	80:20	75:25
Composition B (RDX 60 %: TNT 40%)	57:38:5	54:36:10	51:34:15	48:32:20	45:30:25
Percentage composition Explosive to ZrH_2 (EX: ZrH_2)					
TNT	95:5	90:10	85:15	80:20	75:25
RDX	95:5	90:10	85:15	80:20	75:25
PETN	95:5	90:10	85:15	80:20	75:25
Composition B (RDX 60 %: TNT 40%)	57:38:5	54:36:10	51:34:15	48:32:20	45:30:25
Percentage composition Explosive to $LiAlH_4$ (EX: $LiAlH_4$)					
TNT	95:5	90:10	85:15	80:20	75:25
RDX	95:5	90:10	85:15	80:20	75:25
PETN	95:5	90:10	85:15	80:20	75:25
Composition B (RDX 60 %: TNT 40%)	57:38:5	54:36:10	51:34:15	48:32:20	45:30:25
Percentage composition Explosive to $NaAlH_4$ (EX: $NaAlH_4$)					
TNT	95:5	90:10	85:15	80:20	75:25
RDX	95:5	90:10	85:15	80:20	75:25
PETN	95:5	90:10	85:15	80:20	75:25
Composition B (RDX 60 %: TNT 40%)	57:38:5	54:36:10	51:34:15	48:32:20	45:30:25

Results

EXPLO5 software packages were used to apply to predict the performance of energetic materials containing metal hydrides. The potential of metal hydrides to enhance high explosives materials was investigated using TNT, RDX, PETN and composition B explosive materials. These explosives are mostly applied in military space.

The density of the composite energetic materials

Formulating components of different densities might result in either higher density or lower density depending on the properties of each of the components. Density is an important property in energetic materials as the performance of the energetic materials is also a function of this parameter. Metals are known to have higher densities. High-density and high-enthalpy materials are known as high-energy-density materials. In formulations containing metals, an increase in density is expected and if the metal is energetic then this will result in improved performance. Metal hydrides have less density compared to their respective pure metals. An example of such is aluminium (2.70 g/ml) and aluminium hydride (1.477 g/ml). The density varies with the type of metal hydrides used as seen in **Fig. 1** to **Fig. 4**. Aluminium hydride and magnesium hydride have low density while titanium hydride and zirconium hydride show a very high density.

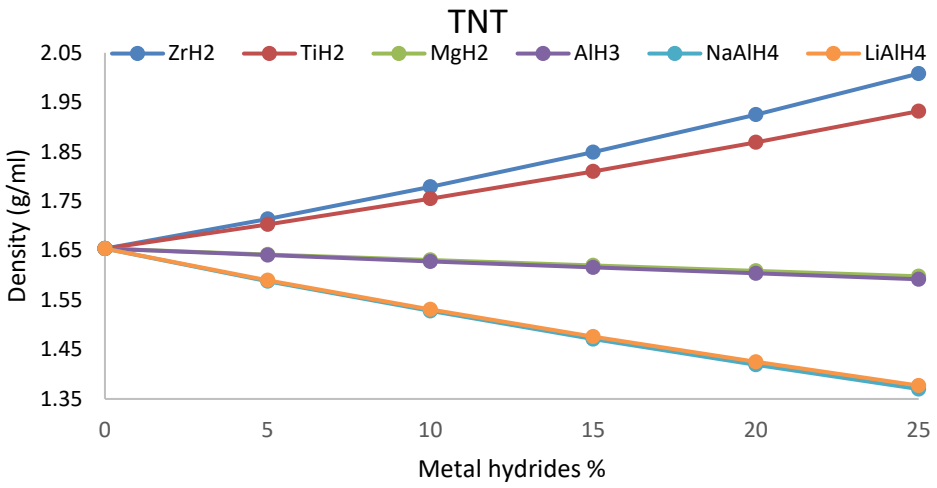

Fig. 1. Density of TNT and metal hydride formulations

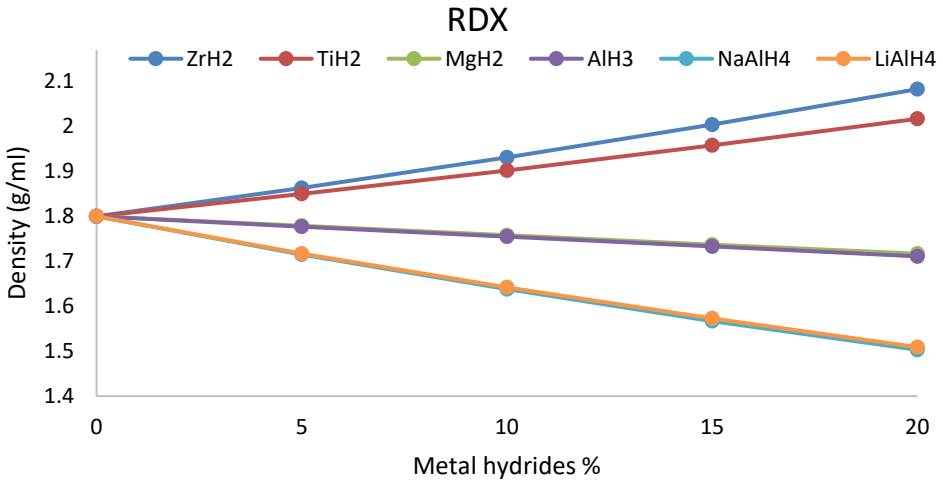

Fig. 2. Density of RDX and metal hydride formulations

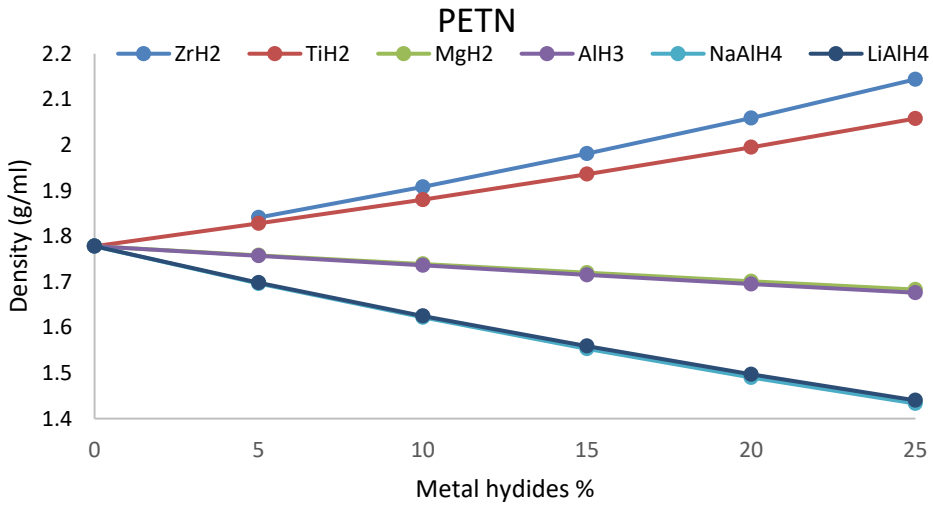

Fig. 3. Density of PETN and metal hydride formulations

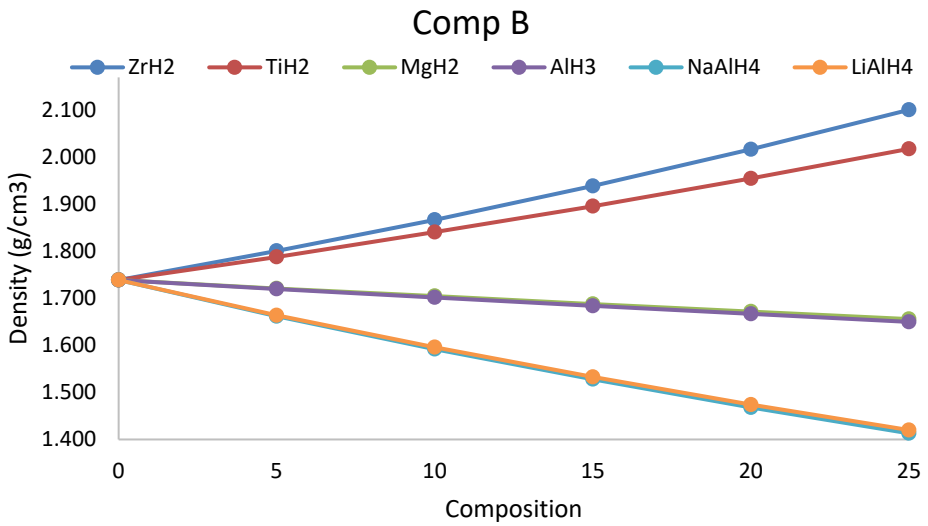

Fig. 4. Density of Comp B and metal hydride formulations

The graphs in **Fig. 1** and **Fig. 4** show the effect of the amount of metal hydrides on the density of explosive formulations. A similar trend is observed for all the explosives. ZrH_2 and TiH_2 are increasing the density of all the explosives. The density of these metal hydrides is high, hence there is an observed increase. For the rest of the metal hydrides, the more they have added to the formulation the lesser the density of the resulting formulation.

Detonation pressure of the formulated materials

A simulation of high explosives containing metal hydrides was completed to explore the potential of metal hydrides as enhancing additives. TNT, RDX, PETN and Comp B were used to study the potential

of ZrH_2, MgH_2, TiH_2, $LiAlH_4$, $NaAlH_4$ and AlH_3. Detonation pressure and detonation velocity were obtained from EXPLO5. These are important in estimating the performance of energetic materials. **Fig. 5** to **Fig. 8** give a graphical representation of the data for all the explosives and their formulations.

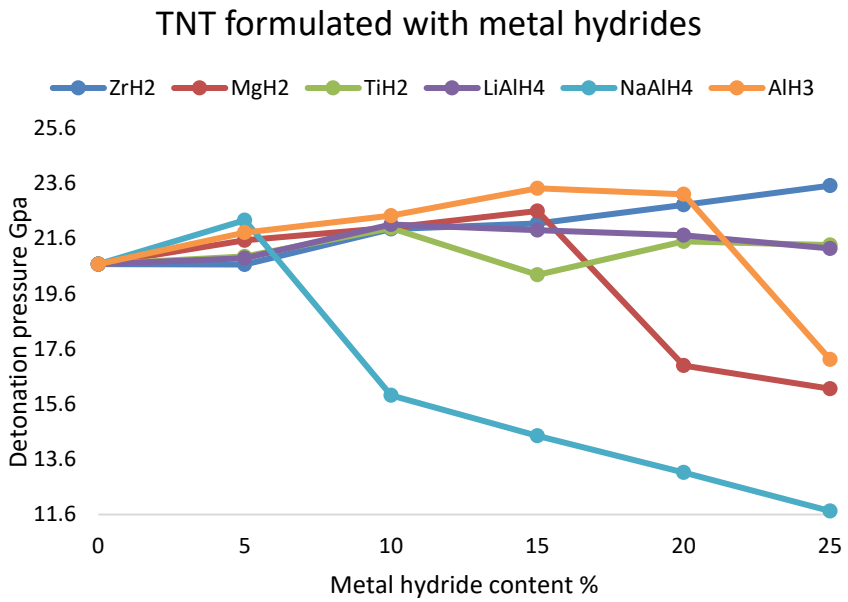

Fig. 5: Effect of metal hydrides quantities on detonation pressure of TNT formulations

It can be seen in **Fig. 5** that for most formulations the detonation pressure increases with increasing % of metal hydride until an optimum is reached beyond which the detonation pressure starts to decrease. $NaAlH_4$ shows higher detonation pressure at 5% which then starts to decrease. AlH_3 shows higher detonation pressure between 5-20%. The same trend is observed with MgH_2, but the resulting detonation pressure is less, and it is between 5-15%. ZrH_2 show an increase and it is the highest at 25%. All the metal hydrides except $NaAlH_4$ show the potential to enhance the detonation pressure of the TNT between 5% to 20% of metal hydride in the formulations.

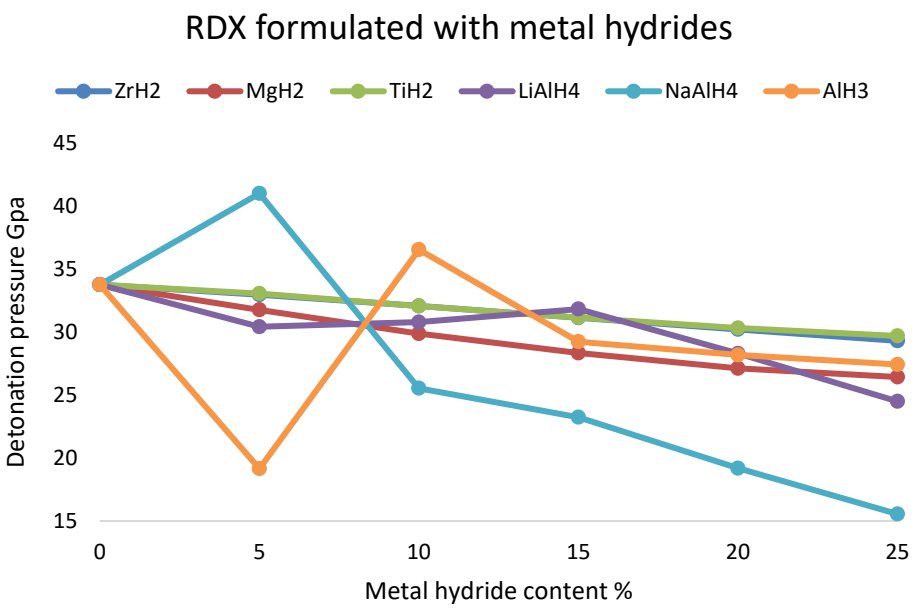

Fig. 6: Effect of metal hydrides quantities on detonation pressure of RDX formulations

In **Fig. 6** formulations of RDX with metal, hydrides show a different trend. $NaAlH_4$ shows a higher detonation pressure of 5% and AlH_3 at 10% the rest of the formulations are showing a decrease in detonation pressure as metal hydride content is increased.

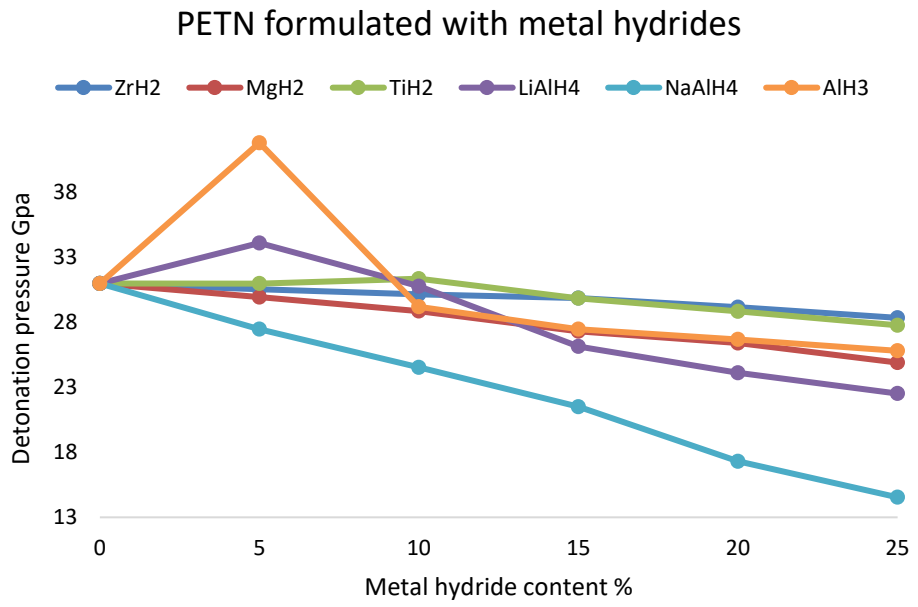

Fig. 7. Effect of metal hydrides quantities on detonation pressure of PETN formulations

Fig. 7 shows PETN formulations with the metal hydrides. AlH_3 shows the highest detonation pressure of 41.7 GPa at 5% followed by $LiaAlH_4$ also at 5%. TiH_2 shows a slight increase at 10%, and the rest of the formulations show a decrease in detonation pressure with increasing quantities of metal hydrides.

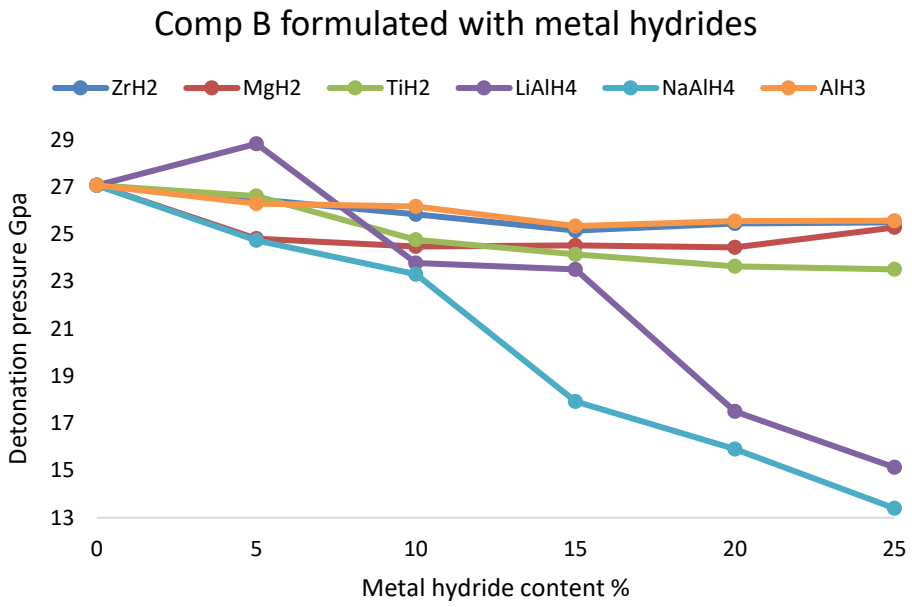

Fig. 8: Effect of metal hydrides quantities on detonation pressure of Comp B formulations

In **Fig. 8**, $LiaAlH_4$ formulation with Comp B is the only formulation that shows higher detonation pressure at 5%. All the other formulations, i.e., ZrH_2, MgH_2, TiH_2, $NaAlH_4$ and AlH_3, are showing a decrease.

The detonation velocity of the formulated materials

Detonation velocity is the propagation velocity of the shock wave through a detonating energetic material. This is one of the parameters that determine the performance of the explosive material. The higher the detonation velocity the better is the performance of the explosive material.

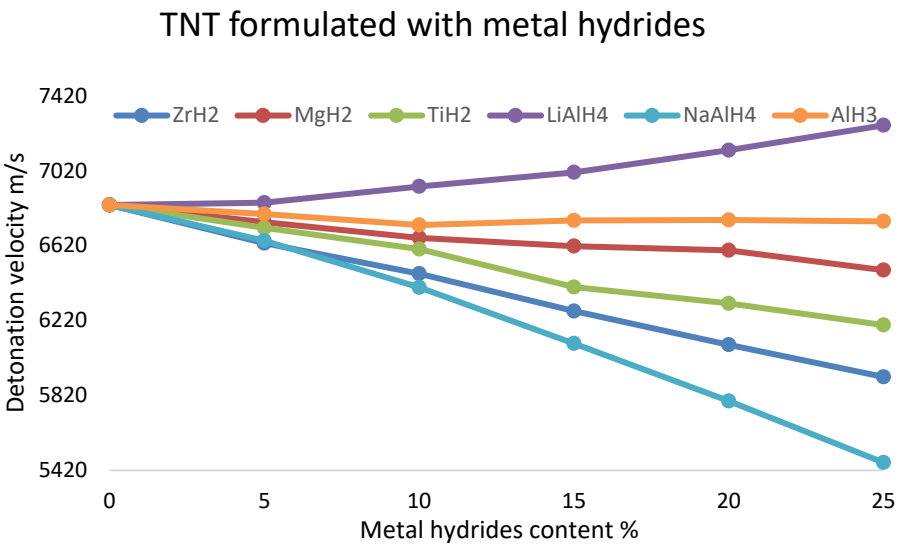

Fig. 9. Effect of metal hydrides quantities on detonation velocity of TNT formulations

Fig. 9 shows the formulations of the TNT with the metal hydrides, $LiAlH_4$ is the only one that shows an increase of detonation velocity with increasing % of $LiAlH_4$. All other metal hydrides decrease the performance of TNT.

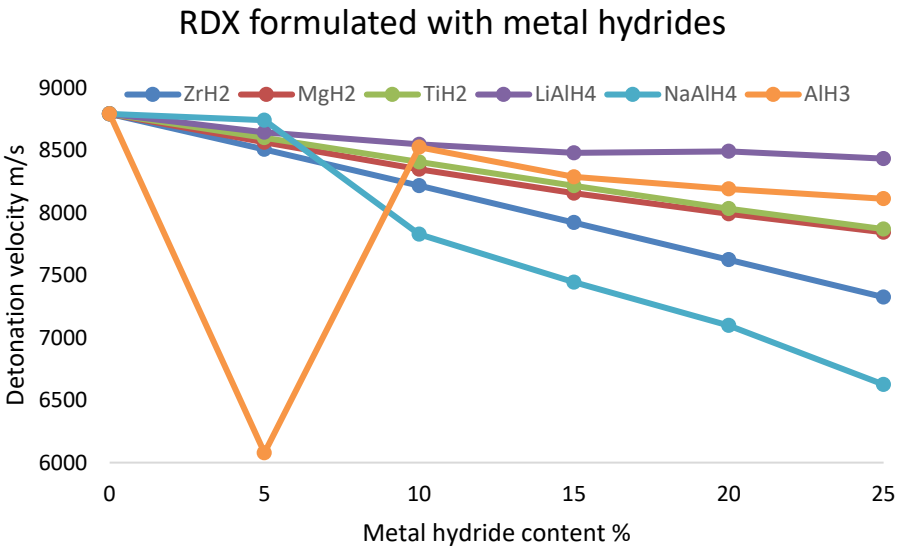

Fig. 10: Effect of metal hydrides quantities on detonation velocity of RDX formulations

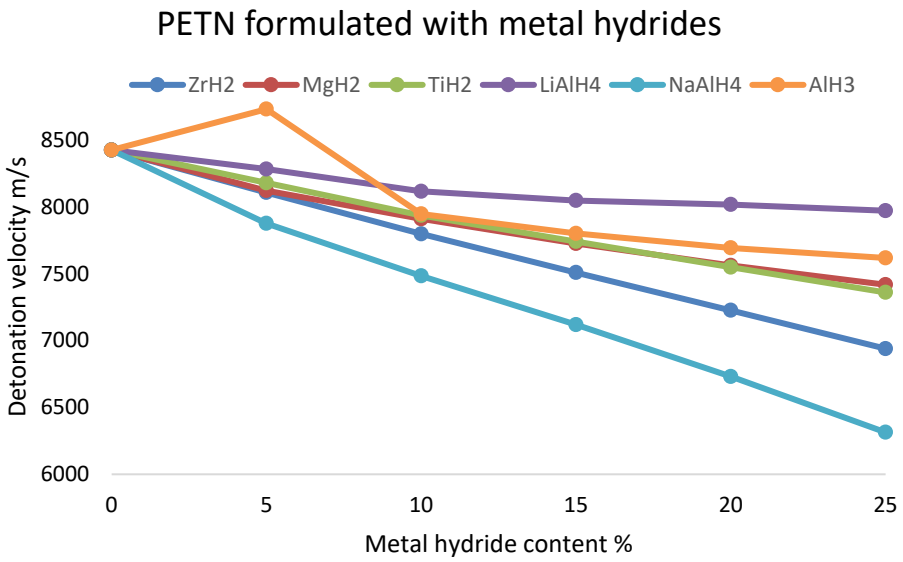

Fig. 11: Effect of metal hydrides quantities on detonation velocity of PETN formulations

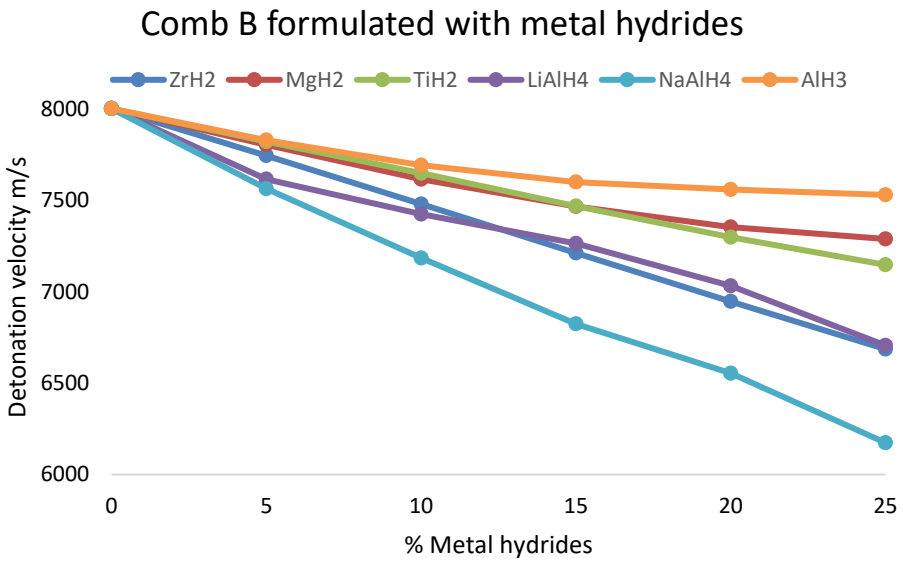

Fig. 12: Effect of metal hydrides quantities on detonation velocity of Comp B formulations

RDX formulations in **Fig. 10** show no enhancement for all the metal hydrides. AlH_3 containing formulation in **Fig. 11** shows an increased detonation velocity of 8700 m/s at 5% metal hydride with the rest of the other formulations showing no enhancement. Comp B consists of 60% RDX and 40% TNT, containing more RDX and that might be the reason that there is no observed enhancement.

Conclusion

The EXPLO5 simulations of the energetic materials containing metal hydride were done successfully. The densities of the formulations were observed to be affected by the addition of metal hydrides where the metal hydrides made from heavy metals increased the formulation densities and the lighter metal hydrides decreased the density. Despite the observed increase in density for some formulations, this did not translate into more increased detonation pressure except for the TNT formulation with ZrH_2. AlH_3 seems to be performing well for all the explosives, including PETN formulation. $LiAlH_4$ and $NaAlH_4$ are shown to be effective at a low percentage (5%) for some of the explosive materials. The metal hydride additives show no considerable effect on the detonation velocity only TNT formulation with $LiAlH_4$ and PETN formulation with AlH_3.

References

1. Pyrotechnics, P.E., Introduction to Explosives and Propellants.
2. Adams, G.F. and R.W. Shaw Jr, Chemical reactions in energetic materials. Annual Review of Physical Chemistry, 1992. 43(1): p. 311-340.
3. Flower, P., et al. Improving the efficiency of metallised explosives. in 2006 Insensitive Munitions and Energetic Materials Technology Symposium. 2006.
4. Cao, W., et al., Detonation characteristics of an aluminized explosive added with boron and magnesium hydride. Propellants, Explosives, Pyrotechnics, 2019. 44(11): p. 1393-1399.
5. Wu, X.-l., et al., Hazard evaluation of ignition sensitivity and explosion severity for three typical MH2 (M= Mg, Ti, Zr) of energetic materials. Defence Technology, 2020.
6. Yang, Y., et al., Hydrogen-enhanced combustion of a composite propellant with ZrH2 as the fuel. Combustion and Flame, 2018. 187: p. 67-76.
7. Rusman, N. and M. Dahari, A review on the current progress of metal hydrides material for solid-state hydrogen storage applications. International Journal of Hydrogen Energy, 2016. 41(28): p. 12108-12126.
8. Lototskyy, M.V., et al., The use of metal hydrides in fuel cell applications. Progress in Natural Science: Materials International, 2017. 27(1): p. 3-20.
9. Yang, Z., et al., Interaction Mechanism between Metal Hydrides and Energetic Compounds: an Extensive Literature Survey. FirePhysChem, 2021.
10. Pang, W., et al., Effect of metal nanopowders on the performance of solid rocket propellants: a review. Nanomaterials, 2021. 11(10): p. 2749.
11. Yang, Y., et al., Reinforced combustion of the ZrH2-HMX-CMDB propellant: The critical role of hydrogen. Chemical Engineering Journal, 2020. 402: p. 126275.
12. Cudziło, S., et al., Effect of Titanium and Zirconium Hydrides on the Detonation Heat of RDX-based Explosives–A Comparison to Aluminium. Propellants, Explosives, Pyrotechnics, 2018. 43(3): p. 280-285.
13. Sućeska, M., Evaluation of detonation energy from EXPLO5 computer code results. Propellants, Explosives, Pyrotechnics, 1999. 24(5): p. 280-285.
14. Štimac, B., et al. Prediction of Gurney velocity based on EXPLO5 code calculation results. in 23rd Seminar New Trends in Research of Energetic Materials. 2020.
15. Štimac, B., et al., Numerical modelling of detonation reaction zone of nitromethane by EXPLO5 code and Wood and Kirkwood theory. Central European Journal of Energetic Materials, 2020. 17(2).
16. Fischer, D., T.M. Klapötke, and J. Stierstorfer, 1, 5-Di (nitramino) Tetrazole: High Sensitivity and Superior Explosive Performance. Angewandte Chemie International Edition, 2015. 54(35): p. 10299-10302.
17. Sućeska, M. EXPLO5–Computer program for calculation of detonation parameters. in Proc. of 32nd Int. Annual Conference of ICT, Karlsruhe, Germany. 2001.
18. Mader, C.L., Detonation properties of condensed explosives computed using the Becker-Kistiakowsky-Wilson equation of state. Vol. 2900. 1963: Los Alamos Scientific Laboratory of the University of California.
19. Tenny, K.M. and J.S. Cooper, Ideal Gas Behavior. 2017.
20. Fried, L.E., W.M. Howard, and J. Zaug, The equation of state and chemistry of detonation products. Theoretical and Computational Chemistry, 2003. 13: p. 193-224.
21. Guillermet, A.F., Thermodynamic properties of the generalized Murnaghan equation of state of solids. International journal of thermophysics, 1995. 16(4): p. 1009-1026.
22. Koukkari, P., R. Pajarre, and K. Hack, Constrained Gibbs energy minimisation. International journal of materials research, 2007. 98(10): p. 926-934.

Characterisation of home-made explosives such as ANFO and NM against a military grade explosive, PE4, in open air environment

[1,2]Thanyani Pandelani, [1]Dithoto Modungwa and [1]David John Reinecke

[1]CSIR, D&S, Meiring Naude Road, Brummeria, Pretoria, 0001,

[2]Department of Mechanical Engineering, School of Engineering, College of Science Engineering and Technology, University of South Africa, Private Bag X6, Florida, 1710, South Africa.

Tpandelani@csir.co.za

Abstract

Detonating an explosive charge generates the propagation of a shock-wave, principally affecting gas-containing organs, such as lungs, middle ear and gastrointestinal tract. In a free-field environment, the pressure-time history resulting from a detonation has a well-known shape, called the Friedlander profile. The use of improvised explosive devices (IEDs) results in more complex waves, with multiple reflections that can interact simultaneously with the soldier, resulting in more severe injuries.

The influence of different explosives such plastic explosives (PE4), home-made explosives, such as nitromethane, ammonium nitrate (fertilizer), and fuel oil (ANFO) which been used in IEDs should be investigated to begin to assess the effectiveness of the performance of materials and personal protective equipment used in this environment. In order to develop equipment to protect soldiers during IED attacks, an important step is to understand the complex blast waves and to quantify the pressure level. In this study, the blast wave characteristic of two home-made explosives in a form of NM and ANFO are investigated and compared with the military grade PE4 explosive charge using the Blast Test Device (BTD).

Keywords— BTD, PE4, ANFO, NM, IEDs

Introduction

The detonation of an explosive charge generates the propagation of a shock-wave, principally affecting gas-containing organs, such as lungs, middle ear and gastrointestinal tract [1]. In a free-field environment, the pressure-time history resulting from a detonation has a well-known shape, called the Friedlander profile [2]. The use of improvised explosive devices (IEDs) results in more complex waves, with multiple reflections that can interact simultaneously with the soldier, resulting in more severe injuries.

The influence of different explosives such plastic explosives (PE4), home-made explosives, such as nitromethane, ammonium nitrate (fertilizer), and fuel oil (ANFO) which been used in IEDs should be investigated to begin to assess the effectiveness of the performance of materials and personal protective equipment used in this environment.

In order to develop equipment to protect soldiers during IED attacks, an important step is to understand the complex blast waves and to quantify the pressure level. In this study, the blast wave characteristic of two home-made explosives in a form of NM and ANFO are investigated and compared with the military grade PE4 explosive charge using the BTD.

Methods

The main test device used to assess the loading that would have faced a human thorax is the Blast Test Device (BTD), which is a cylinder with an outer diameter of 300 mm, a height of 762 mm and wall thickness of 20 mm. It is instrumented with pressure gauges every 90 degree interval at mid-height (Fig 1)

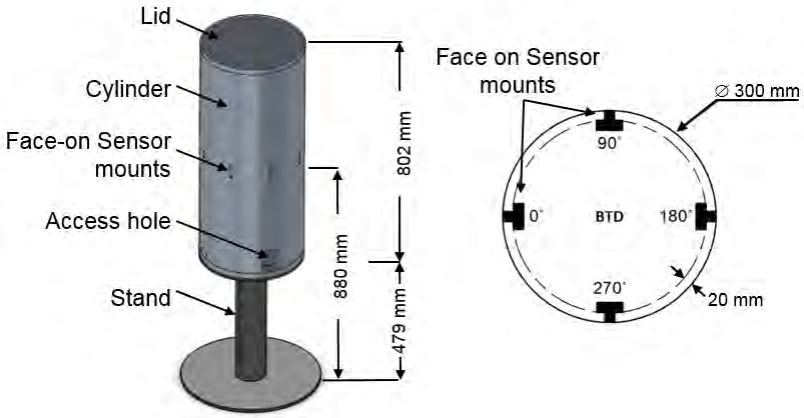

Fig. 1. BTD on a stand and pressure sensor orientation

The test scenario for the BTD considered in this study was the detonation of a spherical charge over a flat solid concrete surface. This configuration generates complex blast wave behaviour, depending on the mass and height of the charge, such as a reflection wave or Mach reflection [3]. The BTD and all other measurement sensors were located at a standoff distance (SOD) of 2 m from the charge (Fig 2). In the vertical direction, the charge was positioned at a height of burst (HoB), 220 mm, which is defined as the distance from the bottom of the charge to the ground. This HoB was selected to reproduce scenarios typically incurred on the battlefield.

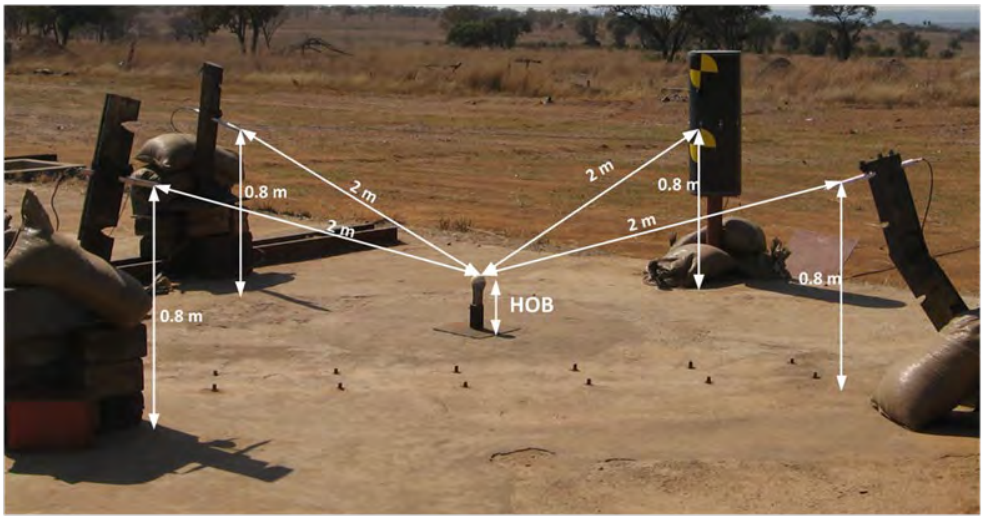

Fig. 2. Experimental setup. The sensors were mounted on custom pencil probe stands at a height of 880 mm. The sensors were angled towards the level of the charge. The BTD was located at the 270˚ position on the BTD stand

Two external high speed Photron SA4 black and white cameras were used to track the propagation of the shock wave. The footage was analysed to determine the triple point path. The recording rate was set to at least 20 000 frames per second for both cameras. Since the meteorological conditions affect the blast propagation, a Kestrel 5000 environment meter was used to measure the ambient conditions during testing.

Results

Fig 3 and Fig 4 show the mean of the reflected pressures and impulses measured on the BTD for all three explosive materials tested, namely PE4, NM and ANFO. PE4 has the highest peak pressure at 345.3 kPa followed by nitromethane at 294.0 kPa and lastly ANFO with a pressure of 124.8 kPa.

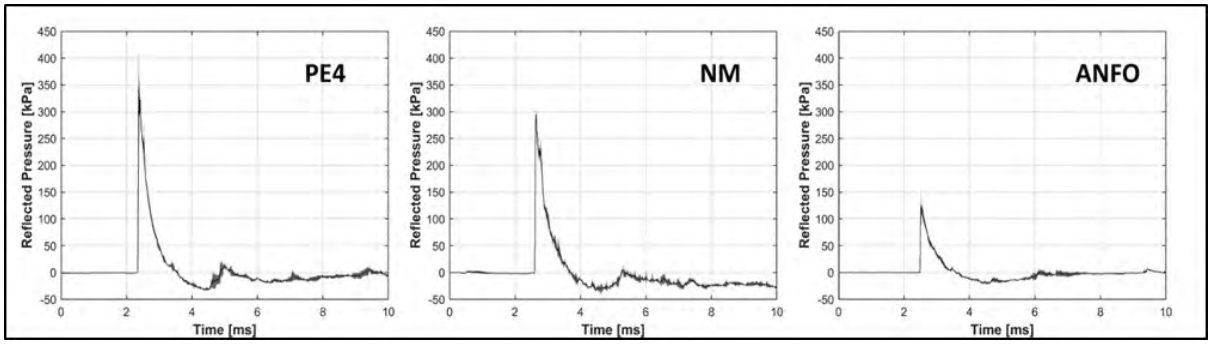

Fig. 3 Reflected pressure profiles for the PE4, NM and ANFO (the average values and standard deviations are plotted).

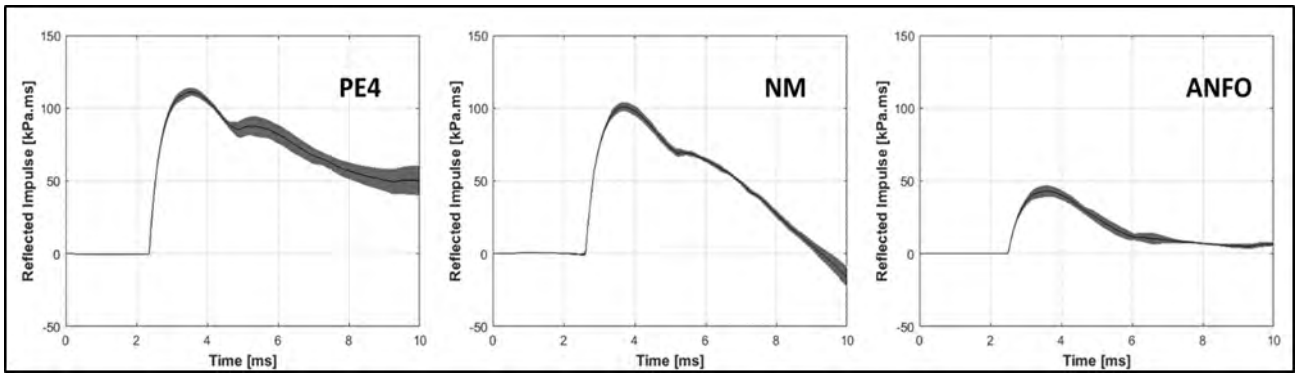

Fig. 4. Reflected impulse profiles for the PE4, NM and ANFO (the average values and standard deviations are plotted)

The PE4 and ANFO have the similar rise time to reach the peak of 24.1 µs, whilst NM reaches the peak after 33.9 µs. The positive phase duration in Table I is the difference in time between the first time the signals goes above zero and the first time that the signal reaches zero again (that is before it becomes negative). PE4 has the longest positive phase duration of 1 237.0 µs, followed by NM at 1 117.6 µs and lastly ANFO has the shortest positive phase duration of 1 107.3 µs. ANFO falls quicker to ambient due to it being a weak explosive that loses wave strength faster.

TABLE I. **BLAST CHARACTERISTICS OF THE THREE DIFFERENT EXPLOSIVES**

Description	PE4	NM	ANFO
Reflected pressure [kPa]	345.3	294.0	124.8
Impulse [kPa.ms]	111.3	101.0	43.1
Time to peak [µs]	24.1	33.9	24.1
Positive phase durations [µs]	1 237.0	1 117.6	1 107.3

Conclusion

As expected, PE4 demonstrate higher peak reflected pressure and impulse compared to the NM and ANFO explosives at the same NEC. This suggests that PE4 is the more energetic explosive and ANFO is the least energetic of the three explosives tested. For the two home-made explosives NM is found to have a higher output than ANFO at the same standoff. PE4 and ANFO have the shortest peak rise time compared to the NM. PE4 has the longest positive phase duration, followed by NM and then ANFO

References

[1] Mayorga, Maria A. "The pathology of primary blast overpressure injury." Toxicology 121.1 (1997): 17-28.

[2] Boutillier J, Mezzo, S.D., Deck C, Ehrhardt, L., Magnan P, Naz P, Willinger R. (2016). New experimental data on blast interaction with instrumented structures, MABS 24.

[3] Ehrhardt, L., J. Boutillier, P. Magnan, C. Deck, S. De Mezzo, R. Willinger, and S. Cheinet. "Evaluation of overpressure prediction models for air blast above the triple point." Journal of Hazardous Materials 311 (2016): 176-185.

Theoretical investigation and experimental validation of 3D printed solid fuels for rocket motors

Tselane Risuna Gail Ndlovu[1 *], Devlin Govender[1], Lafras Fritz[1]

[1]*Flamengro, A Division of Armscor SOC Ltd., Pretoria, South Africa*

gail@flamengro.co.za

Abstract

Hybrid rocket motors suffer from poor regressing rates due to the boundary layer combustion mechanism. Research to overcome this issue is in progress where moulding the port geometry of a widely used solid fuel, Hydroxyl-terminated polybutadiene (HTPB), is being investigated. HTPB is not one of the easily printable plastics therefore in this study Acrylonitrile Butadiene Styrene (ABS) was investigated instead as it has similar thermal properties. This study aims to investigate ABS as an alternative rocket motor solid fuel, and to modify its chemical composition by infusing metal powder in the polymer structure. The hypothesis drawn is that the combustion performance can be improved by increasing the burn surface area as well as chemically modifying the fuel to make it more energetic. The mixing efficiency of the polymer and the metal powder was analysed using Scanning Electron Microscopy (SEM). Theoretical investigation of the combustion performance of the fabricated fuels was done using NASA Chemical Equilibrium with Applications (CEA) and Thermogravimetric analysis (TGA). The aim of these methods is to find the activation energy, adiabatic flame temperature, and specific impulse which was compared to values reported in the literature for HTPB.

Keywords— 3D Printing, ABS, HTPB, CEA, TGA, SABO

Introduction

Hybrid rocket systems have a reputation for being highly manufacturable, and inexpensive compared to other rocket systems [1]. This is because hybrid rocket systems possess the advantages of both liquid propellants as well as solid propellants [2]. Due to the distinct physical states of the fuel and oxidiser, hybrid rockets are relatively safe and are less expensive to fabricate [3]. It is because of these advantages that hybrid rockets are the obvious choice for suborbital flight missions [4]. The large-scale application of hybrid rockets is inhibited because of the low regression rates due to the boundary layer combustion mechanism [5]. Research to overcome this issue has been reported in literature where the commonly used solid fuel, hydroxyl-terminated polybutadiene (HTPB), was fabricated into sophisticated port geometries to increase the surface area of contact with the gaseous oxidiser [6]. However, research to attain further enhancement in combustion properties is ongoing.

Additive manufacturing, commonly known as three-dimensional (3D) printing is a radical evolving technology and is now becoming more accessible [7]. The most commonly used 3D printing method is fused filament fabrication (FFF) in which a thermoplastic filament is melted and extruded through a nozzle. These layers are fused layer by layer onto a heated bed and solidified into the desired end product [8]. Polymers which can be used for FFF 3D printing are considered printable if their thermoplastic properties,

such as the melt viscosity, are adequate to allow extrusion, solidifies fast enough and ultimately provide structural support [9], [10]. It is for this reason that hybrid 3D printing filaments have not yet gained much popularity in that they compromise the printability of the polymer for the intended extra property (such as strength). A common problem when fabricating hybrid filaments is that the additives tend to agglomerate resulting in poor mixing of the fillers and the polymer [7].

Substance mixing is an important aspect of the manufacturing of propellants and explosives. This is because the burning characteristics of the explosive matter need to be uniform (i.e. controlled and repeatable) so that necessary safety measures can be implemented to avoid accidents resulting from unexpected burning patterns of the explosive matter [11]. In chemistry, a substance is a form of matter that has a constant chemical composition and characteristic properties and is composed of one type of atom or molecule. A mixture then becomes something that consists of diverse, non-bonded elements or molecules [12].

A mixture is a material system made up of two or more different substances, which are physically mixed but not chemically bonded/combined [13]. The identities of the individual components of a mixture are retained and separation is often possible. Mixtures take the form of alloys, solutions, suspensions, and colloids. Mixtures can either be heterogeneous or homogenous and the difference is tabulated in TABLE I.

TABLE I. COMPARISON OF HETEROGENEOUS AND HOMOGENEOUS [12]–[14].

Heterogeneous Mixtures	Homogenous Mixtures
A mixture of two or more chemical substances (elements or compounds), where the different components can be visually distinguished.	A mixture of two or more chemical substances (elements or compounds), where the different components cannot be visually distinguished.
Heterogeneous mixtures can easily be separated by physical means.	Separation of a homogeneous mixture is more challenging than separating the components of a heterogeneous mixture.
Examples: mixtures of sand and water, a salad, water, and oil, etc.	Examples: polymers/plastics, tap water, air, etc.

Hydroxyl-terminated polybutadiene (HTPB) is a common thermoplastic that is used as a solid fuel in hybrid rockets. Current port geometries of HTPB propellants are limited to what moulds can be provided [15], and since the propellant performance (regression rate) depends highly on the burn surface area and the chemical composition, there exists a need to modify these parameters [16]. 3D printing (filament fabrication ad FFF) is a tool that potentially allows for such flexibilities and was explored in further detail in this research. One of the drawbacks of HTPB is that it is controlled by the International Traffic in Arms Regulations (ITAR) Part 121, and is not easily accessible in South Africa [17]. In this study, Acrylonitrile butadiene styrene (ABS), a 3D printing thermoplastic, was used as the solid fuel in place of the HTPB with the hope of overcoming the low regression rates of HTBP as reported in literature [18], [19]. The use of ABS as a potential hybrid rocket motor offers the additional benefit of being able to 3D print in complex shapes, thus increasing burn surface area, which in turn will result in an improved rate. Whitmore et al. [19] compared the performance and consistency of ABS fuel grains against equal-size HTPB fuel grains and found that the ABS fuel grains offered a more consistent burn-to-burn consistency with reduced overall performance. Furthermore, increasing the fraction of butadiene in the ABS chemical composition was found to improve the performance of the ABS fuel grains, which demonstrates the potential of ABS as a hybrid rocket fuel grain material [20], [21]

Methods

The theoretical combustion performance of the polymer-metal mix was investigated using NASA CEA (Chemical Equilibrium with Applications) at metal powder content ratios of 0 % (sample group A), 2.5 % (sample group B), 5.0 % (sample group C), 7.5 % (sample group D), and 10 % (sample group

E). The analysis was performed at 10 bar and at a oxygen to fuel ratio of 4 using nitrous oxide as the oxidiser. TABLE II. shows descriptions of what each of the samples labelled A – E contained.

TABLE II. SAMPLE IDENTIFICATION USED IN THIS STUDY

Sample ID	Description
A	100 % ABS
B	97.5 % ABS and 2.5 % Metal Powder
C	95 % ABS and 5 % Metal Powder
D	92.5 % ABS and 7.5 % Metal Powder
E	90 % ABS and 10 % Metal Powder

The polymer powder was mixed in a blender to achieve sample groups A – E as stated above. Thereafter, a random powder sample was taken (after the mixing process was concluded at approximately 5 minutes) to analyse the mixing efficiency of the polymer powder and the metal powder was analysed using Scanning Electron Microscope (SEM).

The decomposition reaction kinetics focuses on the reaction activation energy and was defined from the variable heating rate on the TGA (Thermogravimetric Analyser) data applying Kissinger equation Equation (1).

$$\ln\left(\frac{\phi}{T_m^2}\right) = \ln\left(\frac{AR}{E_a}\right) - \frac{E_a}{RT_m} \quad (1)$$

Where ϕ represents the heating rate, T_m is the maximum temperature for the heat flow, A is the frequency factor, E_a is the activation energy, and R is the gas constant. Each sample defined in TABLE II. was analysed in the TGA with variable heating rates (5 K/min, 10 K/min, 15 K/min, 20 K/min,) and their peak temperatures were noted. The slope of the curve obtained from plotting $\ln\left(\frac{\phi}{T_m^2}\right)$ vs $\frac{1}{T_m}$ was used to calculate the activation energy using the method below, derived from Equation (1).

$$\text{Slope of the curve} = \frac{E_a}{R} \quad (2)$$

Rearranging this, making the activation energy the subject of the formula results in the expression of the activation energy.

$$E_a = (R)(\text{Slope of the curve})$$
$$E_a = (8.314\frac{J}{\text{mol. K}})(\text{Slope of the curve}) \quad (3)$$

Substituting the slope of the curve results in the value of the activation energy, E_a (J/mol. K).

Results

The design of the system began by theoretically simulating the performance of the solid fuel fabricated in this study. Fig. 1 shows results obtained from analyzing different mix ratios of the ABS and the metal

powder. Both the adiabatic temperature and the specific impulse increase as the amount of metal powder is increased. This suggests that adding more metal powder makes the fuel more energetic. However, when 3D printing is concerned there needs to be a balance between adding more additives and keeping the fuel printable (e.g. not too brittle, easy flowing, fast response to thermal changes, etc). In this study, 10 % metal powder content became the maximum additive added. The adiabatic flame temperatures obtained in this study range between 3042 -3307 K for 0 – 10 % metal powder content. These are slightly higher than that of HTPB, 2835 K, obtained under the same conditions. The specific impulse values obtained in this study range between 1072 – 1085. These values are similar to HTPB, 1080, obtained under the same conditions.

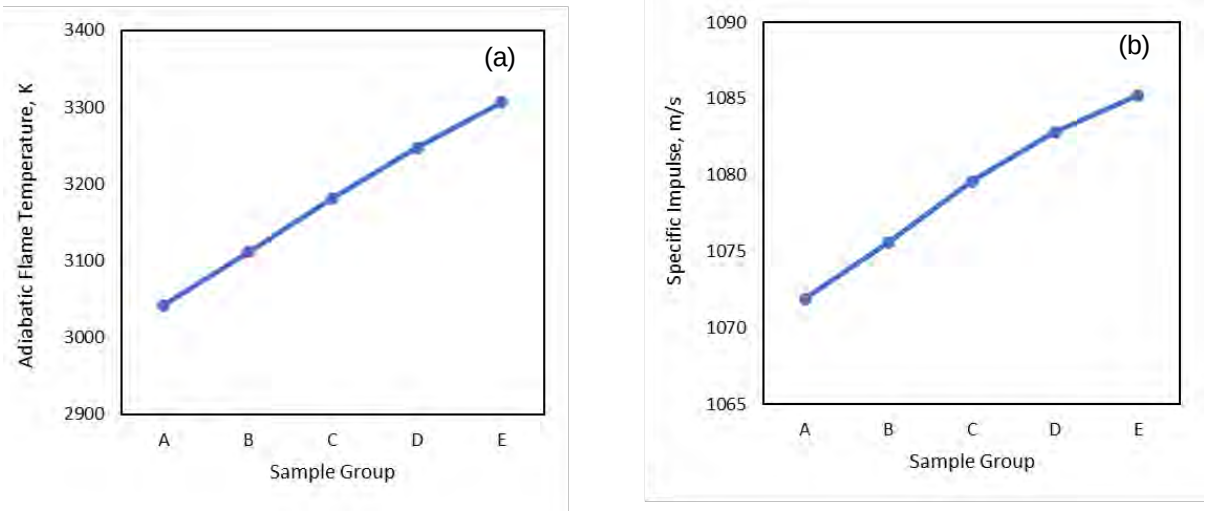

Fig. 1. NASA CEA combustion performance. (a) adiabatic flame temperature (b) Specific impulse

The morphology of the powder mix before extruding the 3D printing filament was analysed to assess the distribution of the metal powder on the polymer matrix was analysed using SEM and the results are shown in Fig. 2. An even distribution of the metal powder was observed in Fig. 2 (a) and (b). Both Fig. 2 (c) and (d) showed that some of the metal powder was lumped together. In addition to lumping, Fig. 2 (c) also showed that the metal powder began to oxidise. This may be because the sample was exposed to air relatively more than the other samples (this may have been internal during sample preparation or external during the SEM analysis).

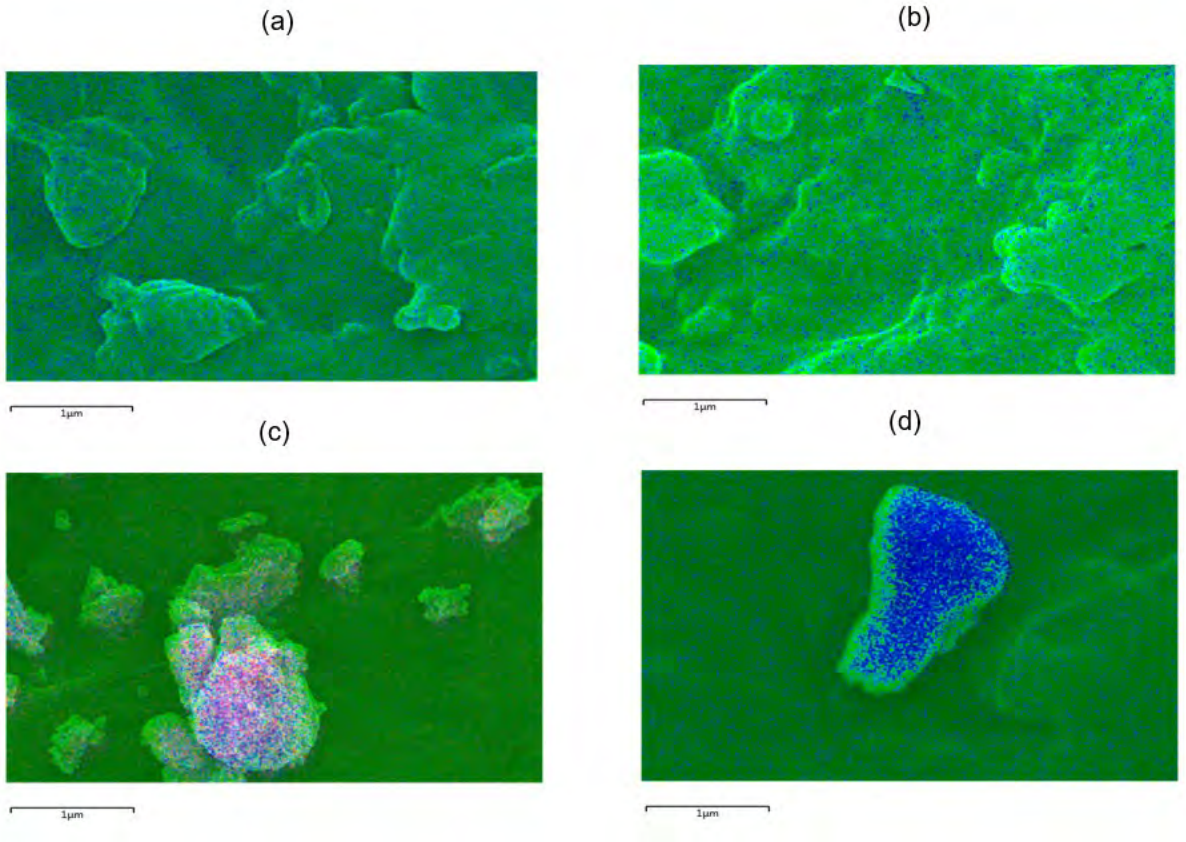

Fig. 2. SEM for the samples with varied metal powder content (a) 2.5 % (b) 5.0 % (c) 7.5 % (d) 10 %

The results obtained from analysing the samples on a TGA at varied heating rates were processed using the Kissinger equation to obtain the activation energies for each of the sample groups. Generally, the values obtained show that as the metal powder content is increased, the activation energy also increases. Fig. 3 (a) shows results for pure ABS, and its activation energy was 234 kJ/mol which is higher than what literature reports for ABS in the range of 134 – 190 kJ/mol [22]. This study aimed to chemically modify pure ABS by making it more reactive to compare with HTPB which has an activation energy of 69 – 141 kJ/mol [23]. This study was able to achieve an activation energy of 186 kJ/mol for ABS with 10 % metal powder content.

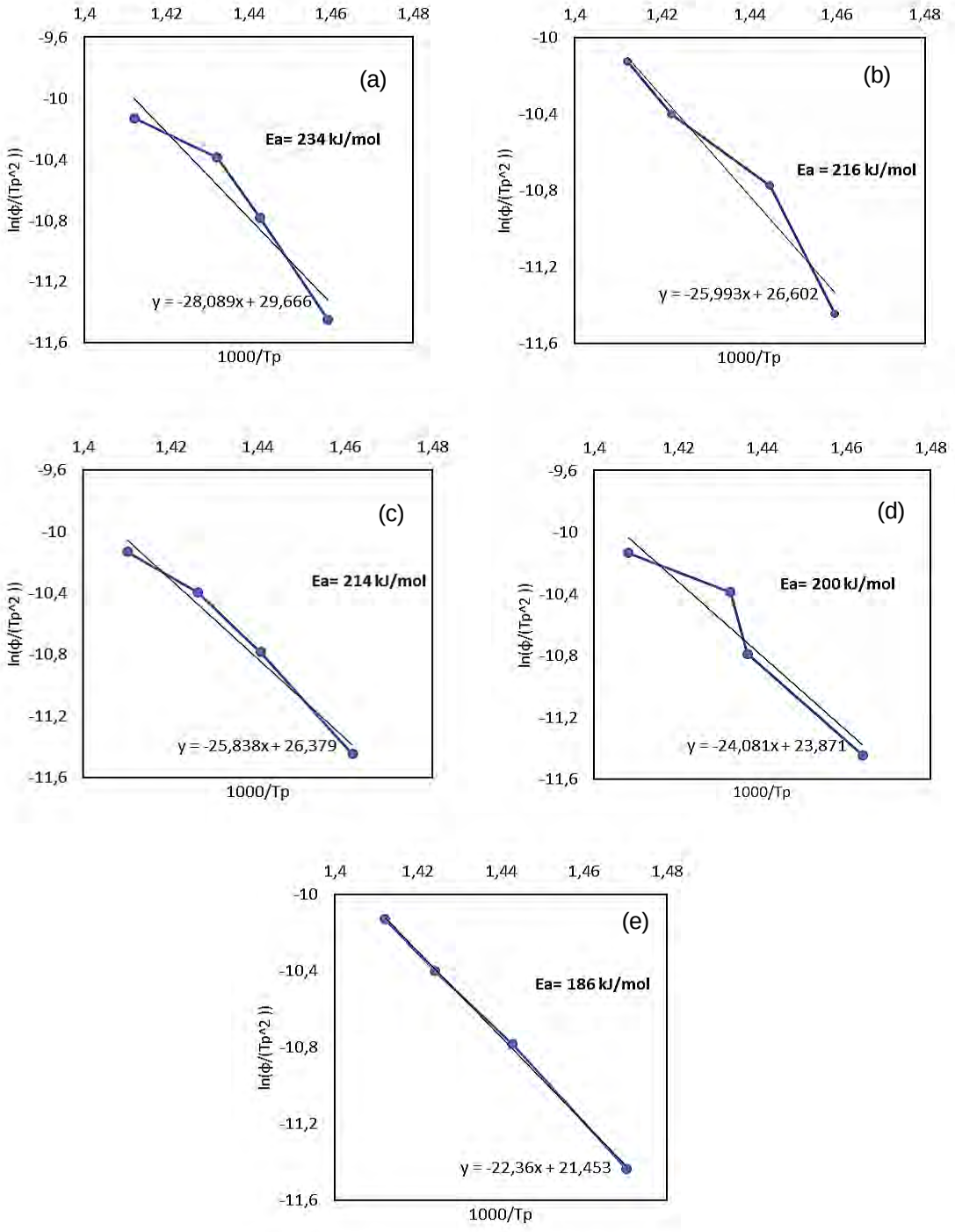

Fig. 3. Activation energy for the samples with varied metal powder content. (a) 0 % (b) 2.5 % (c) 5.0 % (d) 7.5 % (e) 10 %

TABLE III. shows a summary comparison of the thermal/ combustion performance of the metallised ABS fuel fabricated in this study, and that of HTPB. The values obtained in this study are reasonably comparable with those of HTPB and show great potential for the fuel fabricated in this study to act as an alternative fuel for hybrid rocket motors. The amount of the metal powder added was capped at 10 % in this study because

of printability considerations. The study to add more additives that will make the ABS more reactive while retaining its printability is ongoing.

TABLE III. COMPARISON OF THERMAL/COMBUSTION PERFORMANCE OF HTPB AND METALLISED ABS

Sample	Activation Energy, kJ/mol	Specific impulse, m/s	Adiabatic flame temperature, K
HTPB	69 – 141 [23]	1080	2835
Pure ABS	234	1072	3042
ABS + 2.5 % metal powder	216	1076	3111
ABS + 5.0 % metal powder	214	1080	3182
ABS + 7.5 % metal powder	200	1083	3247
ABS + 10 % metal powder	186	1085	3307

Conclusion and Recommendations

This study has shown great potential for the aim intended, and we have learned and discovered a lot in the process. ABS has shown characteristics desirable for use as an alternative fuel for rocket motors (in place of HTPB). More studies are in progress to find more reactive additives which can be infused with the ABS polymer while ensuring that the ABS can still be printed. The metal powder must be handled and stored carefully at all times to avoid oxidation. A study to extend the amount of metal powder used in this study beyond 10 % is in progress, to find out what the printable maximum metal content is.

References

[1] M. King, 'Analysis for Hybrid Rocket Fuel Regression Using Stereolithographic Geometry', *Theses Diss.*, Dec. 2020, [Online]. Available: https://scholar.afit.edu/etd/4542

[2] G. Risha, E. Boyer, R. Wehrman, and K. Kuo, 'Performance Comparison of HTPB-Based Solid Fuels Containing Nano-Sized Energetic Powder in a Cylindrical Hybrid Rocket Motor', in *38th AIAA/ASME/SAE/ASEE Joint Propulsion Conference & Exhibit*, American Institute of Aeronautics and Astronautics, 2012. doi: 10.2514/6.2002-3576.

[3] K. K. Kuo and M. J. Chiaverini, *Fundamentals of Hybrid Rocket Combustion and Propulsion*. Reston ,VA: American Institute of Aeronautics and Astronautics, 2007. doi: 10.2514/4.866876.

[4] A. Mazzetti, L. Merotto, and G. Pinarello, 'Paraffin-based hybrid rocket engines applications: A review and a market perspective', *Acta Astronaut.*, vol. 126, pp. 286–297, Sep. 2016, doi: 10.1016/j.actaastro.2016.04.036.

[5] M. Calabro, 'Overview on hybrid propulsion', in *Progress in Propulsion Physics*, 2011, vol. 2, pp. 353–374. doi: 10.1051/eucass/201102353.

[6] S. Chen *et al.*, 'Combustion enhancement of hydroxyl-terminated polybutadiene by doping multiwall carbon nanotubes', *Carbon*, vol. 144, pp. 472–480, Apr. 2019, doi: 10.1016/j.carbon.2018.12.063.

[7] C. Aumnate, A. Pongwisuthiruchte, P. Pattananuwat, and P. Potiyaraj, 'Fabrication of ABS/Graphene Oxide Composite Filament for Fused Filament Fabrication (FFF) 3D Printing', *Adv. Mater. Sci. Eng.*, vol. 2018, p. e2830437, Nov. 2018, doi: 10.1155/2018/2830437.

[8] S. Singh, S. Ramakrishna, and F. Berto, '3D Printing of polymer composites: A short review', *Mater. Des. Process. Commun.*, vol. 2, no. 2, p. e97, 2020, doi: 10.1002/mdp2.97.

[9] X. Wang, M. Jiang, Z. Zhou, J. Gou, and D. Hui, '3D printing of polymer matrix composites: A review and prospective', *Compos. Part B Eng.*, vol. 110, pp. 442–458, Feb. 2017, doi: 10.1016/j.compositesb.2016.11.034.

[10] J. Zhang, B. Yang, F. Fu, F. You, X. Dong, and M. Dai, 'Resistivity and Its Anisotropy Characterization of 3D-Printed Acrylonitrile Butadiene Styrene Copolymer (ABS)/Carbon Black (CB) Composites', *Appl. Sci.*, vol. 7, p. 20, Jan. 2017, doi: 10.3390/app7010020.

[11] 'Handbook on the Management of Ordnance and Explosives at Closed, Transferring, and Transferred Ranges and Other Sites (Interim Final)', p. 222.

[12] 'Substances and Mixtures | Introduction to Chemistry'. https://courses.lumenlearning.com/introchem/chapter/substances-and-mixtures/ (accessed Dec. 15, 2021).

[13] '7.1 Mixtures | Separating mixtures | Siyavula'. https://intl.siyavula.com/read/science/grade-7/separating-mixtures/07-separating-mixtures (accessed Jan. 05, 2022).

[14] 'Homogeneous vs Heterogeneous Mixtures - Difference and Comparison | Diffen'. https://www.diffen.com/difference/Heterogeneous_vs_Homogeneous (accessed Jan. 05, 2022).
[15] S. Chen *et al.*, 'Innovative Methods to Enhance the Combustion Properties of Solid Fuels for Hybrid Rocket Propulsion', *Aerospace*, vol. 6, no. 4, Art. no. 4, Apr. 2019, doi: 10.3390/aerospace6040047.
[16] M. McClain, I. Gunduz, and S. Son, 'Additive manufacturing of ammonium perchlorate composite propellant with high solids loadings', *Proc. Combust. Inst.*, vol. 37, Jun. 2018, doi: 10.1016/j.proci.2018.05.052.
[17] U. S. O. of the F. Register and N. Archives (U.S.), *Federal Register*, no. v. 79, 1. Office of the Federal Register, National Archives and Records Service, General Services Administration, 2014. [Online]. Available: https://books.google.co.za/books?id=MRH8h9_o6j8C
[18] D. Pastrone, 'Approaches to Low Fuel Regression Rate in Hybrid Rocket Engines', *Int. J. Aerosp. Eng.*, vol. 2012, pp. 1–12, 2012, doi: 10.1155/2012/649753.
[19] S. A. Whitmore and S. D. Walker, 'Engineering model for hybrid fuel regression rate amplification using helical ports', *J. Propuls. Power*, vol. 33, no. 2, pp. 398–407, 2017, doi: 10.2514/1.B36208.
[20] Z. Wang, X. Lin, F. Li, and X. Yu, 'Combustion performance of a novel hybrid rocket fuel grain with a nested helical structure', *Aerosp. Sci. Technol.*, vol. 97, p. 105613, Feb. 2020, doi: 10.1016/j.ast.2019.105613.
[21] S. A. Whitmore, Z. W. Peterson, and S. D. Eilers, 'Comparing Hydroxyl Terminated Polybutadiene and Acrylonitrile Butadiene Styrene as Hybrid Rocket Fuels', *J. Propuls. Power*, vol. 29, no. 3, pp. 582–592, May 2013, doi: 10.2514/1.B34382.
[22] R. Balart, D. Garcia-Sanoguera, L. Quiles-Carrillo, N. Montanes, and S. Torres-Giner, 'Kinetic Analysis of the Thermal Degradation of Recycled Acrylonitrile-Butadiene-Styrene by non-Isothermal Thermogravimetry', *Polymers*, vol. 11, no. 2, p. 281, Feb. 2019, doi: 10.3390/polym11020281.
[23] L. Zhang and X. Zheng, 'Experimental study on thermal decomposition kinetics of natural ageing AP/HTPB base bleed composite propellant', *Def. Technol.*, vol. 14, no. 5, pp. 422–425, Oct. 2018, doi: 10.1016/j.dt.2018.04.007.

Aging of Booster Relay Detonator and Assessment according to AOP46

C.J.H. Oosthuizen[1]

Rheinmetall-Denel Munition, Boskop, Potchefstroom, North West, South Africa, 2531

manus.oosthuizen@rheinmetall-denelmunition.com

Abstract

The remaining shelf life of naturally aged Booster Relay Detonators were investigated by thermal aging and functioning. The remaining shelf life was determined by using the methodology as specified in AOP46. The results indicated that the Detonators had a remaining shelf life of at least 30 years.

Keywords—Relay detonators, shelf life, aging, AOP46, RDX.

Introduction

Shelf life of munitions are a major factor in the product life cycle of weapon systems as the replacement of life expired munitions contributes to the product life cycle cost of the weapon system as well as the cost of the demilitarisation of the expired munitions. The energetic materials is an important part in the design of ammunition as it normally determines the safety and functionality of the ammunition over time. The shelf life of detonics in ammunition is the major contributor as it is usually the most sensitive energetic materials used in ammunition. The detonic train is also responsible for the safe and reliable functioning of the ammunition.

During the design of munitions a wide range of materials are which includes plastics, rubbers, adhesives, explosives and various types of metals. It is therefore crucial that no chemical or physical interaction takes place between these different materials.

Typical degradation mechanisms include:

1) Thermal (Chemical) reactions causing slow decomposition of such materials of which the reaction rate is increased by elevated temperatures and humidity.
2) Mechanical mechanisms which include fatigue and applied stresses causing cracks.
3) Thermomechanical mechanisms which involves mechanical stresses induced by thermal effects resulting in mechanical failures.

A request to determine whether the shelf life of Booster Relay Detonators, filled with two increments of RDX, which was manufactured in 1988 and stored in a magazine since manufacturing could be extended and for how long. The proposed methodology was to evaluate the detonators against the product acceptance specification to determine a baseline of functionality of the detonators and then to age the detonators by a thermal process at 60°C for seven days. AOP46 was used to determine the shelf life evaluated by the seven day aging [1]. The functionality of the detonators will then be evaluated again after the aging.

AOP46 is an Allied Ordnance Publication promulgated in July 2006, with the title: The Scientific Basis for the Whole Life Assessment of Munitions. AOP46 is not a well-known NATO document. The purpose of

AOP46 is to “describe munition life limiting factors and their scientific basis and describe the methodology used for conducting whole life assessments of munitions” [1].
The definition of shelf life can be defined as presented graphically in Fig. 1.

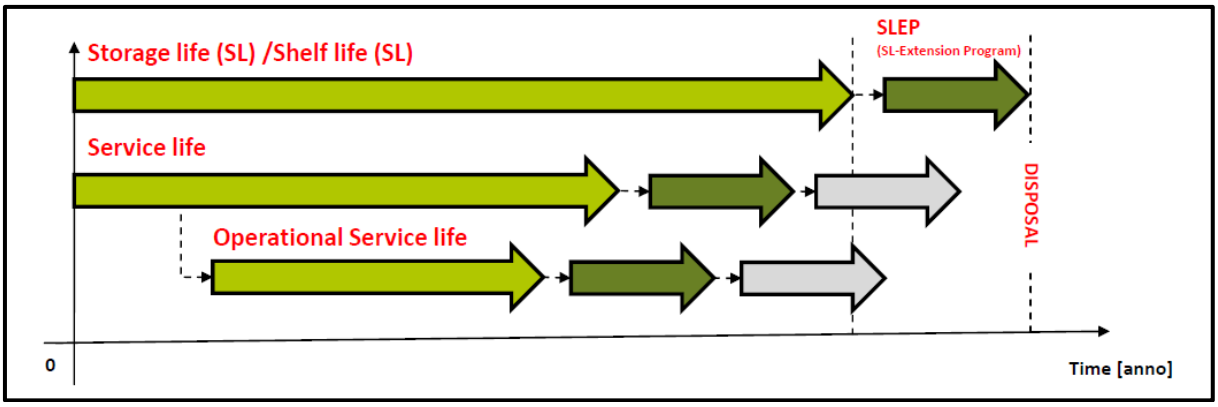

Fig. 1. Graphical Definition of Shelf Life [2].

As presented in Fig. 1 the definition of shelf life includes the service and operational life of a munition. The service life of a munition is defined as the time during which a munition, in specified storage conditions and when used in its specified operational and/or training condition, may be expected to remain safe and suitable for service. The operational life time is defined as the time during which a munition may be expected to remain safe and suitable for service when used under service or training conditions, when these are different from its storage conditions, but which is within the envelope of its life cycle [2].
The service and operational life is verified as defined by STANAG 4224 [3], STANAG 4225 [4] or the new AAS3P-23 [5]. This verification does however not evaluate the full shelf or storage life of the munition.

Methods

The shelf life evaluation of the Booster Relay Detonators was based on the chemical deterioration of the RDX filling in the detonators. The acceleration failure mode of AOP46 which was used for the evaluation was the Thermal (chemical) failure mode. For this method AOP46 uses chemical reactions which is temperature dependant and the reactions are defined by activation energy changes. A slightly modified Arrhenius rate equation indicates the relationship between the reaction rates at different temperatures as defined in Fig. 2.
Studies performed on the decomposition of RDX and RDX in a binder complex indicated activation energies in the order of 205 kJ/mole for RDX only and activation energies in the order of 153 kJ/mole for RDX in a binder complex [6].

$$F = \frac{k_1}{k_2} = e^{\left(-\frac{E}{R}\left\{\frac{1}{T_1} - \frac{1}{T_2}\right\}\right)}$$

where	F	=	Acceleration reaction factor
	k_1, k_2	=	Reaction rates at temperatures T_1 and T_2 separately
	T_1	=	Test temperature (K)
	T_2	=	Reference temperature (K)
	E	=	Activation energy (J mol^{-1})
	R	=	Universal gas constant (8.314 $mol^{-1} K^{-1}$)

Fig. 2. Modified Arrhenius Equation as used in AOP46 [1].

The average storage temperature, T2, was taken as 20°C and test temperature, T1, was taken as 60°C. The Activation Energy was taken as 150 kJ $mole^{-1}$, which is at the lower end of activation energies for secondary explosives. A value of 150 kJ/mole was chosen as the detonators were already more than 30 years old. The test duration at temperature, T1, was 7 days. The shelf life of the Booster Relay Detonator, tested at 60°C for 7 days, was calculated to represent 31 years at an average storage temperature of 20°C (1 week x (F)1619 = 1619/52 weeks = 31 years)

The shelf life guaranteed on ammunition is usually 10 years after manufacturing but it was decided to have a built-in safety factor of at least 3 as the detonators were already 34 years old. Two hundred Booster Relay Detonators were subjected to an aging test by conditioning at a constant temperature of 60°C for 7 days.

The shelf life investigation consisted of three parts namely;

1) Testing of the Booster Relay Detonators in the current naturally aged condition to establish a base line by using the acceptance test specification test conditions.
2) Artificial aging of the Booster Relay.
3) Testing of the artificially aged Booster Relay Detonators again according to the acceptance test specification conditions.

One hundred of the naturally aged Booster Relay Detonators were subjected to the different environmental tests according to the acceptance test specification e.g. transport vibration, jolt, a 9 meter drop test and a temperature cycling at -54°C to 70°C for 3 cycles of 24 hours.

After the detonators were subjected to the different tests, the detonators were fitted into an SK test set-up, see Fig 3, to test the power output of the detonators. The Primer Detonator was initiated by dropping a ball on the striker.

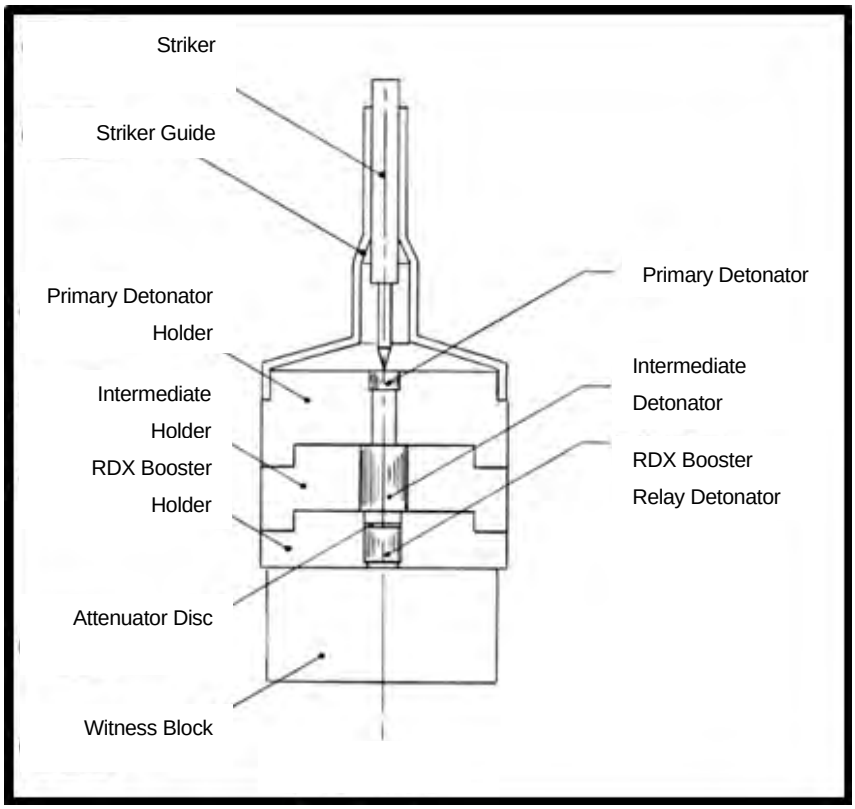

Fig. 3. RDX Booster Relay Detonator Power Output Test Set-up.

The Primer Detonator initiated an Intermediate Detonator which then initiated the Booster Relay Detonator. The detonation wave output of the Booster Relay detonators impact a steel witness block, indenting the steel witness block (see Fig 4). The indentation was measured and this indentation is used as an indication of the power output of the detonator.

Fig. 4. Typical indentation of a Booster Relay on a witness block.

The indentation specification, as specified in the acceptance specification, for an acceptable indentation value is > 0,30 mm for a single value and > 0,35 mm for a group average indentation value.

Results

The indentation results for the naturally aged Detonators are presented in Table I.

TABLE I. POWER OUTPUT INDENTATION DATA FOR THE DETONATORS NATURALLY AGED.

Serial	Functioning (mm)	Vibration (mm)	Jolt (mm)	Temperature Cycle (mm)	Drop Test 9 meter (mm)
Average	0.39	0.39	0.39	0.39	0.38
Standard Deviation	0.027	0.033	0.027	0.044	0.043

The test results indicated that the functioning of the detonators are still conforming to specification after 34 years of natural aging during storage.
The artificially aged Booster Relay Detonators, at 60°C, were also tested for functioning and power output as discussed above. The test results are presented in Table II.

TABLE II. POWER OUTPUT INDENTATION DATA FOR THE BOOSTER RELAY ARTIFICIALLY AGED.

Serial	Functioning (mm)	Vibration (mm)	Jolt (mm)	Temperature Cycling (mm)	Rest Functioning (mm)	Drop Test 9m (mm)
Average	0.37	0.37	0.38	0.38	0.38	0.38
Standard Deviation	0.033	0.039	0.066	0.058	0.034	0.034

The test results as presented in Table 2 still conforms to the specification although one Booster Relay Detonator did not register an indentation to specification. The indentation was only 0,06 mm instead of the 0,3 mm minimum.

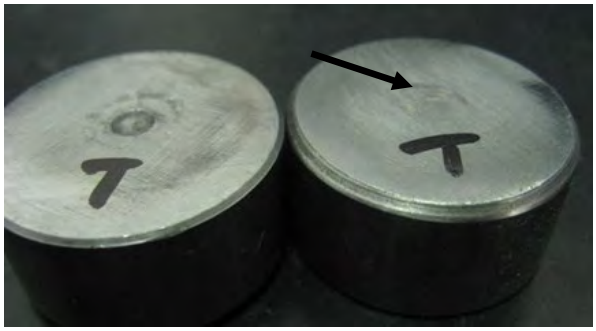

Fig. 5. Indentation Failure on the Temperature Cycle (right hand side).

The aging effect of the Temperature Cycling was calculated according to AOP46. The Temperature Cycle caused the Booster Relay Detonators to spend 13 hours per cycle at 70°C. For a total of three cycles another 34 years of aging was added, to the already artificially aged detonators, causing the Temperature Cycled detonators to be aged artificially for a total of 31 + 34 years, namely 65 years.

CONCLUSION

The Booster Relay Detonators were therefore aged in total for 99 years (34 + 31 + 34) before indicating a reduction on explosion properties. The use of AOP46 to predict the shelf life of munitions provides a scientific basis and is therefore essential to the management of operational stocks. In a study to determine the shelf life of RDX as discussed in [6], it was found that RDX can keep its explosion properties and safety for 70 years using an activation energy of 205 kJ $mole^{-1}$.

References

[1] AOP46. The Scientific Basis for the Whole Life Assessment of Munitions (Ed 1). Allied Ordnance Publication, July 2006.

[2] Michael Koepf, Overview on Shelf Life / Life Time / Operational Life / Storage Life. Presentation, Neuenburg 03/08/2020.

[3] STANAG 4224, Large Calibre Artillery and Naval Gun Ammunition greater than 40 mm, Safety and Suitability for Service Evaluation (Ed 5). NATO Standard, July 2007.

[4] STANAG 4225, The Safety Evaluation of Mortar Bombs (Edition 2). NATO Standard, August 2001.

[5] AAS3P-23, Safety and Suitability for Service Assessment Testing for Mortar Cartridges. NATO Standard, July 2018.

[6] Nguyen Trung Toan, Phan Duc Nhan, Duong Cong Hung, Vo Hoang Phuong. Thermal decomposition behavior and shelf-life of polymer-bonded explosives and hexogen - An experimental study. Vietnam J. Chem., 2018, 56(5), 654-659, September 2018.

Evaluation of Weapon Dynamics and Weapon Mount Dynamic Response

L. Fritz, K. Winnaar

Flamengro, a Division of Armscor SOC Ltd., Pretoria, South Africa

lafras@flamengro.co.za

Abstract

The evaluation and measurement of the dynamic response of weapon systems is a continual challenge. The measurements of interest are usually estimated using accelerometers, or laser-based displacement sensors. The sensors used must have adequate full-scale range to ensure limits are not exceeded, as well as sufficient dynamic range to ensure the internal resonance frequency is not activated. The typical shock-loadings experienced during weapon firings are of a small-time scale. Very often, the entities-of-interest are not accelerations, but rather displacements and velocities.
The computing of these quantities by numerical integration also poses some risks. The frequency response of the signal, the integration strategy, and the initial conditions are often responsible for the incorrect integration results. Added inconveniences are that accelerometers can sometimes not be placed at the location of interest (due to thermal constraints or inaccessibility of cabling), and that multiple uniaxial accelerometers, or another triaxial accelerometer) would be required for every location of interest. Flamengro has developed an algorithm to utilise Computer Vision (CV) to obtain full-field displacements of a tracked object, or “marker”. The algorithm determines the position of a marker in the image, and the displacements are calculated from the positions. The velocities and accelerations are determined by numerical differentiation instead.

Keywords—DIC, Marker Tracking, Displacement, Cameras

Introduction

The evaluation and measurement of the dynamic response of weapon systems is a continual challenge. The measurements of interest are usually estimated using accelerometers, or laser-based displacement sensors. The sensors used must have adequate full-scale range to ensure limits are not exceeded, as well as sufficient dynamic range to ensure the internal resonance frequency is not activated. The typical shock-loadings experienced during weapon firings are of a small-time scale.

Very often, the entities-of-interest are not accelerations, but rather displacements and velocities. The computing of these quantities by numerical integration also poses some risks. The frequency response of the signal, the integration strategy, and the initial conditions are often responsible for the incorrect integration results.

Added inconveniences are that accelerometers can sometimes not be placed at the location of interest (due to thermal constraints or inaccessibility of cabling), and that multiple uniaxial accelerometers, or another triaxial accelerometer) would be required for every location of interest.

Flamengro has developed an algorithm to utilise Computer Vision (CV) to obtain full-field displacements of a tracked object, or “marker”. The algorithm determines the position of a marker in the image, and the displacements are calculated from the positions. The velocities and accelerations are determined by numerical differentiation instead.

Methodology

The method describes how DIC is performed to perform marker tracking. The marker tracking techniques are explained and the benefits and challenges of DIC is pointed out. The underlying mathematics behind camera calibration, marker tracking, and stereo triangulation is described. This is followed by the steps required for DIC which includes camera calibration, marker detection and stereo triangulation.

DIC/marker Tracking Algorithm

The DIC/marker tracking algorithm was developed entirely by Flamengro, using the Python language, and the OpenCV Computer Vision (CV) libraries.

Camera Calibration

Camera calibration is required to estimate the parameters of the camera and lens of an image or video. The intrinsic parameters relate to the parameters of the camera, whilst the extrinsic parameters relate to the relative position of the camera relative to the world. These parameters are used to:

1. Correct for lens distortion,
2. Measure the size of objects within an image, and
3. Measure the location of an object within an image.

The Flamengro code uses the modified pinhole camera model by OpenCV [3] with lens distortion. The pinhole model is illustrated in Fig. 1 below.

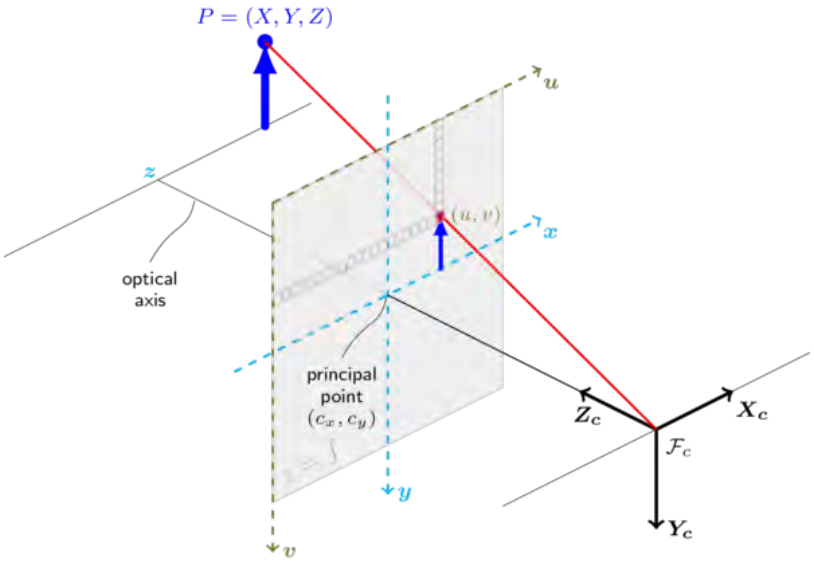

Fig. 1. Pinhole Camera Model. [4]

In this model, a 3D point in a scene is projected into a 2D image plane using the following perspective transformation:

$$\lambda \begin{bmatrix} u \\ v \\ 1 \end{bmatrix} = \begin{bmatrix} f_x & s & c_x \\ 0 & f_y & c_y \\ 0 & 0 & 1 \end{bmatrix} \begin{bmatrix} r_{11} & r_{21} & r_{31} & t_1 \\ r_{21} & r_{22} & r_{32} & t_2 \\ r_{31} & r_{23} & r_{33} & t_3 \end{bmatrix} \begin{bmatrix} X \\ Y \\ Z \\ 1 \end{bmatrix} \tag{1}$$

$$\lambda m' = K[R|t]M'$$

Where (X, Y, Z) is the coordinate of a 3D point in the world frame, (u, v) is the coordinate of the projected image in the 2D image plane, (f_x, f_y) are the focal lengths, (c_x, c_y) is the principal point of the image, s is the pixel skewness, λ is a scaling factor, K is the camera matrix and completely describes the intrinsic parameters of the camera, and R and t are the relative rotation and translation between the camera and the 3D point and completely describes the extrinsic parameters of the scene,

The transformation of a 3D point (X, Y, Z) to a 2D plane is as follows:

$$\begin{bmatrix} x \\ y \\ z \end{bmatrix} = R \begin{bmatrix} X \\ Y \\ Z \end{bmatrix} + t \tag{2}$$

Real lenses introduce radial and tangential distortion. The lens distortion is assumed to be fourth order. The model is extended to correct for lens distortion using the algorithm by Wang et al. as follows: [1]

$$\begin{aligned} x' &= \frac{x}{z} \\ y' &= \frac{y}{z} \\ x'' &= x' \frac{1 + k_1 r^2 + k_2 r^4 + k_3 r^6}{1 + k_4 r^2 + k_5 r^4 + k_6 r^6} + 2p_1 x' y' + p_2\left(r^2 + 2x'^2\right) + s_1 r^2 + s_2 r^4 \\ y'' &= y' \frac{1 + k_1 r^2 + k_2 r^4 + k_3 r^6}{1 + k_4 r^2 + k_5 r^4 + k_6 r^6} + p_1\left(r^2 + 2y'^2\right) + 2p_2 x' y' + s_3 r^2 + s_4 r^4 \end{aligned} \tag{3}$$

Where x'' and y'' are the corrected image coordinates in the world frame, $k_1, \ldots, k_6$ are the radial distortion coefficients, p_1 and p_2 are the tangential distortion coefficients, $s_1, \ldots, s_4$ are the thin prism distortion coefficients, and $r^2 = x'^2 + y'^2$.

It is also assumed that the lens may not be perfectly parallel to the image sensor, due to lens and camera tolerances. It is assumed that the lens may be tilted relative to the image sensor, and thus introduces a perspective distortion of x'' and y''. The pixel locations x'' and y'' are replaced by x''' and y'''. The distortion is modelled using the algorithm by Hamrouni et al. as follows: [4]

$$\begin{aligned} \lambda \begin{bmatrix} x''' \\ y''' \\ 1 \end{bmatrix} &= \begin{bmatrix} R_{33}(\tau_x, \tau_y) & 0 & -R_{13}(\tau_x, \tau_y) \\ 0 & R_{33}(\tau_x, \tau_y) & -R_{23}(\tau_x, \tau_y) \\ 0 & 0 & 0 \end{bmatrix} R(\tau_x, \tau_y) \begin{bmatrix} x'' \\ y'' \\ 1 \end{bmatrix} \\ R(\tau_x, \tau_y) &= \begin{bmatrix} cos\,\tau_y & sin\,\tau_y\, cos\,\tau_x & -sin\,\tau_y\, cos\,\tau_x \\ 0 & cos\,\tau_x & sin\,\tau_x \\ sin\,\tau_y & -cos\,\tau_y\, sin\,\tau_x & cos\,\tau_y\, cos\,\tau_x \end{bmatrix} \end{aligned} \tag{4}$$

Where $R(\tau_x, \tau_y)$ is the rotation of the lens relative to the image sensor, and τ_x and τ_y are the parameters used to estimate the angular perspective distortion. The pixel locations are then transformed to the image coordinates as follows:

$$\begin{aligned} u &= f_x \cdot x''' + c_x \\ v &= f_y \cdot y''' + c_y \end{aligned} \tag{5}$$

Camera calibration is performed by using an object of known size and shape, and then determining the camera intrinsics and extrinsics using the pixel location of the object. The method laid out by Zhang et al. is used to estimate the camera parameters. Fig. 2 shows one of the many images used for calibration.

a) Original calibration image.

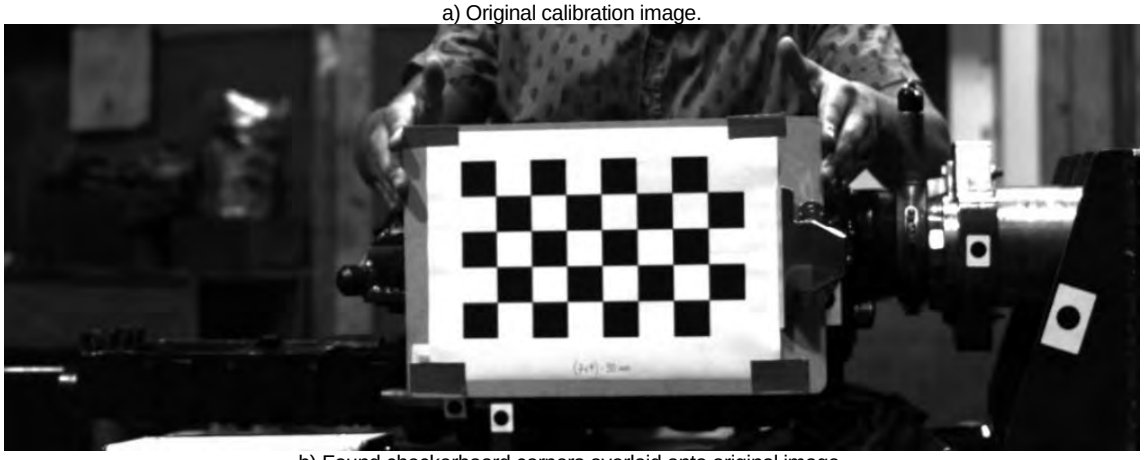

b) Found checkerboard corners overlaid onto original image.

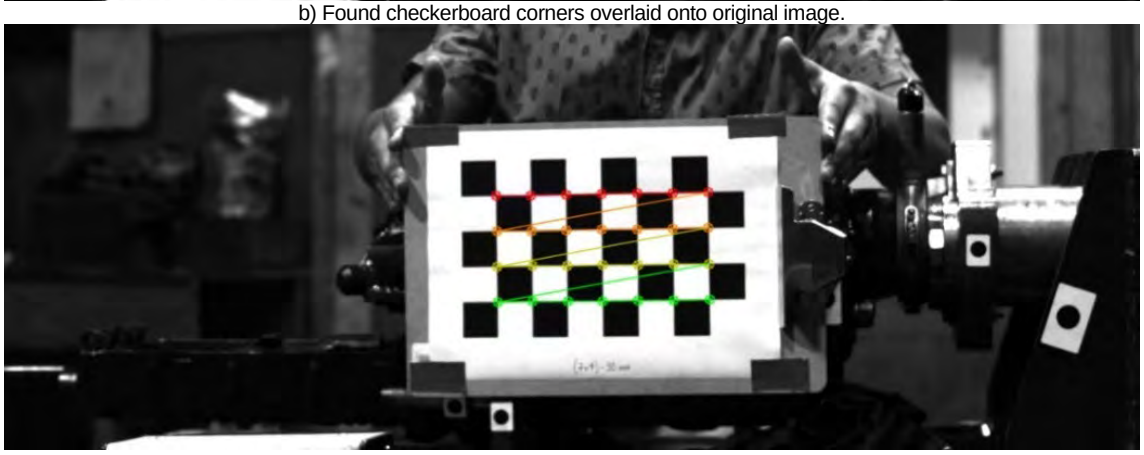

Fig. 2. Camera Calibration Checkerboard Corner Detection.

The Flamengro calibration code utilises a checkerboard pattern of known grid size and dimensions to estimate the camera intrinsic and extrinsic parameters. Multiple images of the calibration board are captured, and a non-linear least squares minimisation approach is used to estimate the camera parameters. For this method to be reliable and provide accurate camera parameter estimations, multiple images are required. The Flamengro code can achieve sub-pixel reprojection using the method developed by Wang et al. Flamengro currently use at least 20 images to provide reprojection errors smaller than 0.25 pixels [1].

A pair of cameras placed in a stereo setup are used to obtain full-field measurements. It is required that each individual camera must be calibrated to determine the relative transformation between the stereo pair. It is assumed that each camera is also individually calibrated - i.e., the intrinsic parameters and distortion coefficients are known.

Stereo rectification is performed once both cameras in a stereo setup have been calibrated. Stereo rectification is a transformation process in which the images from each camera are projected onto a common image plane. Stereo rectification is used in CV to simplify the determination of the correspondence between two matching points between images.

To rectify a pair of stereo images, the transformation between a pair of stereo cameras is required. The fundamental and essential matrices of the stereo camera are required. The fundamental and essential matrices are 3x3 matrices which relate corresponding points in stereo images. The fundamental and essential matrix are related as follows:

$$F = K_2^{-T} E K_1^{-1} \tag{6}$$

Where F is the fundamental matrix, E is the essential matrix, and K_1 and K_2 are the intrinsic camera matrices for the first and second camera, respectively.

It is assumed that if you have a stereo camera where the relative position and orientation of two cameras is fixed, and if you computed poses of an object relative to the first camera and to the second camera, (R_1, T_1) and (R_2, T_2), respectively, then those poses relate to each other. This means that, given (R_1, T_1), it should be possible to compute (R_2, T_2). You only need to know the position and orientation of the second camera relative to the first camera. This is computed as follows:

$$\begin{aligned} R_2 &= R' \times R_1 \\ T_2 &= R' \times T' + T_1 \end{aligned} \tag{7}$$

Where R' is the relative rotation between the cameras, T' relative translation between the cameras, R_1 and R_2 are the rotations of the first and second cameras in the global coordinate, and T_1 and T_2 are the translations of the first and second camera in the global coordinate system.

Once the essential matrix is known, it is also possible to determine, not only the orientation and translation of the stereo camera pair in the global coordinate system, but also the relative orientation and translation between the cameras. This is defined as follows:

$$E = \begin{bmatrix} 0 & -t_3' & t_2' \\ t_3' & 0 & -t_1' \\ -t_2' & t_1' & 0 \end{bmatrix} \times R' \tag{8}$$

Where $T' = (t_1', t_2', t_3')$ is the relative translation between the cameras.

Marker Detection

The marker detection algorithm is used to determine the location of an arbitrarily shaped marker in a frame. The marker centroid locations are determined for every image frame in the pixel coordinate space for each camera.

The marker detection algorithm utilises cross-correlation to locate the marker template in the image, and then blob detection is used to determine the marker centroid location. To improve marker detection fidelity, a cross correlation algorithm is used to place a region of interest (ROI) around the marker prior to blob detection. The ROI is then continually updated to move with the marker – the marker is continually placed in the centre of the ROI.

The normalised cross-correlation algorithm requires a source image, I and a template image, T. The template image is compared to the source image by sliding the template over the source image pixel by pixel. For each location of T over I, the metric is stored in the result matrix, R. The normalised cross-correlation is applied as follows:

$$R(x,y) = \frac{\sum_{x'y'}[T(x',y') - I(x+x', y+y')]}{\sqrt{\sum_{x'y'} T(x',y')^2 \cdot \sum_{x'y'} I(x+x', y+y')^2}} \tag{9}$$

All pixels outside the ROI are turned off (i.e., black for “Light” markers and white for “Dark” markers) and the image is binarized for blob detection. The marker centroid is determined using the algorithm by Suzuki et al. [5]

Once the marker centroid locations are determined in each image (for both camera views), the marker centroid location can be determined by simple stereo triangulation.

Stereo Triangulation

For a single camera setup, there exists a Euclidean transformation between the camera coordinate system, and the world coordinate system. This is called the projection matrix, and is defined as follows:

$$P = K[R|t] \tag{10}$$

Where P is the 3 × 4 projection matrix between the camera plane and the world coordinate system.

Once the projection matrices of each camera are known, it is possible to triangulate any pair of corresponding points in the stereo camera setup. This is calculated as follows:

$$P_2 = R'T'(P_1 - T') \tag{11}$$

Where P_1 and P_2 are the projection matrices for the first and second camera, respectively.

Once the stereo rectification is completed, any pair of corresponding points – i.e., as determined by a marker tracking algorithm – can be triangulated using the corresponding image point locations, and the projection matrices of the cameras.

Equations of motion

After stereo triangulation is performed, and the corresponding marker positions are known, the displacement, velocity and acceleration of the marker can be determined.

The displacement is determined by the change in position of the marker between two or more image frames:

$$\boldsymbol{s} = \boldsymbol{x}_{i+1} - \boldsymbol{x}_i \tag{12}$$

Where $\boldsymbol{s}$ is the displacement vector, and $\boldsymbol{x}_{i+1}$ and $\boldsymbol{x}_i$ is the position vector of the following and previous image frames, respectively.

The velocity and acceleration are simply the derivatives of the displacement and velocity with respect to time, respectively:

$$\begin{aligned} \boldsymbol{v} &= \frac{d\boldsymbol{s}}{dt} \\ \boldsymbol{a} &= \frac{d\boldsymbol{v}}{dt} = \frac{d^2\boldsymbol{s}}{dt^2} \end{aligned} \tag{13}$$

Where $\boldsymbol{v}$ is the velocity vector, $\boldsymbol{a}$ is the acceleration vector, and t is the time.

The displacement vector is calculated directly, whereas the velocity and acceleration vectors are calculated by numeric differentiation. The algorithm used is based on finite differences and utilise 1st-order accurate forward and backward differences at the boundaries, and 2nd-order accurate central differences at the mid-points. The time vector is easily determined by the frame rate of the cameras.

Camera Setup

Fig. 3 shows the cameras setup. Two Photron Mini UX100 cameras were used, each equipped with a 25 mm focal-length lens. The cameras were placed 1500 mm from the weapon mount with 20 deg included angle between the cameras.

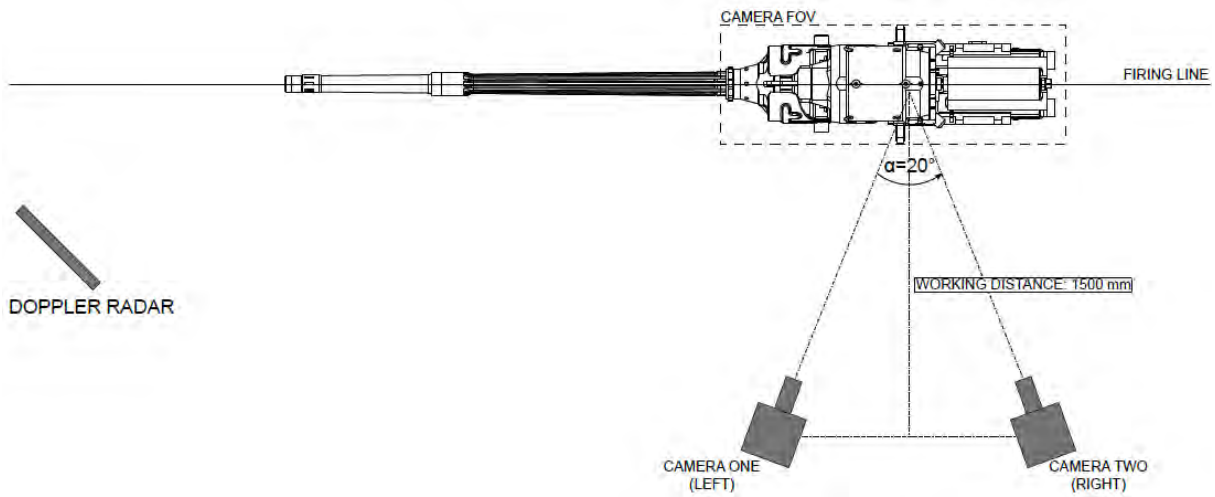

Fig. 3. Camera Test Setup

The camera setup parameters are summarised in TABLE I.

TABLE I. CAMERA SETUP SARAMETERS.

Camera Calibration								
Hor. Resolution [px]	Vert. Resolution [px]	Frame Rate [fps]	Shutter Speed [1/s]	F-stop [nodim]	Trigger [nodim]	Num Rows [nodim]	Num Cols [nodim]	Square Size [mm]
1280	480	10000	1/200000	2	Centre	7	4	30

Results

To investigate the effectiveness of using DIC to perform marker tracking the example of markers placed on a weapon mount is used as shown in Fig. 4. The focus is not on the actual weapon and the results obtained but rather the accuracy and error margins achieved making use of DIC marker tracking.

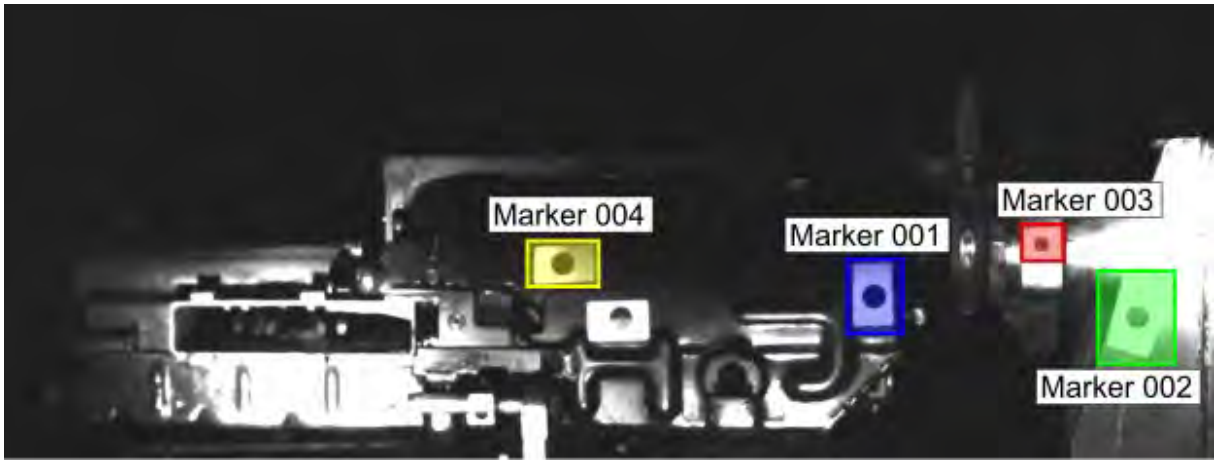

Fig. 4. Markers placed on the weapon and weapon mount.

The relative displacement, relative velocity and relative acceleration is measured between marker 002 and marker 001 as well as marker 002 and marker 004. The displacement for each marker is calculated making use of equation (12). Once the displacement for each marker is calculated the relative displacement for

marker 001 and 004 is calculated by subtracting the displacement from marker 002. The velocity and acceleration are calculated using equation (13).

Fig. 5 A) shows the axial displacement results between marker 002 and marker 001. The displacement results are given for five different single shots. The results clearly show the accuracy that can be achieved making use of DIC marker tracking. The cameras were able to capture the change in displacement between the markers within less than a 0.01 mm and captured 3000 images in 300 ms.

a) Marker 001. b) Marker 004.

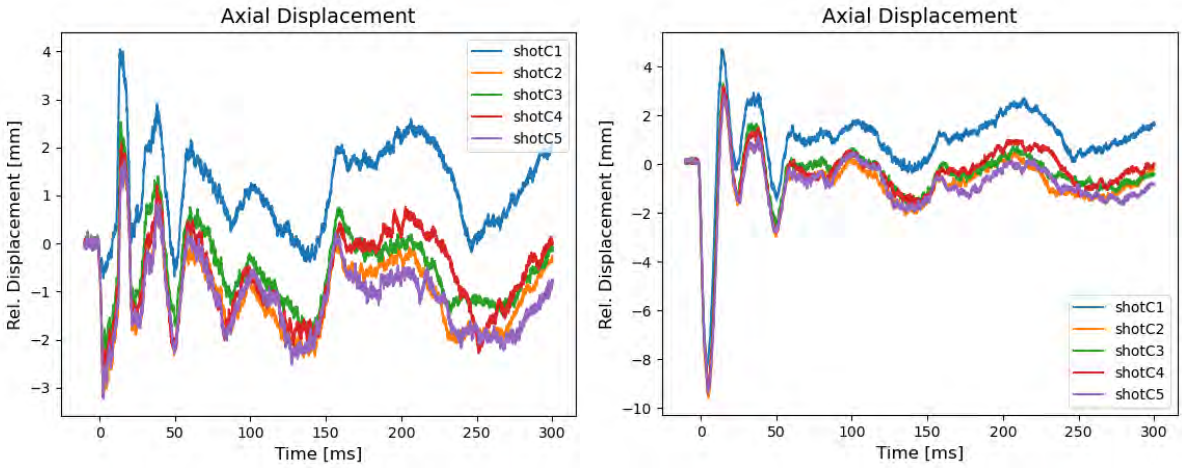

Fig. 5. Relative axial displacement.

Fig. 5 B) shows the axial displacement between marker 004 and marker 002. The results between Fig. 5 A) and Fig. 5 B) are different because the markers are placed at different locations. The results show how the cameras were able to capture the change in displacement for such a small-time frame.

The axial velocities are shown in Fig. 6. The axial velocities were calculated taking the derivate of the displacement between the markers. Both Figures show a higher velocity at time close to zero. This is expected as this was the moment the weapon was fired. The dampening effect can then be seen by the decrease in axial velocity.

a) Marker 001. b) Marker 004.

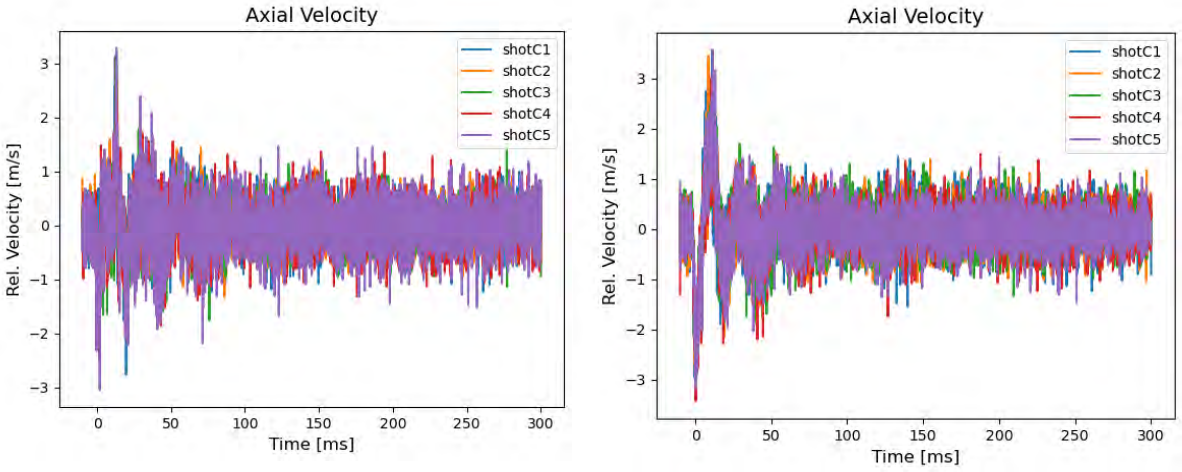

Fig. 6. Relative axial velocity.

Fig. 7 shows the axial acceleration between the respective markers. The axial acceleration is derived from the axial velocity results.

a) Marker 001. b) Marker 004.

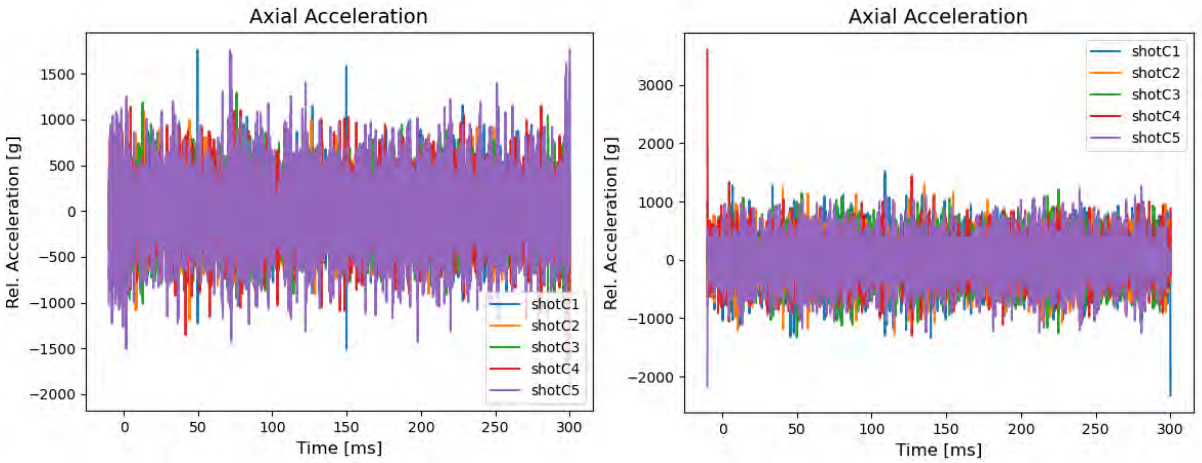

Fig. 7. Relative axial acceleration.

Statistical Significance of the Results

The axial displacement, velocity and acceleration plots only show the x-direction component. The y and z-direction components were also captured. The next step is to prove that the results obtained are statistically significant. A students t-test was performed on the noise component of the axial displacement. The t-test compares the mean between samples. During testing the first 100 ms only captured the noise component of the estimated axial displacement because during the first 100 ms the weapon was not yet fired. The null hypothesis, $\boldsymbol{H_0}$ is that the mean of the noise has an absolute magnitude less than 0.1 mm. The results are shown in Table II. The t-statistic is smaller than the t-critical value indicating that the null hypothesis cannot be rejected. This means that we are 95 % certain that the mean of the absolute magnitude of the noise is smaller than 0.1 mm.

TABLE II. T-TEST PARAMETERS

T-test Parameter	Result
Null hypothesis, H_0:	μ >= 0.1 mm
Alternative hypothesis, H_a:	μ < 0.1 mm
Significance level, α	0,05
Degrees of freedom, $df = n - 1$	14
Critical t-value, t_{crit} (from t-distribution):	-1,761
Decision rule:	if $t < t_{crit}$, Reject H_0
Sample mean, $\bar{x}$:	0,047
Hypothesised mean, μ:	0,1
Sample standard deviation, s	0,031
Sample count, n	15
t-statistic, T	-6,657
Reject H0 [Y|N]?	Reject H0

A further test can be done by calculating the signal-to-noise (SNR) ratio of the axial displacement, velocity, and acceleration. The SNR was calculated by taking the Root-Mean-Square (RMS) of the measured data divided by the RMS of the noise.

A higher SNR value is better as it means that the effect the noise has on the actual measured data is relatively small compared to the measured signal. The SNR results are shown in Fig. 8. The axial displacement SNR results gave a large value which indicates that the noise has little to no effect on the

axial displacement. The same cannot be said for the SNR results for the axial velocity and axial acceleration. Some of the measured results had a SNR value close to or smaller than 1. This indicates that the effect the noise has on estimated results exceeds the effect of the actual data. The velocity and acceleration terms are derived from the displacement terms. The displacement was the direct measurement given by the marker tracking results. The author also notes that the results are unfiltered, as this was not the scope of the project.

It is hypothesized that the noisy velocity and acceleration signals are due to the "relatively" course time-step of 0.1 ms (10 000 fps). Reducing the frame rate should yield better results.

The axial displacement results agree with the t-test results indicating that high accuracy displacement measurements can be taken making use of DIC/ marker tracking.

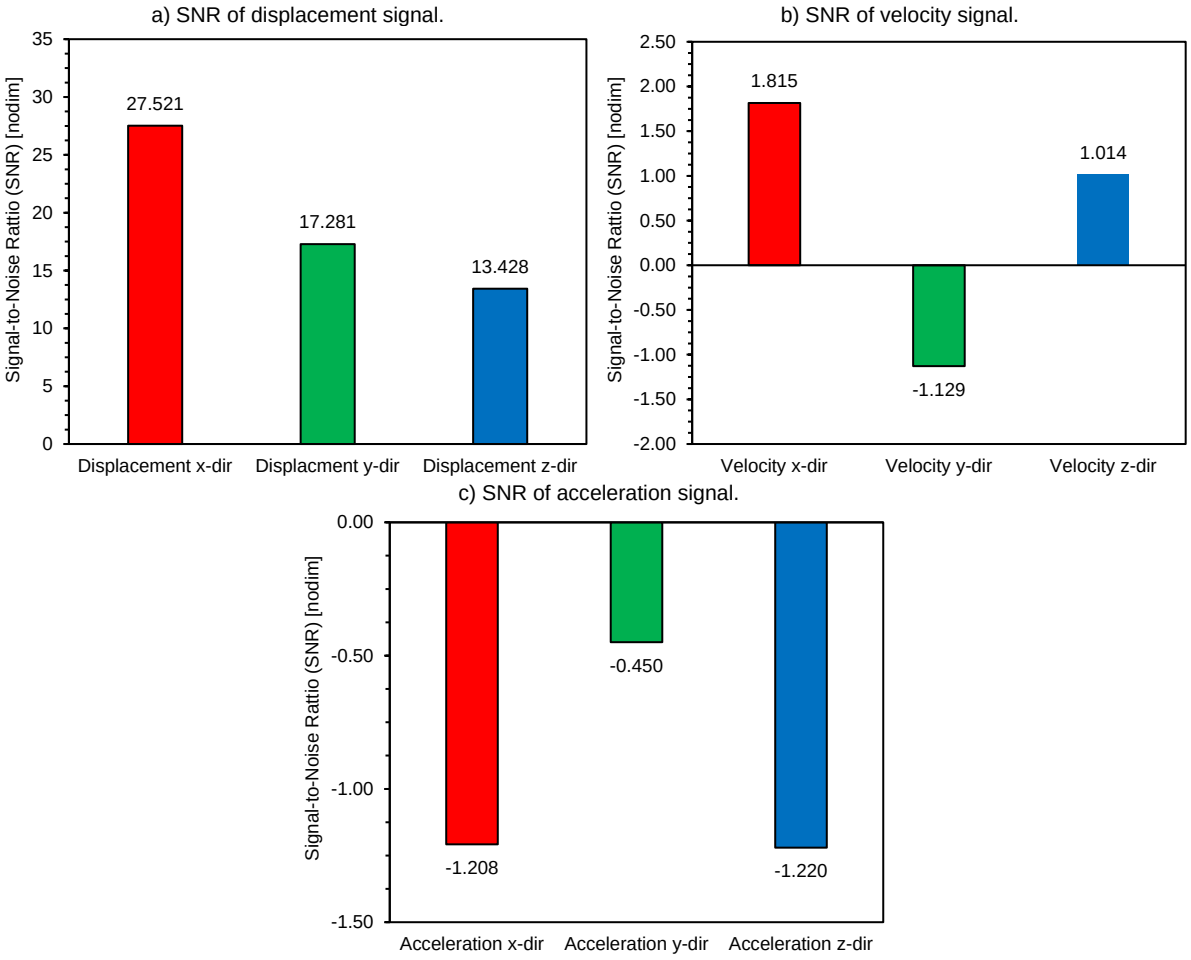

Fig. 8. Signal-to-Noise Ratio.

Discussion and Conclusion

The axial-displacement results yielded great results with high resolution values. It is possible to make use of the algorithm, to accurately track the displacement of any given point. The noise present in the data had an absolute mean less than 0.1 mm to a significance of 95 %. By knowing these results the data can be filtered to further increase the resolution and accuracy. The axial velocity and acceleration results had bad SNR results. This could be potentially improved upon by first filtering the displacement data and then deriving the velocity and acceleration terms.

The lenses used on the cameras were not ideal for the application. By making use of higher quality lenses the resolution can also be improved upon further reducing the noise and yielding better velocity and acceleration results. The lighting was also not ideal. The good news is these issues are easy to remedy.

Accelerometers are ideal for when acceleration measurements are required but decreases in accuracy if displacement and velocity is required. In the defence sector and specifically at Flamengro it is often preferred to capture the displacement instead of the displacement and acceleration terms. This means that making use of high-speed video and marker tracking would provide exceptional accuracy. A bonus, is that the only upper limit to the number of data points obtainable are due to computing requirements.

References

[1] J. Wang, F. Shi, J. Zhang, and Y. Liu, 'A new calibration model of camera lens distortion', *Pattern Recognit.*, vol. 41, no. 2, pp. 607–615, Feb. 2008, doi: 10.1016/j.patcog.2007.06.012.
[2] J. Javh, J. Slavič, and M. Boltežar, 'High frequency modal identification on noisy high-speed camera data', *Mech. Syst. Signal Process.*, vol. 98, pp. 344–351, Jan. 2018, doi: 10.1016/j.ymssp.2017.05.008.
[3] OpenCV, 'OpenCV Documentation'. OpenCV, 2018.
[4] S. Hamrouni, H. Louhichi, H. B. Aissia, and M. Elhajem, 'A New Method for Stereo Cameras Self-Calibration in Scheimpflug Condition', *Int. Symp. Flow Vis.*, vol. 15, p. 10, Jun. 2012.
[5] S. Suzuki, 'Topological Structural Analysis of Digitized Binary Images by Border Following', p. 15.

Performance Testing of Metalized Acrylonitrile Butadiene Styrene (ABS) Hybrid Rocket Fuel Grains

[1]Devlin Govender, [1]Lafras Fritz and [1]Gail Ndlovu

[1]Flamengro, A Division of Armscor SOC Ltd, Pretoria, South Africa
devlin@flamengro.co.za

Abstract

Flamengro designed, manufactured and assembled a hybrid rocket motor for an initiative into propellant replacements for the ITAR controlled Hydroxyl Terminated Polybutadiene (HTPB) fuel. The primary objective was to investigate the use of additive manufacturing technologies in fuel grains for hybrid rocket and ramjet propulsion systems using metallized acrylonitrile butadiene styrene (ABS). The first phase of the technology establishment involved the design, modelling, and simulation of the fuel grain and HBR motor. The second phase involved the demonstration of this technology through live-fire testing, at Flamengro's dynamic testing laboratory .The aim of the live-fire test was to acquire performance data to make a reliable comparison between ABS fuel grains, metallized ABS fuel grains and HTPB fuel grains. The results of the live-fire test showed that a ABS/aluminum (10%) fuel grain had a 35.70% higher regression rate than pure ABS fuel grains and a 67.5% higher regression rate compared to HTPB fuel grains reported in literature. Although the regression rate does not provide a complete assessment of fuel grain performance, these results imply that additively manufactured fuel grains perform comparably, in terms of burn rates, to legacy fuels such as HTPB**.**

Keywords—Flamengro, rocket motor, ABS, fuel grain, aluminum, regression rate

Introduction

Conventional solid rocket motors have been developed to a high state of capability; however, for a variety of reasons, these systems have become increasingly expensive to operate. Some of these reasons include manufacturing and operational complexity, safety, and environmental regulations for dealing with hazardous materials. However, there is an emerging requirement for low complexity propulsion systems where a lower system performance is acceptable in exchange for reduced operational costs, quicker design, reduced manufacturing turn-around and lower environmental impact. Hybrid rocket motors, illustrated in Fig 1, are becoming significantly more popular than solid rocket motors due to their low cost, safety, and overall performance.

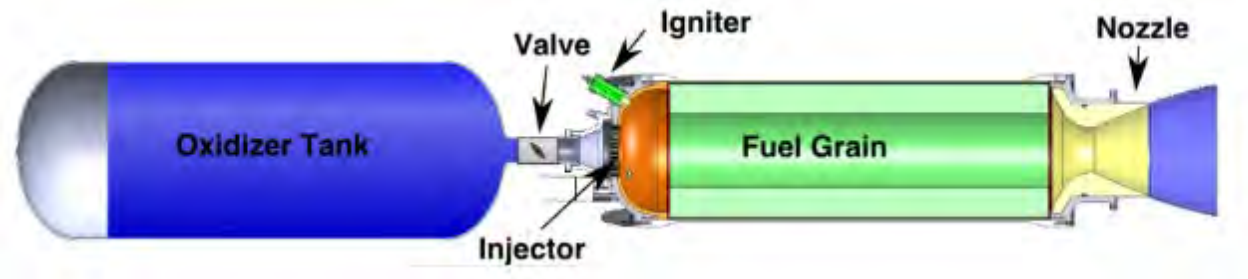

Fig. 1. Hybrid Rocket Motor Schematic [1]

The most used hybrid rocket fuel grain, hydroxyl-terminated polybutadiene (HTPB), is a thermosetting polymer that cannot be shaped and manufactured using fused deposition modelling (FDM) methods such as through 3D printing. Once cast, the HTPB grain cannot be reshaped, reused, or recycled. Furthermore, to increase the structural strength of HTPB, the material is cross-linked with additives that are controlled by International Traffic in Arms Regulations (ITAR). This makes sourcing of high-strength HTPB a problem.

The proposed replacement material, acrylonitrile-butadiene-styrene (ABS), is an inexpensive, recyclable thermoplastic that melts at a relatively low temperature, 250°C. This melting point can be precisely controlled and allows ABS to be reshaped and recycled multiple times with little to no degradation of the material properties. Furthermore, ABS is widely available in South Africa. Unlike HTPB, ABS can be formed into a wide variety of shapes using modern additive manufacturing techniques such as 3D printing. It is possible to further enhance the performance of ABS, by producing metallized filament and to utilize additive manufacturing technology to produce the fuel grains. The technological capability proposed here could form part of any future upgrades to extended range mortars, artillery projectiles, artillery rockets and missiles.

The aim of this investigation was to estimate the performance of additively manufactured acrylonitrile butadiene styrene (ABS) fuel grains, and metallic enhanced ABS grains, as a potential fuel for hybrid rocket motors. The performance of a propellant (a fuel and oxidizer combination) is linked to several physical variables such as its thrust performance and specific impulse. Furthermore, it is required to measure the regression rate of the fuel grain to establish its burn performance.

ABS is a solid homopolymer made by combining three components:

- Acrylonitrile,
- Butadiene and,
- Styrene

The addition of metal powders augment the performance of standard fuel grains. For this investigation, aluminium metal powder was added to the ABS fuel grain, due to aluminium's commercial availability and noteworthy burning effects. It was also intended to assess the performance of metallised ABS fuel grains that contain different mass percentages of aluminium powder. One of the problems existing is the lack of information regarding the performance of additively manufactured fuel grains. There is no industry standard value for the regression rates since those that have been published, vary widely [2,3].

There is a drive to establish technologies to increase the range of current artillery systems even further. Greater ranges will involve the exploration of newer and more advanced propulsion concepts. The hybrid rocket motor (HBR) will act as a vessel to test multiple propellant combinations and acquire relevant performance data such as its regression rate. Being a static system, the maintenance and running costs will be significantly smaller than dynamic systems.

Methods

The test campaign comprised of 20 burn tests, with each test running for 16 seconds. Each fuel grain was statically fired from the HBR motor, located in Flamengro's dynamic testing laboratory. Five (5) sets of fuel grains were printed and tested, with each set enhanced by a different aluminium mass percentage i.e. 0%, 2.5%, 5%, 7.5% and 10% respectively. Each set comprises of four (4) fuel grains to assess the reliability and the consistency of the tests.

The test setup for the demonstration consisted of the hybrid rocket motor technology demonstrator, the concept 3D printed fuel grain, an ignitor (E-match), a nitrous oxide (N_2O) supply tank and mass scale, a HBM Quantum data acquisition (DAQ) system, a LabVIEW control system, and a C270 HD Webcam. Live data acquisition will consist of:

1. Force measurements from a HBM U9C 100 N load cell to assess the motors thrust performance,
2. Temperature measurements from K-type thermocouples that are placed at three different positions on the HBR motor,
3. N_2O flow rates from a programmable mass scale and,
4. Video footage of each burn test from the HD Webcam.

The design of the HBR motor was done by Flamengro but manufactured by an external entity. The design of the motor included a motor pre-combustion chamber, main combustion chamber, post

combustion chamber, front and back-end caps, and sensor port plugs. All the parts were manufactured from 304 stainless steel. The test setup is shown in Fig 2.

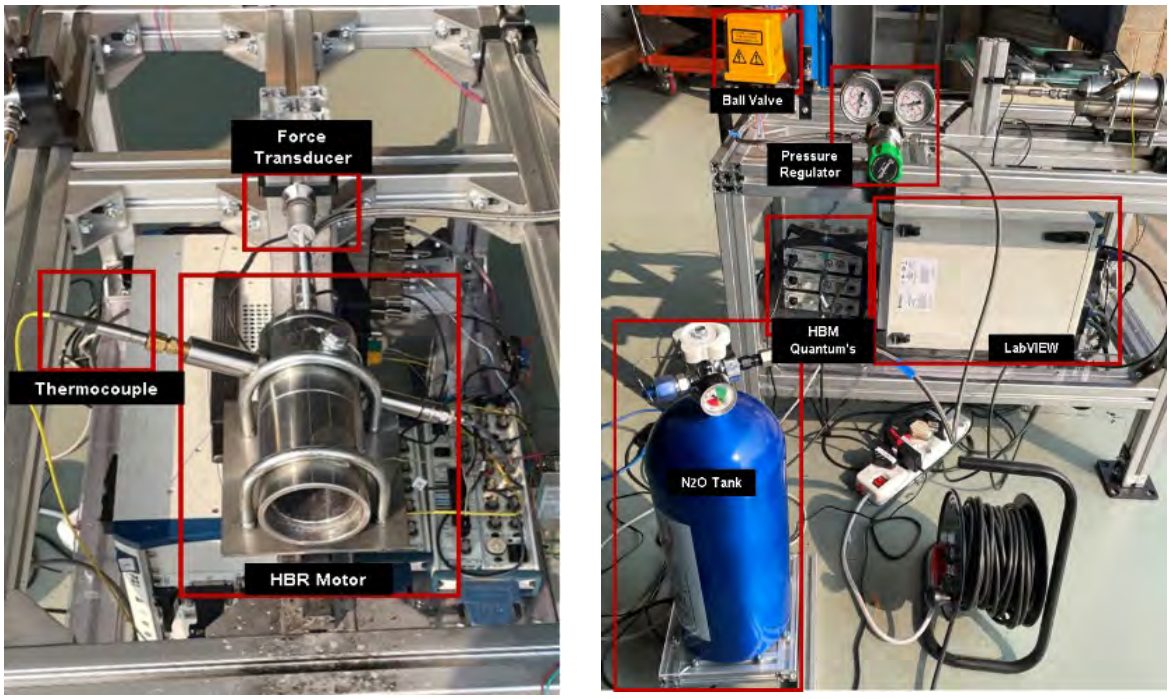

Fig. 2. Test Setup

ABS and metallised ABS fuel grains were 3D printed using a Creality Ender 3D printer. The printers required an upgrade that involved physical and software modifications to allow for metallised ABS printing capabilities. All fuel grains were printed as hollow cylinders, with an approximate length, diameter and port diameter of 97 mm, 47 mm and 13 mm, respectively. The 3D printed fuel grains are shown in Figure 3 below. The fuel grains were 3D printed using a composite filament produced by Flamengro. ABS/Al filament was produced my mixing ABS powder with the desired amount of aluminium powder and fed to Flamengro's filament extruder pilot plant. The fuel grains were 3D printed into quarters and glued together to form the entire test sample.3D printing ABS/Al fuel grains is a complicated process due to the different material properties of ABS and aluminium. ABS filament melts at 250 °C, which is significantly lower than melting temperature of pure aluminium powder (660 °C). As a result, solid aluminium particles clog the printer nozzle, which causes printing to be irregular. Nozzle clogging worsened as the percentage of aluminium increased therefore it was decided to limit the ABS/Al mixture to a maximum of 10 % aluminium by mass. The fuel grains were printed in quarters to shorten the printing time. This prevented print failures especially for samples with 5 – 10 % aluminium. The 3D printed fuel grain samples are shown in Fig 3 below.

Fig. 3. 3D Printed Fuel Grains

The E-match is the ignition system designed by Flamengro. It consisted of a pyrotechnic grain that is attached to a high voltage (12 V) wire. The pyrotechnic grain is made by combining sucrose ($C_{10}H_{22}O_{11}$) and potassium nitrate (KNO_3) in a 1:1.5 ratio, respectively. E-matches' are required to start combustion within the HBR motor and are triggered by the LabVIEW control system. The E-matches' are illustrated in Fig 4 below. A mass scale was designed and assembled by Flamengro to monitor the oxidiser flowrate, and to track oxidiser loses via connection points. The scale frame consisted of aluminium extrusions, a polycarbonate base sheet and a 100 kg load cell. Figure 2 shows how the N2O tank is placed on top of the mass scale throughout the test.

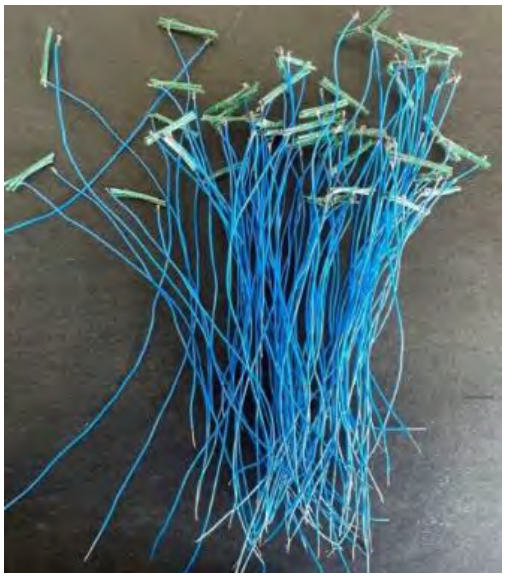

Fig. 4. E-Match Ignitors

Results

Fuel Regression Rates

Each sample was weighed and measured before each test. The results are shown in TABLE I

TABLE I TEST CONDITIONS

Test Number	Aluminium Percentage [%]	Test Duration [s]	$L_{fuel,initial}$ [mm]	$M_{fuel.initial}$ [g]	$D_{port,initial}$ [mm]
A1	0.00	16.00	96.50	154.90	14.40
A2	0.00	16.00	96.70	154.80	13.20
A3	0.00	16.00	97.10	156.36	13.70
A4	0.00	16.00	96.10	152.30	14.10
B1	2.50	16.00	97.70	161.52	14.10
B2	2.50	16.00	97.70	160.16	14.00
B3	2.50	16.00	98.00	164.80	14.80
B4	2.50	16.00	95.90	160.24	14.10
C1	5.00	16.00	98.60	155.44	13.80
C2	5.00	16.00	97.60	155.82	14.20
C3	5.00	16.00	98.00	147.86	13.80
C4	5.00	16.00	96.80	154.20	13.80
D1	7.50	16.00	96.90	159.52	14.40
D2	7.50	16.00	96.40	159.84	14.20
D3	7.50	16.00	96.70	162.68	14.20
D4	7.50	16.00	97.70	161.48	14.70
E1	10.00	16.00	95.60	157.54	13.10
E2	10.00	16.00	96.40	117.06	13.60
E3	10.00	16.00	96.90	157.36	14.20
E4	10.00	16.00	96.10	151.82	13.80

One of the main objectives of the test was to assess the regression rate of each sample. Fuel regression rate is the rate that the fuel surface recedes over the course of the burn time. This was calculated using the initial and the final port diameter for each test sample, divided by the total burn time. This regression profile can also be observed through a physical inspection of each test sample. The burn profiles of samples A1-E1 (one from each sample set) are shown in Fig 5 - 9 below. It must be noted that the samples were not photographed to scale, and that the outer diameter did not change significantly after each burn test.

(a) (b)

Fig. 5 : Sample A1 (a) before combustion (b) after combustion

(a) (b)

Fig. 6 : Sample B1 (a) before combustion (b) after combustion

(a) (b)

Fig 7. Sample C1 (a) before combustion (b) after combustion

(a) (b)

Fig. 8. Sample D1 (a) before combustion (b) after combustion

(a) (b)

Fig. 9. Sample E1 (a) before combustion (b) after combustion

From Fig 5 - 9, all samples showed signs of regression. It was also evident that each sample showed a slightly different burn profile, and that each sample set (A – E) did not necessarily burn consistently throughout the set. Variation in the burn profile could be due to the chemical composition of the fuel grain, the structural integrity of each 3D printed fuel grain and/or slight differences in the oxidiser flowrate. The pre -test images above, depict small crevices (caused during fuel grain manufacturing) that were possibly exacerbated during burning. This abnormality in grain structure could have resulted in different burn rates and/ or burn directions for certain samples.

The regression rate results are shown in Fig 10 -14, below. For each sample, the regression rate was plotted against its oxidiser mass flux to obtain a best fitting trend line through each sample set. This method is used to acquire the Marxman equation model (see equation 1) and used to calculate the regression rate constants for each sample set.

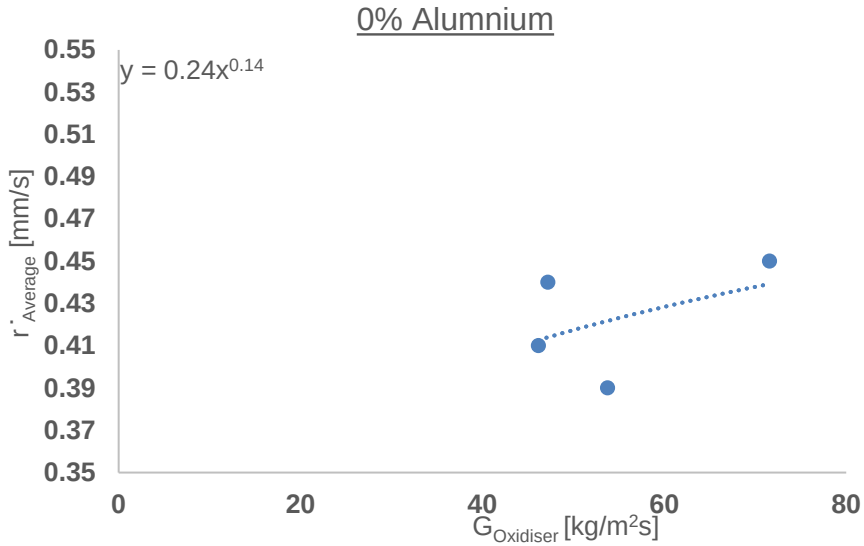

Fig. 10. Marxman Model for Sample Set A

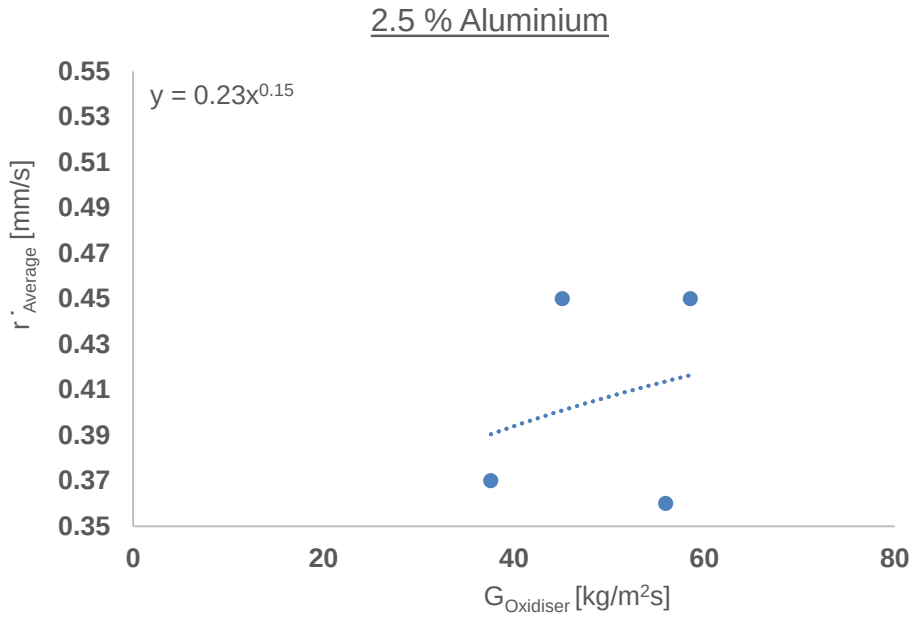

Fig. 11. Marxman Model for Sample Set B

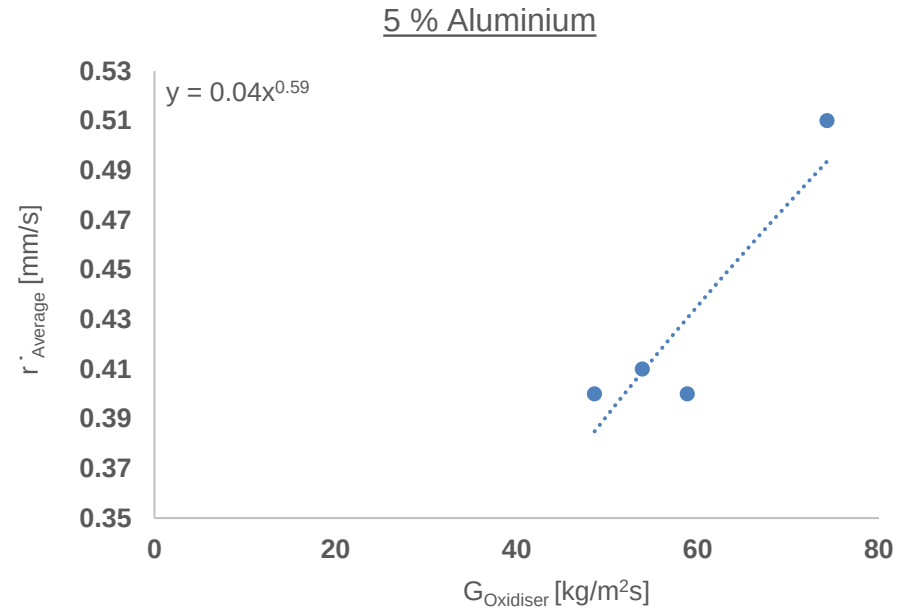

Fig. 12. Marxman Model for Sample Set C

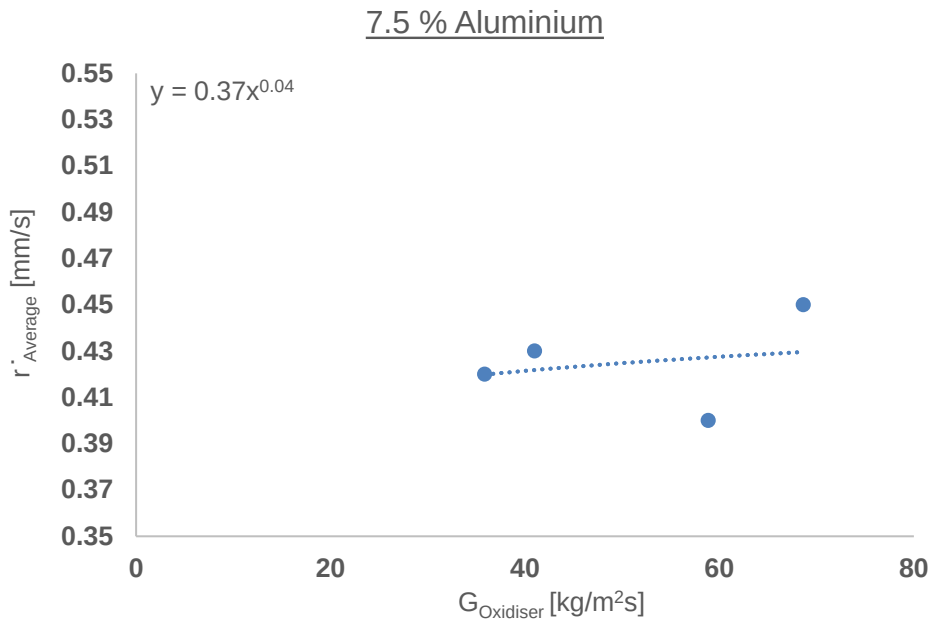

Fig. 13. Marxman Model for Sample Set D

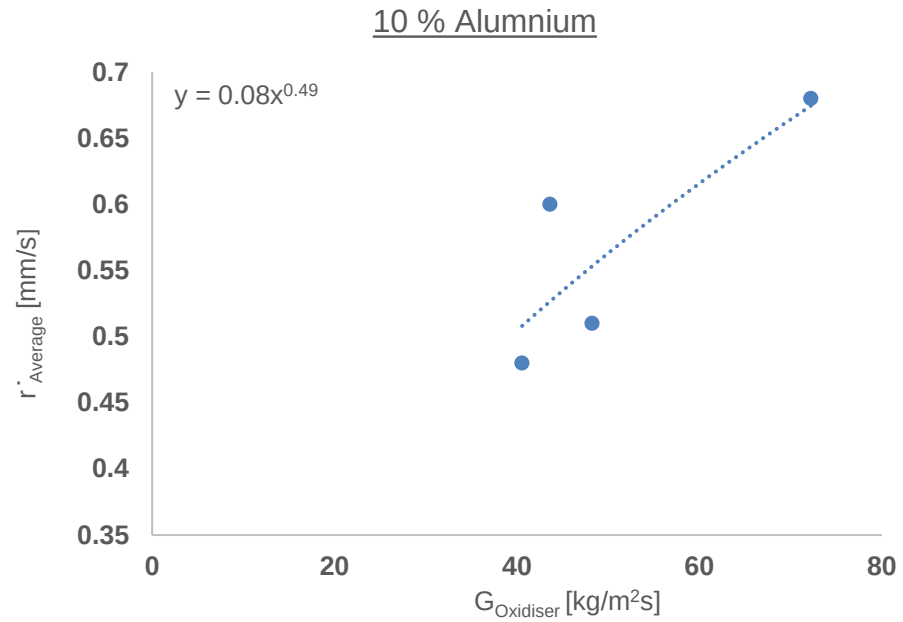

Fig. 14. Marxman Model for Sample Set E

TABLE II.REGRESSION RATE RESULTS

Test Number	$L_{Fuel,final}$ [mm]	$M_{Fuel.final}$ [g]	ΔD_{Port} [mm]	$\dot{M}_{Fuel, average}$ [g/s]	$G_{Oxidiser}$ [kg/m^{2}s]	$\dot{r}_{Average}$ [mm/s]	Regression Rate Constants [nodim]
A1	97.60	137.50	6.35	1.08	53.76	0.39	a = 0.24
A2	97.30	137.06	7.05	1.10	47.20	0.44	n = 0.14
A3	96.70	135.12	7.25	1.32	71.57	0.45	
A4	97.00	130.68	6.70	1.35	46.15	0.41	
B1	98.10	143.58	6.05	1.04	37.57	0.37	a = 0.23
B2	97.50	140.94	7.30	1.20	58.53	0.45	n = 0.15
B3	95.70	143.64	5.90	1.32	55.95	0.36	
B4	94.90	137.80	7.25	1.40	45.08	0.45	
C1	96.30	135.16	6.55	1.26	48.61	0.40	a = 0.04
C2	97.70	133.58	6.45	1.39	58.85	0.40	n = 0.59
C3	98.10	123.68	8.30	1.51	74.28	0.51	
C4	96.70	135.84	6.70	1.14	53.88	0.41	
D1	97.60	143.22	6.80	1.01	35.86	0.42	a = 0.37
D2	94.10	138.30	6.55	1.34	58.85	0.40	n = 0.04
D3	97.70	138.32	7.35	1.52	68.63	0.45	
D4	93.90	137.14	7.00	1.52	40.99	0.43	
E1	95.60	140.24	7.80	1.01	40.56	0.48	a = 0.08
E2	92.00	93.36	10.90	1.34	72.23	0.68	n = 0.49
E3	93.40	136.52	8.30	1.52	48.23	0.51	
E4	95.40	130.44	9.60	1.52	43.62	0.60	

From **TABLE II** above, it can be seen that the length of each fuel grain did not change significantly. This was expected because burning did not occur in an axial direction. The slight deviations in fuel grain length are due to warping and/or expansion of the grain during combustion. This is usual for a thermoplastic material such as ABS.

The mass flowrate of the fuel refers to the rate at which fuel gasifies and combines with the oxidizer. On average, every sample set with aluminium (sample set B-E) showed a higher mass flowrate than the sample set with no aluminium (sample set A). Sample set D (7.5 % aluminium) showed the highest percentage increase, 10.95 %, in the fuel mass flowrate when compared to sample set A (0 % aluminium). This difference in flowrates between pure ABS fuel grains and metallised ABS fuel grain lies in the grains bulk density. The addition of aluminium powder was aimed to increase the bulk density of the fuel grain and thus increase the burn surface area. This was intended to result in a higher overall mass flowrate that was in fact observed in this investigation.

On average, sample set E (10 % aluminium) showed a 33.82 % increase in regression rate when compared to sample set A (0 % aluminium). Again, this observation confirms the better burn performance of metallised fuel grains when compared to pure ABS fuel grains. Although there is no clear trend between the fuel mass flowrate and regression rate, a higher fuel mass flowrate generally leads to a higher regression rate and vice versa. Higher regression rates imply better burn performance and potentially better motor performance due to the production of greater thrust forces.

Lastly, the regression rate constants, a and n, are part of the Marxman model equation (equation 1) that is used to predict propellant performance [3]. The regression rate constants are specific to each propellant combination and aluminium percentage composition. Currently, literature does not provide values for the regression rate constants for each of our fuel grain compositions. Therefore, calculating theses values will provide valuable insight for current and future research work.

$$r = a\,(G_{oxidser})^{n} \quad (1)$$

Also, the Marxman model equation was used to predict the performance of HTPB/N_2O for the oxidiser flowrates used in this investigation. The regression rate constants were acquired from literature for the same propellant combination as our investigation i.e. HTPB with N_2O as the oxidiser. The values for a and n were reported as 0.094 x 10^{-3} and 0.325 respectively [4]. The regression rate of HTPB was calculated using the regression rate coefficients from [4] and the average oxidiser mass fluxes for each sample set from our investigation .The results are shown in TABLE **III.** below.

TABLE III. REGRESSION RATES FOR ABS/ALUMINIUM AND HTPB

Sample set	$G_{N2O,average}$ [kg/m^{2}s]	$\dot{r}_{Average}$ [mm/s]	$\dot{r}_{HTPB}$ [mm/s]
A	54.68	0.42	0.35
B	49.28	0.41	0.33
C	58.91	0.43	0.35
D	51.09	0.43	0.34
E	51.16	0.57	0.34

From TABLE **III.** , the regression rate of ABS and ABS/aluminium fuel grains performed better than the HTPB option, in terms of the fuel grains burning performance. On average, every sample set from our investigation (sample set A-E) showed a higher regression rate than HTPB reported in literature. On average, sample set A (pure ABS) showed a 22% increase in regression rate when compared to HTPB, and sample set E (10% aluminium) showed a 68% increase in regression rate when compared to HTPB.

Inspection of the Exhaust Flames

The exhaust flames were inspected to assess if there are any differences between each sample set. Fig 15-19 shows the exhaust flame images, for samples A1–E1, captured from video footage that was recorded during the test. The images show that as the percentage of aluminium is increased, there is no significant discrepancy in the exhaust flame for sample A1 – D1. Sample E1 clearly produced the largest flame. It was also noticed, during the tests, that the amount of sparks and flares increased as the aluminium percentage increased .It was later discovered that the sparks are actually aluminium particles that are heated and blown out the motor, with the exhaust gases. This observation may imply that large quantities of the aluminium did not burn during the test, and as a result, it did not optimally influence the fuels burn capacity.

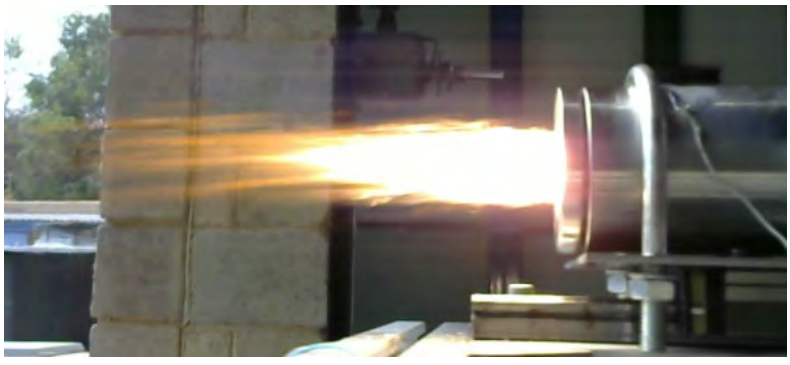

Fig. 15. Exhaust flame of Sample A1

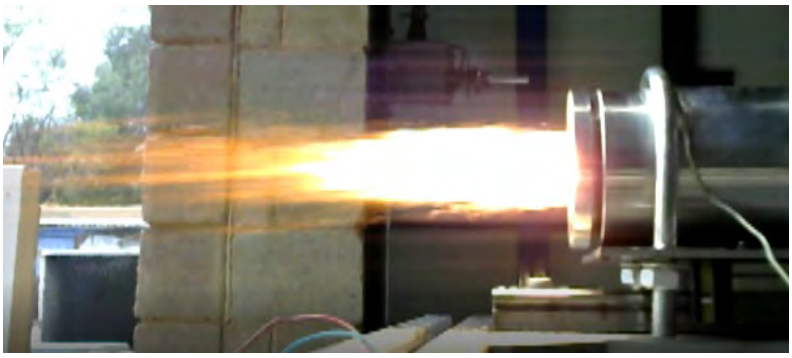

Fig.16. Exhaust flame of Sample B1

Fig.17. Exhaust flame of Sample C1

Fig.18. Exhaust flame of Sample D1

Fig.19. Exhaust flame of Sample E1

Conclusion

Flamengro produced twenty (20), 3D printed fuel grains to demonstrate and validate the capabilities of additively manufacturing techniques for rocketry and artillery systems. Furthermore, fifteen (15) 3D printed fuel grains were infused with aluminium to demonstrate the capabilities of additive manufacturing techniques for composite fuels. On average, the 3D printers produced fuel grains to a 96.97 % accuracy in desired length, 97.64 % accuracy in desired port diameter and 99.13 % accuracy in desired outer diameter.

On average, the 3D printed fuel grains showed an overall increase in regression rate as the mass percentage of aluminium increased. However, an inspection of an ANOVA analysis revealed that this increase is not significant for sample set B-D i.e. 2.5 % to 7.5 %.The ANOVA analysis also revealed that sample group E (10 % ABS/Al) showed a significant increase in regression rate compared to pure ABS fuel grains. This implies that only the 10 % ABS/Al fuel grains showed an improvement compared to pure ABS fuel grains in terms of the burn performance. Also, the 3D printed ABS/Al fuel grains showed an overall higher regression rate when compared to HTPB reported in literature. Although the regression rate does not provide a complete assessment of fuel grain performance, these results imply that additively manufactured fuel grains perform comparably, in terms of the burn rate, to legacy fuels such as HTPB.

The following recommendations are put forth for the continuation of this investigation. It was noticed that the fuel grain continues burning after the oxidizer supply is cut off. Therefore, an extinguisher gas such as nitrogen (N_2) or helium (He) should be used to safely stop burning immediately after a test. A larger range of aluminum percentages (greater than 10 %) should be investigated to assess possible effects of higher concentrations of aluminum. A smaller particle size of aluminum powder should be used to ensure better amalgamation during fuel grain production, and consequently better burning during combustion. To improve on the thrust force created during combustion, it is required to add a nozzle to the HBR motor. From literature, it is common to use a nozzle to increase the thrust generated by the HBR motor to acquire significant thrust data.

References

[1] 'Hybrid Rocket Motor Overview –'. http://www.spacesafetymagazine.com/aerospace-engineering/rocketry/hybrid-rockets-overview/ (accessed Oct. 06, 2022).

[2] 'F2-BP-2018SonkaIvanBP_3D_Printed_Fuel_Grain_for_Hybrid_Rocket_Engine_IvanSonka.pdf'.

[3] McFarland and Antunes, 'Small-Scale Static Fire Tests of 3D Printing Hybrid Rocket Fuel Grains Produced from Different Materials', *Aerospace*, vol. 6, no. 7, p. 81, Jul. 2019, doi: 10.3390/aerospace6070081

[4] B. Geneviève, 'Development of a Hybrid Sounding Rocket Motor', p. 213.

Evaluation of bio-remediation techniques for the treatment and management of explosives in ballistic testing range

[1]Phumzile Dladla

[1]*Alkantapan Test Range a Division of Armscor SOC Ltd, Admin Building, SHEQ Domain, Copperton, Northern Cape*

phumzilen@armsordy.co.za

Abstract

Explosives are regarded as highly energetic chemicals that release large amount of energy and gaseous products upon detonation in a short period. As a result testing, detonation and disposal of explosives contaminates soil, ground water, thus posing a threat to humans, living organisms and natural resources. The most commonly used explosives in artillery shells, bombs and other munitions are 2,4,6 Trinitrotoluene (TNT), Hexahydro-1,3,5 – trinitro -1,3,5 – triazine (RDX) etc (Clark and Boopathy, 2007). Through previous investigation on the matter of explosives contaminating soil and posing risks to human; bioremediation treatment/ method processes are often considered as best methods, since these are usually the least expensive means of dealing or destroying organic pollution.

These methods of bioremediation can be undertaken in any ballistic testing range without causing a major disturbance to human activities and environment. The processes are more than just eliminating radiation sources, however they are about protecting people and environment against potential harmful effects from exposure to ionizing radiation. Clean-up of contaminated areas by explosive is now mandated due to human health and safety concern. There are three categories of bioremediation techniques which are recommended, the in-situ land treatment for soil and ground water, bio filtration for the air, and bioreactors which is predominantly involved in water treatment.

The advantage of bioremediation is eco-friendly and sustainable methodology that is able to destroy a pollutant or transform harmful contaminants into harmless substances. This paper examines the best bioremediation method or treatment that can be explored by the ballistic testing ranges to minimise the environmental impacts and risk threats to human. Two types of bioremediation investigated which is soil slurry reactor and in-situ bioremediation with promising results. Both methods have advantages and disadvantages.

The soil slurry reactor is able to remove the explosive contaminates within three weeks; the advantages of this process is that it's a short term process with disadvantages of labour intensive when executed and expensive. Whereas; the in-situ bioremediation the treatment time is approximately 12 months, the advantage of this process is that the treatment is cost effective.

Keywords— ***Explosives, ballistic, bioremediation, TNT, RDX, soil slurry reactor, in-situ, environmental impact, human health and safety, soil contaminates,***

Introduction

Worldwide most defence sites including the ballistic testing ranges are contaminated with explosives which are normally released during the manufacturing, testing, firing, and training operations; loading assembly and packing activities and demilitarization operation., Celin S.M (2002). Explosive waste generation is a universal problem because of its complex and hazardous nature. According to Lewis A.T *et al.,* (2003) stated that in the US the Army alone has estimated over 1.2 million tons of soil have been contaminated with explosives, and the impact of explosives contaminated in other countries is of similar magnitude. In South Africa, explosives industry has developed significantly since the discovery of gold in 1886 in Witwatersrand, with Johannesburg emerging as the most engaging markets for dynamite globally.

Over the past years, the industry has grown exponentially. The explosive industry, being an integral component of modern society, conducts activities leading to the production of waste because of explosive production and destruction, Mmolai, (2003). In recent years, growing concern about health and ecological, threats posed by man-made chemicals have led to many issues. Soil contaminated with explosives are major threat to the environment. Explosives in the soil can migrate to the ground water leading to harmful effects on human life and environment. Despite the well-known negative impacts of explosive waste on the environment, there has been very little research on the governance of the explosives waste streams, especially in the evaluation of the legislative framework and legislative compliance to ensure that the explosives waste or ordnance is being treated and managed properly.

The purpose of this paper is to examine the treatment methods/ bioremediation methods to deal with unexploded ordinance; determine the human and environmental risk associated with explosives – contaminated soil, and provide an overview of the environmental fate and degradation pathways of the explosives substances that commonly contaminated. There are numerous publications on this topic, however, this paper contains an extreme enough to guide the ballistic testing ranges more comprehensive information on how to properly deal with the unwanted explosives and unexploded ordinances without impacting the environment and also harming human beings who are dealing with explosives directly (Dimitrios and Kalderis, 2011). The evaluation of the bioremediation methods that are addressed in this paper is pointing out the advantages and disadvantages of each process and leading all the ballistic testing ranges to improve these processes and exploring new ones. This research paper presents two bioremediation technologies for the treatment of explosives contaminated soil. These technologies include soil slurry reactor and in-situ bioremediation.

Methods

In recent years, growing concern about the health and ecological threats posed by man-made chemicals have lead to many issues, and those man-made chemicals includes the manufacturing and testing of the explosives. Explosives are classified as primary or secondary based on their susceptibility of initiation. Kalderis *et al*., (2011) state that priamry explosives are highly susceptible to initiation and are often used to ignite secondary exxplosives, such as TNT (2,4,6-trinitrotoluene), RDX (1,3,5

trinitroperhydr0-1,3,5-traizine), HMX (1,3,5,7-tetranitro -1,3,5,7 – tetrazocone), and tetryl (N-methyly, N-2,4,6, - tetranitro-aniline). Still to date, there are many cases of soil ccontaminated with explosives, either nearby ballastic testing ranges or in areas whre military activities are being performed or have been performed previously. However, due to the lack of comprehensive information regarding these activities, reports on authentic explosives – contamination cases are rather scarce.

According to previous researchers the explosives compounds has the possibility to enter the environment during their production stage, disposal stage through open burning, storage stage or usage (dispersed or unexploded ordanance) resulting in contamination of ground water, surface water, marine and terrestrial environments, which does not only affect the environment specifically aquatic species but affects the human beings who might be directly exposed to contaminated water due to consumption. Currently South Africa is regarded as the water scarce country, therefore contamination of water should be prevented by any means.

The ballistic testing ranges has a huge potential to results in environmental impacts through disposal of explosives by open burning. This activity may result in an adverse impacts on the surface and ground water quality, air pollution and human health (Shen et al., 2009). These impacts may also lead to global effects such as ozone depletion and global warming. The environmental impacts of activities, products and services are fast-moving up the priority level of industries today (Duijim and Markert, 2002). The Johannesburg and Beyond: 2002 World Environment Summit United Nations (2002) and the Sustainable Development Goals (United Nations, 2015) emphasise the importance of sustainable development and its relationship to environmental protection. These requirements are equally applicable to the explosives sector. There is a understanding for the need to minimise the environmental impacts from all affected stakeholders, and the explosive sector is no exception (Alverbro et al., 2009).

The explosives, on other hand are, are considered to be a mixture of various solid and liquid substances that might later on become capable of creating an explosion as being addressed by Rigby et al., 2019. The researcher argued that explosives are harmful to the environment and to the health and safety of humans (Akhavan, 2011). Therefore, the storage and disposal of explosive through open burning need to be well managed. Explosives are categorised as Class 1 dangerous goods in accordance with SANS 10228:2012 (Table 1-1). The level of hazard associated with the different divisions of explosives are outlined in Table 1-1, with Division 1.1 presenting mass explosion hazards, while division 5.1 explosives are very insensitive (and less hazardous in terms of risks of explosion) (SANS, 2012)

TABLE I. EXPLOSIVE DIVISIONS ACCORDING TO SANS 10228:2012

Class 1: Explosive	
Division 1.1	Mass explosion hazard from the explosives
Division 1.2	Projection hazard from the explosives
Division 1.3	Fire hazard and either a minor blast hazard or a minor projection hazard or both from the explosion.
Division 1.4	No significant blast hazard from the explosive
Division 1.5	Explosives with a mass explosion hazard and a very insensitive.

Source: SANS 10228: 2012 Edition 6 (SANS, 2012)

Legislation on Explosives Management

A numerous pieces of legislation have been gazetted – some focusing on the protection of health and well-being, and others on the enviornmental protection. According to the South African Constitution RSA (1996a), in particular Section 24, provision is given to everyone with the right to an "environment that is not harmful to their health and well-being, and the right to have the environment protected through reasonable legislative and other measures". Coulson (2018), stated that the Occupational Health and Safety Act (85 of 1993) (OHS Act) focuses on the protection and safety of the employees that are actively involved in the production, handling, storage, testing or transportation of the explosives in the country. The OHS Act has requirements for the handling, storage, use and disposal of explosives and related processes that it should be handled in a safe manner that is not exposing employees to danger or posing a risk to human life. It further provides a detailed structure of the handling procedures by the well trained personnel who are explosives expects; and the safety precautions that each ballastic testing or explosive industry must have in place for the safety of the employees handling explosives. National Environmental Management Act (107 of 1998) (NEMA) in one of the objective of the duty of care principle (also known as extended producer responsibility (EPR) in the NEMWA) is to ensure that manufacturing and testing ranges) are responsible to practice duty of care to all the unexploded ordanances or unwanted explosives (Nahman, 2010). Implementing an effective EPR programme will assist the explosive industry to move away from landfill disposal and implement the waste management system in favour of recycling, minimisation, bioremediation and avoidance.

Negative Impact of explosives

According to Eom et al (2019), the most significant negative of explosive is pollution of the environment (soil, water, air and land), which may possibly cause environmental degradation. Health effects may be directly or indiectly related to exposure to explosives. Direct exposure to TNT can severe health issues

to human being handling explosives, for example, induce blood disorders such as anaemia, abnormal fuction of the liver, enlargement of the spleen, immunological deficiency and other health-related problems. Indirect exposure to explosive may include exposure through soil, water and air that may contaminated by by-prodcts or wastes from explosive industry/ testing ranges (Letzel et al., 2003).

Impact of explosive on air

In South Africa, thermal destruction of all explosives is required to render the destruction in a safe way in terms of Explosive Act (26 of 1956). Open burning and open detonation (OB/OD) is one of the methods used for unwanted explosives destruction, internationally, and is currently used for the treatment of unwanted explosives in South Africa. Whilst unavoidable from a safety, perpective, OB/OD treatment results in uncontrolled air emissions that may include an array inorganic, organic and metal compounds of concern. The quantification of potential air quality, health risks from OB/OD operations is a prerequisite for responsible management, but poses a significant challenge given the highly variable composition of waste streams, complex source emissions and differing thermodynamic conditions under releases occur (Martin et al., 2012).

Explosives contaminated soil

The destruction of explosives during OB/OD may contaminate the soil and groundwater due to the leaching of chemicals from the destructed components. Soils in close proximity to explosives manufacturing plants, explosive burning grounds and explosives testing ranges may be polluted by various residues of explosives. Soil concentration as high as 38 600mg/g were reported for 2,4,6-trinitrophenol (TNT, trinitro-toluene) in soils located within 1km of explosives manufacturing sites. Other explosives detected in such soil included: 2-amini-4,6-dinitrotoluene (z-am-DNT), 2, 4 – dinitrotoluene (2,4-DNT) and hexogene (RDX) (Fuller et al., 2005) all of which are known to be harmful to the environment.

Human health effects of munitions

Constituents of munitions have the potential to cause adverse human health effects. Table II summaries the potential health effects of five munition constituents closely associated with military munition as listed by EPA

TABLE II. POTENTIAL EFFECTS OF MUNITIONS CONSTITUTES CLOSELY ASSOCIATED WITH MILITARY MUNITION.

Consituent	Potential toxicity/ effects
TNT	The liver, cataracts and skin irritation are infectionemaniting from exposure of TNT and the possibility of human carcinogen
RDX	Due to labotory exposure towards animals, there are indicative prospects of organ damage. There are human related risks like human carcinogen, nervous system callenges, postate challenges nausea and vomiting possibilities.
Perchlorate	Being exposed to perchlorate may result into tearing, itching, and pai; accidental ingestion, which maycreate gastroenteritis with abdormal pain. The infections can further result into nausea, vomiting, and; other systemic effects may follow which includes ears irritation, dizziness, elevated blood pressure, blurred visio, and tremors amongst other illness. Metabolic dysfunction of the thyroid is one of the possible chronic effects.
HMX	Based on animal studies there is a prospective liver damage and breakdown of the central nervous system.
White phosphorus	Inhalation may cause liver, heart or kidney damage; severe exposure can lead to death; mild exposure may cause burning of skin, throat irritation and affecting the proper functioning of the lungs, causing vomiting, creating stomach cramps, with drowsiness and possible reproductive effects.

Source: Appendix 1 Table of 9GAO, 2003)

Destruction of unwanted explosives

Hart and Stock (2019) unfolded that the destruction of the unwanted explosives in South Africa is one of the main objectives of the Department of Defence (DoD), and is incoporated under the Installation Resoration Program. Open burning or open detonation of explosives is still considered one of the most preferred destruction methods in South Africa so far. However; the control of emission from burning gronds are regulated in terms of GNR 893 of 2013 9list of activties which result in atmospheric emissions which have or may have a significant detrimental effect on the environment, including health, social conditions, economic conditions, ecological conditions or cultural.

Bioremediation Techniques

There are numerous publications on this topic; with the research findings presented from previous studies boiremediation techniques are proving to be economic methods for the effective treatment of effluent nad rehabilitation of the pollued site. Two bioremediation methods, namely, soil slurry and and in-situ techniques were evaluated for the treatment of soil contaminated with explosives and health issues on humans/ employees posed by the explosives in ballistic testing ranges.

In-situ bioremediation technologies

The contaminated soil is treated in place and essentially remains undisturbed during treatment. The most common form of in-situ treatment is the biodegradation of contaminants within the saturated zone of the soil. In-situ technologies have been used mostly to remediate the contaminated sites include soil-washing, low temperature thermal treatment, soil bioventing and enhanced bioremediation or landfarming. It has been proven by the previous researchers that the effectiveness of the in-situ biormediation can be highly dependant on the permeability of the soil. It has ben futher investigated that the treament conditions are dificult to control, due to difficulties in nutrient delivery and maintenance of adequate consortiums and levels o microorganisms. Sufficient mixing may also be a problem, and this is due to these factors that the researchers has discovered that biormediation would take longer in-situ than woulb be expected on the soil-slurry.

Soil Slurry bioremediation technologies

Where the disadvantanges of in-situ bioremediation out weigh the advantges, the soil slurry treatment is always considered as the preferred bioremedition technique. The greatest advantage of the soil-slurry treatment is that a closer control over parameters can be exercised. Previous researchers have examined that most of the in-situ treatment can also be employed in soil slurry such as bioventing and landfarming. In this case the biocells or bioreacts are used to contain the contaminated soil and treatment manifolds .

Results

Recovery of unexploded ordanance/ explosives in a properly guided procedure is mandatory for the explosive inductries as I can cause significant harm to the environment and human health. The explosive industry is associted with extremely harmful chemicals in their waste streams, hence it becomes necessary to properly recover those unexploded ordance/ explosives to avoid any physical harm to the environment and human health. From the interviews that were conducted with employees at the ballistic testing range that are responsible for recovery, it has been identified that lamost 95% of the responded perceive the recovery of unexploded explosives to be performed in a proper way with 5% of respondents indicated that they were uncertain.

The unwanted explosive destruction through open burning and testing of explosives in the ballastic testing ranges contaminates the water in the surrounding areas (Ronen, 2020). As per views of Istvan & Ronen (2020) groundwater is easily contaminated in the areas where explosives are tested. The burning grounds and firing grounds of the explosives ballistic range are the main areas where groundwater is polluted (as observed during the 2020 environmetal monitoring studies). The boreholes which are in close proximity to the burning grounds and shooting points indicated level of lead, iron and manganese. However, the level at the current moment are not too high.

Based on the air quality studies that were done as well in 2020, the air pollution is the main issue that is created from destruction of unwanted explosives and firing of explosives in the ballistic testing range. Air pollution caused by the process of thermal destruction through open detonation of explosives and open burning of unwanted explosives. Joy et al (2016) denotes that the rules and regulations imposed by the air quality officers have reduced the air pollution from ballastic testing ranges. The results of the evalution of the air quality monitoing, indicated that the ballstic testing range were in compliance with the condition of the NEMAQ and are in process of applying for the Atmospheric Emissioon Licence (AEL). Changes in air quality due to explosives destruction and firing is, thus, not currently cause of concern as it is being monitored. Therefore, no environmental degradation and human health issues were ruled on the air quality.

Based on the soil contamination study that was conducted in the ballistic testing range, the soil had a high concentration of the 2,4,6-trinitrotoluene (TNT) 10 000mg/kg of soil and meduim level contamination of RDX 1900 mg/kg and HMX 900mg/kg of soil. The results indicated that the soil slurry under co-metabolic condition with molasses as co-sustrate has the potential to remove TNT more effectively than in-situ method. TNT removal efficiency is guarantide at 99% in the soil slurry reactor compared to 82% in the in-situ after 182 days. HMX and RDX, the potential removal was observed from the soil in both methods (soil slurry and in-situ)., but the removal efficiency is predicted to be very low. The examined that the soil microbes mineralize the TNT. It was anticipated that the mass balance of

TNT has a ptential to indicate 23.5% of TNT miniralized to CO(2), 22.6% converted to biomass, and 53.3% converted to various TNT intermediates in the soil slurry reactor. The study reveals that both methods maintained high bacterial population fairly well.

Burning grounds need to be maintained in order to ensure that the successful destruction of unwanted explosives and to prevent pollution to the water course nearby. Explosives indcustries/ ballstic testing ranges should work closely with local authorities and fire departments to verify any additional requirements, which may apply to a specific area to esnure the safety of human beings.

Continous monitoring on ground water and air quality should be performed to monitor the possible effects of destruction and firing of explosives on ground water and air quality. Continous ground water and air quality monitoring will ensure that the testing ranges are in position to identify any potential sources of water pollution. The results of this desktop study are promising with regard to transferring the technology to full scale application in one of the ballistic testing ranges.

References

Akhavan, J. 2011. *The chemistry of explosives*, Royal Society of Chemistry.

Alverbro, K., Björklund, A., Finnveden, G., Hochschorner, E. & HägvalL, J. 2009. A life cycle assessment of destruction of ammunition. *Journal of hazardous materials,* 170**,** 11011109.

Clark, B & Boopathy, R.2007. Evaluation of bioremediation methods for the treatment of soil contaminated with explosive in Louisiana Army Ammunition Plant. *Journal of hazardous materials*, 143 (3):643-8

Coulson, N. 2018. The role of workplace health and safety representatives and the creeping responsibilisation of occupational health and safety on South African mines. *Resources Policy,* 56**,** 38-48.

Duijm, N. J. & Markert, F. 2002. Assessment of technologies for disposing explosive waste. *Journal of hazardous materials,* 90**,** 137-153.

Eom, T., Chaiprapat, S. & Charnnok, B. 2019. Enhanced enzymatic hydrolysis and methane production from rubber wood waste using steam explosion. *Journal of environmental management,* 235**,** 231-239.

Fuller, M. E., Lowey, J. M., Schaefer, C. E. & Steffan, R. J. 2005. A peat moss-based technology for mitigating residues of the explosives TNT, RDX, and HMX in soil. *Soil & sediment contamination,* 14**,** 373-385.

Investigation into a Surrogate Test System for Kinetic Energy Less Lethal Projectile Validation

[1]Philip Roach and [1]Winnie Pelser

[1]*Defence & Security, Council for Scientific and Industrial Research, Pretoria, South Africa*

wpelser@csir.co.za

Abstract

Non-lethal or less-lethal weapons are designed and developed to minimize permanent injury or death, repel, or dissuading belligerents to continue with their selected course of action by inflicting pain and/or temporarily incapacitating the individual or target group. There are weapons, which are 100% lethal, but thus far unfortunately there are no weapons, which are 100% non-lethal. Non (or less)-lethality is dependent on the inherent nature of the weapon, the way a weapon is used and the vulnerability of the opponent or equipment [1]. As different parts of the body differ in vulnerability, and because people vary in physiology, any weapon powerful enough to incapacitate may be capable of killing under certain circumstances. Thus "less-lethal force" does have some risk of causing death: in this context "less-lethal" means only "not intended to kill or permanently injury" [2]. This aim of this paper is to investigate ways of testing kinetic energy less-than-lethal projectile (KELTLP) weapon ammunition in a reliable and repeatable way using materials that closely replicate human skin and soft tissue.
The paper include a literature study investigating international methods for such an approach and to find possible test methods for application against civilians during riots or unrests in South Africa. The most viable solution is with materials available in South Africa, and the process to identify these will be described.

Keywords— Quantifying injury risk of non-lethal projectiles, Surrogate Test System, Skin surrogates, Soft tissue surrogate, less than lethal, kinetic energy.

Introduction

Non-lethal or less-lethal weapons are designed and develop to minimize injury or death, repel, or dissuade people ‘low probability’ and ‘unnecessary suffering’. There are weapons, which are 100% lethal, but thus far unfortunately there are no weapons, which are 100% non-lethal. Non (or less)-lethality is dependent on the inherent nature of the weapon, the way a weapon is used and the vulnerability of the opponent or equipment [1].

As different parts of the body differ in vulnerability, and because people vary in weight and fitness, any weapon powerful enough to incapacitate may be capable of killing under certain circumstances. Thus "less-lethal force" does have some risk of causing death: in this context "less-lethal" means only "not intended to kill or permanently injury" [2].

This aim of this study is to investigate ways of testing kinetic energy less-than-lethal projectile (KELTLP) weapon ammunition in a reliable and repeatable way using materials that closely replicate human skin and soft tissue.

In the document, “Test Methodologies for the Assessment of Less-Lethal Kinetic Energy Rounds” by Wayne State University they strived to formulate a testing methodology by which less-lethal kinetic energy munitions can be assessed. The intent was to determine whether the blunt and penetrating trauma risks are appropriate [3].

Literature Study

According to Kuhne and Papi [1], animal tests are inferior to a good simulant, because a less than lethal projectile impact on tissue has no special effects. Tissue is inhomogeneous and often gives irreproducible results. A good simulant is homogeneous because it allows experiments to be repeatable and reproducible. Simulants should be practical, and available at an acceptable cost. The most difficult requirement though is that of dynamic equivalence of simulant to tissue. The biomechanical response of the body has three components: (a) inertial resistance by acceleration of body masses, (b) elastic resistance by compression of stiff structures and tissues, and (c) viscous resistance by rate-dependent properties of tissue.

Less-lethal kinetic energy test standard

The document "*Test Methodologies for the Assessment of Less-Lethal Kinetic Energy Rounds*" [3], is based on the Draft National Institute of Justice (NIJ) less-lethal kinetic energy test standard. The goal of this research was to develop a testing methodology for the evaluation of less lethal kinetic energy munitions. Two key aspects of testing were proposed including performance of the round (accuracy) and injury risk (blunt and penetrating). The parameters evaluated include accuracy, precision, penetration, and the Viscous Criterion (VC).

Viscous Criterion (VC) – "An injury criterion empirically derived to correlate impact to severity of injury. The VC is calculated based on the amount of sternal deflection and the velocity at which the deflection occurs. VC has been validated as a useful tool in determining injury severity related to blunt ballistic impacts" [3].

The evaluation of potential testing surrogates was included in the study. Key considerations included applicability and feasibility of the testing techniques. Testing was conducted to determine if a proposed methodology provided the expected results [3]. Various surrogates have been identified for use in a possible standard. A new system for monitoring deflection in the surrogate, called 3-Rib Ballistic Impact Dummy, has also been included. This is a test rig developed by Wayne State developed to establish a lethal impact, and not commercially available [4].

The draft NIJ less-lethal kinetic energy test standard (Wayne State University) calls for the munition to be assessed using three tests:

- Accuracy and precision (impact characteristics evaluated at 5 m and 15 m),
- Blunt trauma (risk of injury to the bony thorax and the underlying soft tissues evaluated at 1.5 m), and
- Penetration (risk for the round to penetrate the skin evaluated at 1.5 m) [3].

The North Atlantic Treaty Organization (NATO) approved the Allied Engineering Publication (AEP) "*Skin Penetration Assessment of Non-Lethal Projectiles*", to quantify the skin injury risk of non-lethal projectiles [4]. This document considered two methods to be applicable for the aimed risk assessment method. One method is based on a skin simulant where actual damage to different skin layers resulting from an impact by a non-lethal projectile is used as penetration criterion. The second method is based on the maximum force applied to a "rigid wall" (blunt trauma) by a non-lethal projectile as an injury criterion. The maximum contact force correlates to injury severity [5].

Penetrating trauma and measurement

Three classical experimental evaluation methods exist, i.e. (a) clay back face impact tests, (b) ballistic Gelatin tests, and (c) biomechanical surrogates (crash dummies) tests.

(a) **Clay back face impact tests**

The Chavant company produce Roma Plastilina No 1 which is used in these tests. A whole ballistic impact rig can by procured for this purpose where the projectile displacement of the clay material is measured to determine 'Go/No-Go suitability.

(b) **Ballistic Gelatin tests**

This method of testing appears to be extensively used by law enforcement (Forensic Laboratories) and in Academia for kinetic projectile analysis. It a messy method of evaluation due the preparation.

(c) **Biomechanical surrogates**

Anthropomorphic test devices are expensive and could be prone to damage from the kinetic projectile impacts. A sacrificial polymer membrane could be placed over the impact area to distribute the force, but this would call for recalibration and a factor to be applied.

The risk of penetrating trauma is important to assess due to the increase in severity of injuries seen once the munition penetrates the body cavity. One factor to consider is the amount of energy generated by the munition. One factor to consider is the amount of energy generated by the munition. In addition, it is important to determine the energy per area of presentation ratio (E/a value). Other papers use the term "Energy Density" (Ratio of kinetic energy to the area depending on whether the round is flexible or not) which has the same units of "J/cm^{2}". The current tolerance for penetration is based on the region of concern on the body. Recent research has demonstrated various E/a required to produce a 50% risk of penetration for various regions of the body [3]. See Table I.

TABLE I. RISK OF PENETRATION FOR VARIOUS REGIONS OF THE BODY [6]

Location	50% Risk (J/cm^2)
Skin	24
On Anterior Rib	23.99
Between Anterior Rib	33.30
Liver	39.88
Lateral to Umbilicus	34.34
Proximal Femur	26.13
Distal Femur	28.13

The 3-Rib-Ballistic Impact Dummy (3RBID)

Prof Bir, *et al* from Wayne State University [3], developed the 3RBID for testing acceleration of the chest wall or sternum area by less lethal projectiles and vehicle impact studies.

The 3-Rib-ballistic impact dummy (3RBID) consists of a modified side impact dummy with extra polyurethane damping pad and a neoprene coat. The system is equipped with a RibEye deflection measurement system, allowing to measure the 3D displacement of the 3 ribs with a 20-kHz frequency. Due to reliability issues when undergoing ballistic impacts, additional modifications are added here, replacing the RibEye measurement system by a single axis PCB200C20 accelerometer screwed on the central rib. Additionally, the modified 3RBID is laterally fixed on a rigid structure, instead of placing it horizontally allowing to measure the inner displacement of the ribs using a high-speed camera. This second measurement is used to validate the accelerometer measurement [7]. Refer to **Fig. 1**.

The 3RBID is not a Commercial-Off-The-Shelf (COTS) product and will not be available for the CSIR to use. A testing methodology is purposed that will allow for objective evaluations to be made for

currently manufactured rounds prior to deployment. The 3RBID was intended for use to measure trauma in vehicle accidents.

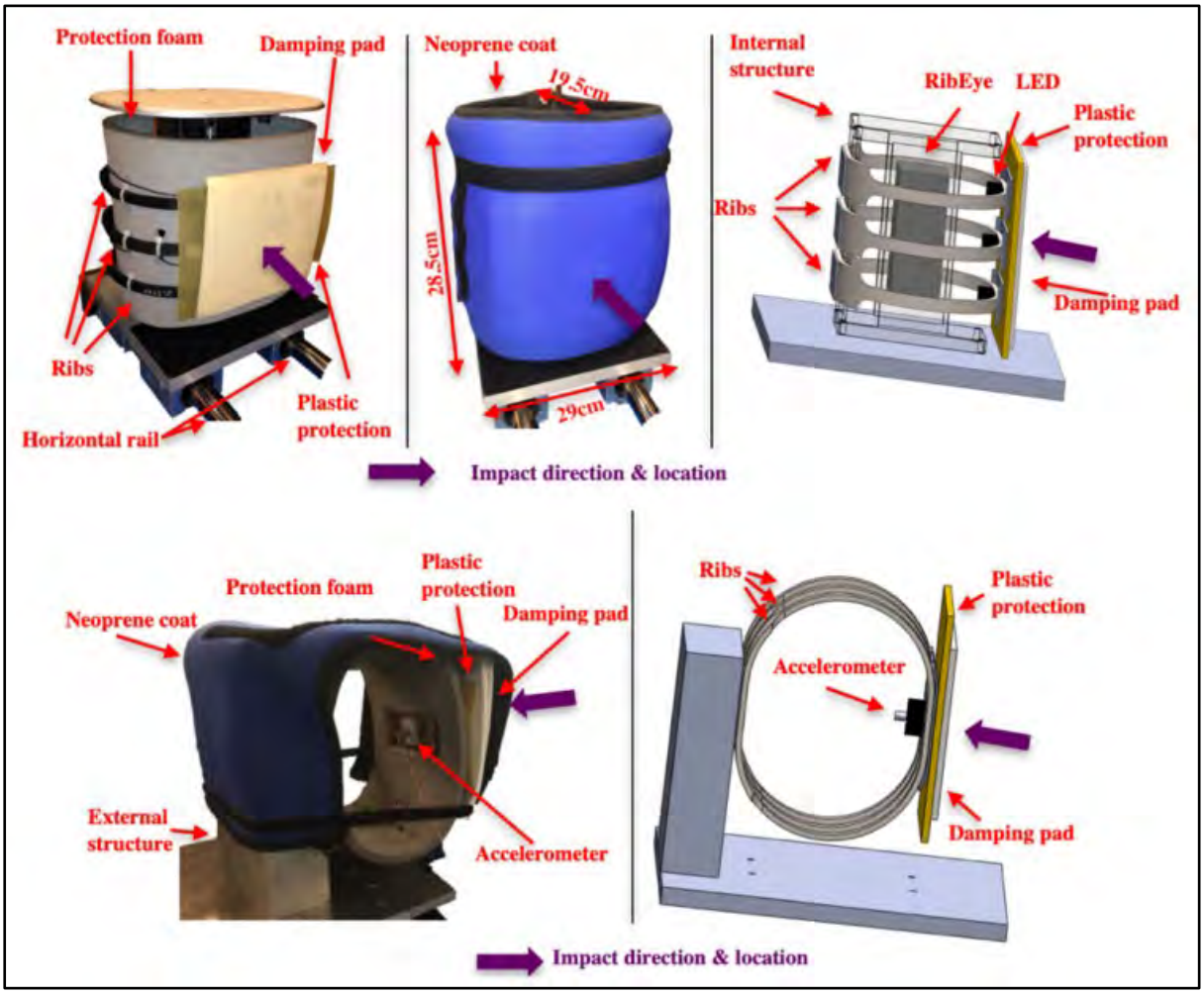

Fig. 1: 3RBID dummy [7]

Force Sensor, The Rigid Wall

As described in the NATO Standard AEP-94, the skin's mechanical resistance depends on its structure, the network of fibres, the point of impact, age, and fundamentally on the strain and strain rate during a blunt ballistic impact. Research carried out over the past few years on the critical stress induced by blunt impacts required to cause damage to the skin show that the mean value of this stress is less than10 MPa (see No 1 and 2 in Figure 2) [4].

If the mean value (V_{50}) is 10 MPa, then the maximum value for penetrations should be used as a threshold to ensure that the “less-than-lethal” definition is abided by.

The purpose of the rigid wall method of testing is to verify that this critical stress is not reached for any given projectile. This ensures that the skin is not perforated during the impact, regardless of the speed of impact and of what part of the body the projectile might strike [4].

The rigid wall is a method for measuring force and cross-sectional area during the impact of a less lethal projectile against a rigid wall [4].

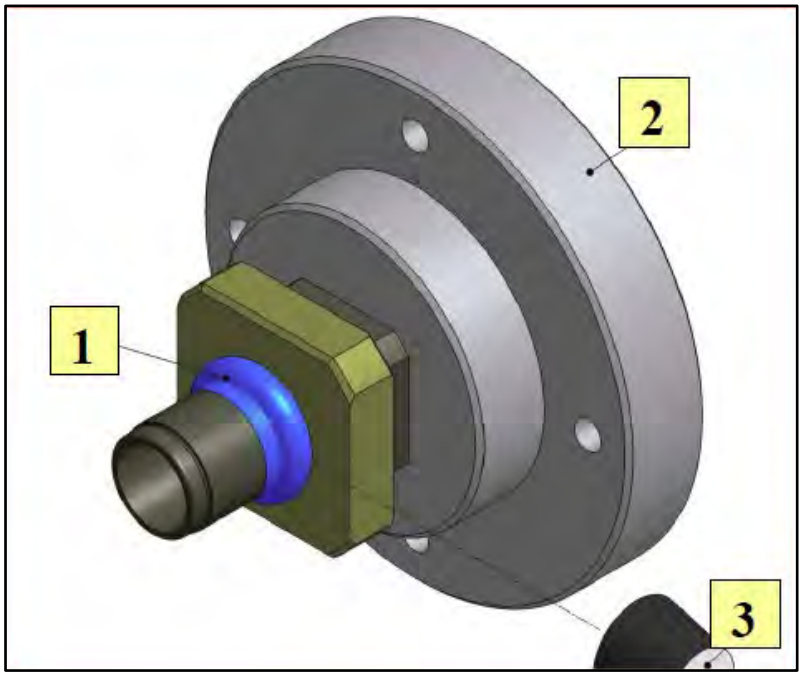

Fig. 2. Method for measuring force and cross-sectional area during the impact of an NL projectile against a rigid wall [4]

Robbe, Pappy and Nsiampa [7] describes a “rigid wall” that consists of a force sensor (Kistler 9061a) (1), fixed on a 300 mm× 65 mm aluminium cylinder (2), using an aluminium “impact pad” (3), and a washer and nut (4). The cylinder is supported on a steel beam structure. The sensor allows measuring the impact force as a function of time and the consequent maximum force.

The rigid wall is not considered as a biofidelic surrogate used to perform injury prediction. Using this rigid wall implementation with such impacts requests the use of dedicated post-processing filters, to attenuate the effect of the resonance frequency of the structure [7]. Refer to Fig. 3.

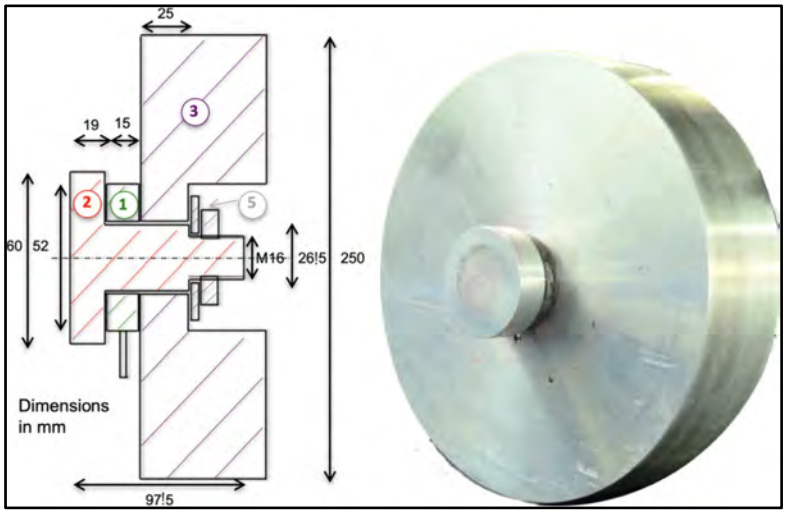

Fig. 3. The rigid wall mechanical assembly [7]

Tissue Surrogate

The internal component of the surrogate used to assess the occurrence of penetration is composed of Ballistic Gelatin. Usually 10 or 20% (weight) is used to evaluate penetrating impacts.

One of the major limitations of using ballistic Gelatin as a tissue simulant is procedural differences among researchers. As early as the mid-1980's, researchers at the Letterman Army Institute of Research began publishing papers in professional journals based on their model for ballistic research and, on the work of Dr. Martin Fackler. Fackler established one standard, 10% Gelatin cured at 4°C [8].

Others such as NATO use 20% concentrations of Gelatin at 10 °C and the Federal Bureau of Investigation (FBI) recommend a 10% formulation at 4 °C.

According to Maiden, et al, in an article titled "*Ballistics ordnance Gelatin – How different concentrations, temperatures and curing times affect calibration results*" [9], neither of the NATO 20% concentrations of Gelatin at 10 °C, or a 20% concentration of 285 Bloom Gelatin at 10 °C, met the same calibration standard as the FBI recommended 10% formulation at 4 °C. A 20% concentration of 285 Bloom at 20 °C met the same calibration/ penetration criteria as a 10% concentration of 250 bloom at 4 °C after 100 h of curing. Therefore, it can be classed as matching the FBI calibration standard for a soft tissue simulant for wound ballistics research [9]. The 10% formulation at 4 °C is easier and does not require such a long curing time.

In the study "*Kinetic Non-lethal weapons*" Koene, Papy and Id-Boufker regard 10% Gelatin better for penetrating impacts [1].

In their study, Maiden, et al, compared results using three different water types and curing times. Between curing times of 21 hours, 100 hours and three weeks and tap water, de-ionised water, reverse osmosis water of 10% ordnance Gelatin at 4 °C, and de-ionised water at 3 °C no significant difference was found. When testing (calibrating) 20% ordnance Gelatin at 10 °C using tap water, and de-ionised water, there was a significant difference between curing time of 21 hours and 100 hours. There is a significant difference between the FBI formulation and the NATO formulation [9].

Physical preparation of the Gelatin may cause variations. Methods have used cold or hot water to dissolve the powdered gel. Heating the gel above 40°C weakens gel strength and viscosity (Fackler). Some methods are not concise. Gelatin used at 10 °C is often taken from the refrigerator and allowed to "warm up" to 10 °C, not accounting for differences in temperature from the outside to the inside of the block. It is important to calibrate tissue simulants [8].

Koene and Papy described three classical experimental evaluation methods of the biomechanical response to impact. These are clay back face signature tests, ballistic Gelatin tests and biomechanical surrogates (e.g., crash dummies) tests. According to them clay is good to evaluate body armour. They prefer the use of Gelatin as a soft tissue simulant. Specifically, they consider 10% Gelatin to be better for penetrating impacts [9].

The document, "*The use of Gelatin in wound ballistics research*", quote the following: "Bullet muzzle velocity is often quoted, but it is arguable that the impact velocity at the target is more useful especially when considering the development or overmatching of personal protective equipment (PPE). Impact velocity can be equated to an estimated engagement distance" [10].

A big issue for using Gelatin blocks for ballistics testing is the fact that they are only good for one shot. As a result, some researchers find using Gelatin time consuming and expensive. Additionally, the user must still interpret the data collected from wound profiles to determine projectile efficiency or lethality.

Human Skin Surrogate

For experimental terminal ballistic research good simulants for human skin must be used. The three materials that the investigation returned are: Natural Chamois leather; car inner tube and a thermoplastic polyurethane film (tuftane).

According to Koene and Papy, skin resistance should be considered [11].

The "*Skin Penetration Assessment of Non-Lethal Projectiles*" NATO AEP 94 document suggest the use of two layers as skin substitute. The first layer is 6 mm closed cell foam and the outer layer natural chamois, but its thickness should be recorded. The optimum thickness chamois is 1.39 mm (1.15 to 1.80mm) [4].

Bir *et al*, tested several materials for the surrogate skin, such as chamois, leather, 0.6 cm foam, 0.93 cm foam, 48 to 64 kg/m^3 foam and 112 to 128 kg/m^3 foam. The best is an outer layer natural Chamois and inner layer of 6 mm thick closed cell foam [4]. This is per the NATO AEP 94 Standard, above.

The NATO STANREC committee on blunt impact kinetic energy non-lethal weapon (Defence Research and Development Canada), has identified two major limitations with the surrogate proposed in the draft NIJ standard to assess the risk of skin penetration.

First, the inherent variability of the natural chamois is not desirable for a test standard where consistency and repeatability is critical.

Second, the use of a foam sheet complicates the analysis of penetration with the addition of an intermediate layer between the chamois and the ballistic Gelatin. Experimental trials were conducted to identify an alternative material to replace the natural chamois and to remove the foam layer of the current NIJ skin-soft tissue surrogate (Anctil, 2013).The alternative surrogate skin is one layer of a thermoplastic polyurethane film (400 µm thick) that provides similar penetration limits (V_{50}) to the natural

chamois currently specified in the NIJ draft standard. In addition, it was found that the foam layer of the NIJ skin-soft tissue surrogate can be removed without affecting the penetration limit (V_{50}) obtained when using the thermoplastic polyurethane film as the first layer (Tuftane grade TFL-1EA 400 µm). The findings of this study suggest that the surrogate can be modified to simplify the setup and analysis techniques while providing similar outcomes [12].

Koene and Papy in the document "*Towards a better, science-based, evaluation of kinetic non-lethal weapons*" emphasised the necessary to include skin in the model. They concluded that fresh abdominal pigskin of 3 to 4 mm thickness has been shown to give the most comparable results but is not practical [11]. They suggest the use of car inner-rubber tube of 1.3 to 2.0 mm thickness gave the next best results. This material is easy to obtain and offers no difficulties in storage.

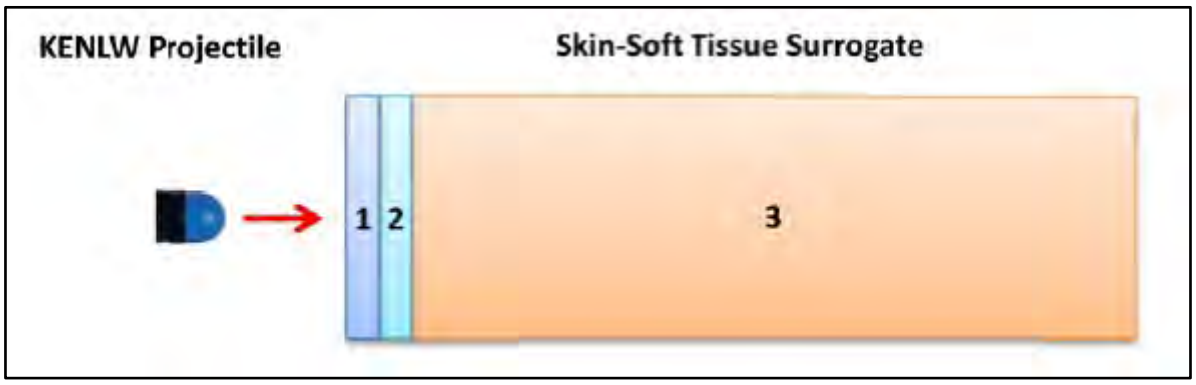

Fig. 4. Skin penetration schematic test setup [12]

Methodology

Accuracy / Precision Testing Methodology

The accuracy testing phase utilized a universal receiver to mount the 12-gauge barrel. A paper target containing a bull's eye and grid marks was mounted down range at distances of 5 m and 15 m. After each impact, the target was replaced, and key-testing information recorded. X and Y coordinate data was measured from the point of impact to the axis using digital callipers. They shot 10 rounds with each round at each distance. To measure accuracy, the distance from the centre point is measured for each shot. [3]. For the CSIR tests a 12-gauge shotgun was used at 10 m and 20 m increments.

Energy Density of the different rounds is calculated from the projectile cross-sectional area, mass, and velocity.

Gelatin block sizes

Fackler preferred using blocks 25 x 25 x 50 cm [8]. The suggested FBI Block size is 16 x 16 x 40 cm [13]. Anctil in the document *KENLW Testing Methodology* suggests a block size of 10 x 10 x 30 cm [12]. (This is in line with the draft NIJ penetration standard).

In the document "*Definition of a standardised skin penetration surrogate for blunt impacts", Papy et al as well as the NATO Standard AEP-94 describe the use a Gelatin cube with an edge length of* 25 cm [4] and [6].

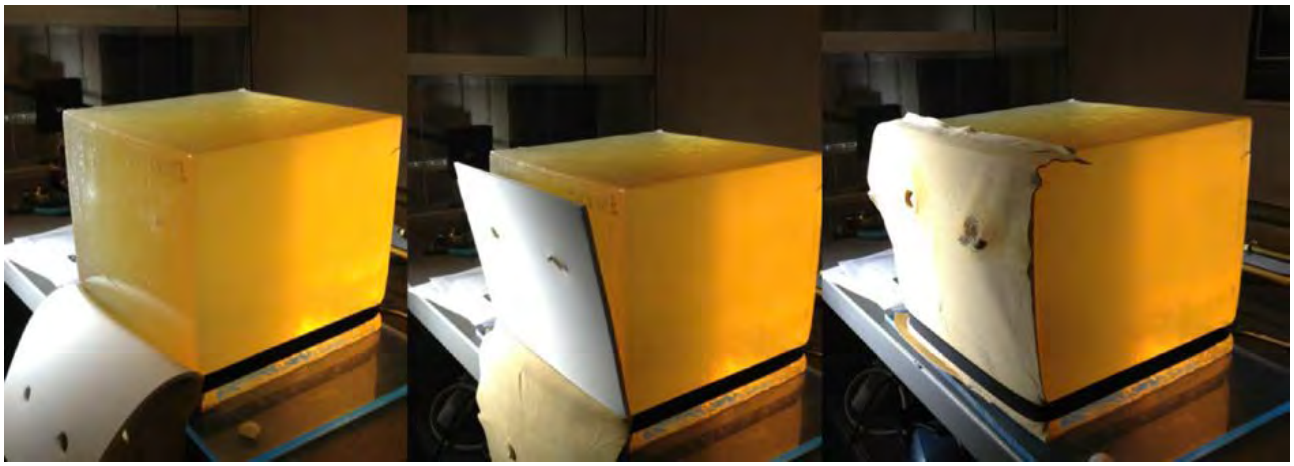

Fig. 5: Surrogate construction [4]

Prof Rian Stopforth from the University of Kwa Zulu Natal described a method of producing a ballistic Gelatin block in the R&D Journal of the South African Institution of Mechanical Engineering [14].

Surrogate setup examples

Different methods can be used to adhere the surrogate skin to a Gelatin block. Bir *et al* used metal clips attached to elastic straps. Refer to **Fig. 6**. For 9 mm and 5.56 mm testing, the longer 400 mm blocks shall have to be produced and placed end-to-end.

Fig. 6. Test setup for evaluation of skin and tissue surrogate materials [5]

A similar setup is shown in Figure 7.

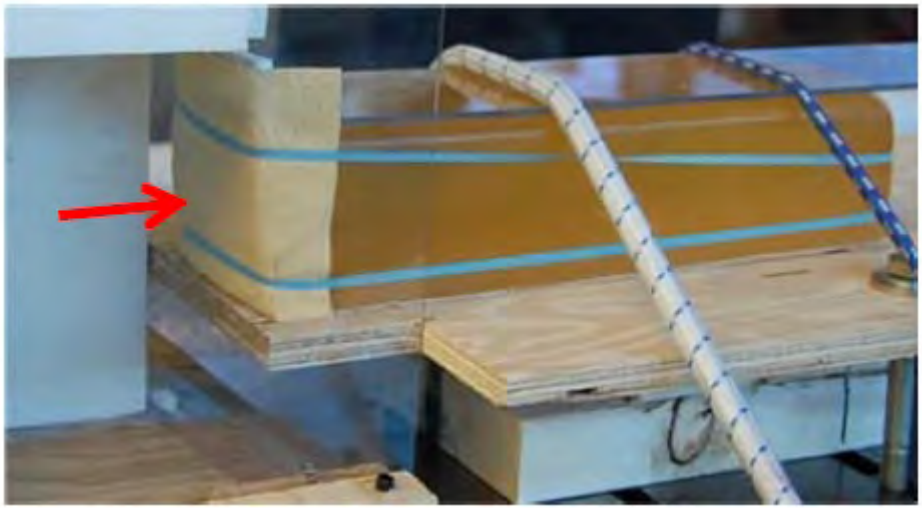

Fig. 7: NIJ skin soft tissue surrogate [12]

Calibration of Gelatin blocks

Fackler was the first researcher to introduce calibration into 10% ordnance Gelatin testing. They suggested a series of penetration tests using calibre .177 (4.5 mm) steel BBs at a velocity of 180 ±4.5 m/s. The calibration method outlined was later adopted by the FBI as their standard [9]. The acceptable penetration depth is 84 mm, ±10 mm. The Gelatin was placed 3 m from the muzzle of the test weapon [13].

Prof Papy describe that on a three layers surrogate (ballistics Gelatin, foam, chamois skin) the Gelatin block must be checked for the presence on cracks after impact.

Anctil, describe a similar method of calibration for 20% Gelatin. They also describe the use of a copper plated 0.177 calibre BB projectile traveling at a velocity of 179 m/s (± 4.5 m/s). The BBs are fired from a distance of 3 m. Due to a lack of calibration requirements for 20% Gelatin, a penetration depth of 38.1 to 76.2 mm would be used as an acceptable pass/fail range. Calibration will be completed for each Gelatin block used prior to the test sequence [12].

Maiden *et al*, in an article in, "*Ballistics ordnance Gelatin – How different concentrations, temperatures and curing times affect calibration results*", came across the following conclusions: [9]

- Temperature and curing times directly affect Gelatin projectile penetration.
- Penetration results are not affected by different water types during manufacture.
- The best consistency for shooting is Gelatin with Bloom Number between 250 and 300. Consistency may be determined not only by the Bloom Number but also by the concentration and temperature of preparation.
- A 10% w/w concentration of 250 Bloom Type 'A' Gelatin at 4 °C is widely accepted as an equivalent human soft tissue simulant based on porcine penetration tests conducted by Fackler and Malinowski.

Results

The manufacture of the Ballistic Gelatin Blocks (BGB) and subsequent calibration with the Daisy BB rifle using a 4.5 mm steel spherical pellet with an averaged velocity at ~5 m of 598 fps with seven pumps. The penetration must fall between 74.3 to 94.3 mm, the red-dotted line indicates the 94.3 mm threshold (Fig. 8).

A velocity of 596 fps resulted in pellet penetration of ~108 mm, 14 mm over the 94 mm upper threshold (Fig. 8).

The 10% BGBs therefore failed the accepted depth criterion.

Fig. 8: BB Pellet depth of 112 mm at a velocity of 598 fps

Seven compression pumps of the Daily BB rifle resulted in the majority of five out of six BB 4.5 mm steel pellets velocities falling within the minimum/maximum criteria. The slowest velocity with seven pumps was 596 fps and the maximum, 610 fps.

The Gelatin block concentration was changed to 15% with a curing time of 5 days. The Gelatin block was 5 kg. 4.5 mm pellet was shot into the BGB from 3 m. The pellet penetration was 82.3 mm with a velocity of 614 fps. This falls in the threshold for the Gelatin block calibration. Velocity would be lower at 10 m. The result is shown in Fig. 9.

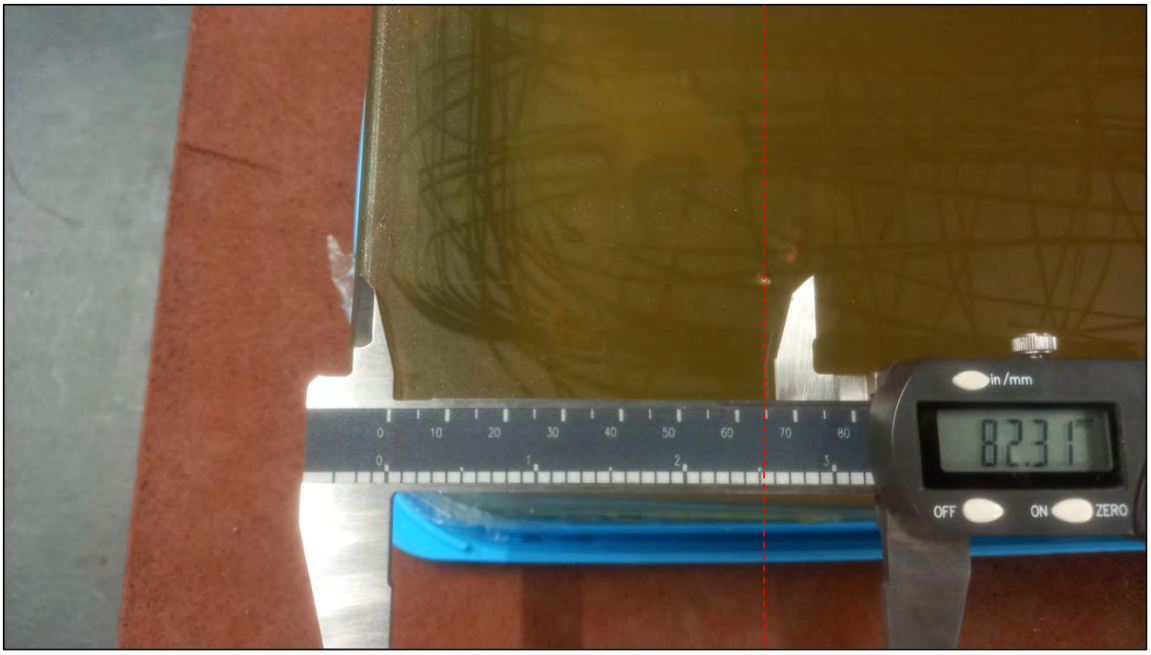

Fig. 9. BB Pellet depth of 82 mm

A double layer of Chamois leather was placed over the BGB providing a thickness of 1.1 mm.

Koen *et al* state “a Chamois thickness of 1.39 mm” [15].

Beanbag Projectile Test: The Beanbag impacted the Chamois at less than 68 m/s and left a 5 mm deep imprint in the leather with a spherical imprint in the BGB, refer to the lower left-hand side (LHS) in **Fig. 10**.

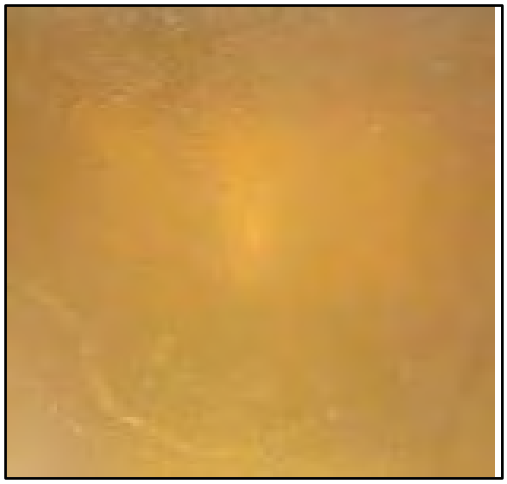

Fig. 10. Beanbag impact through Chamois

Rubber Projectile Test: The Rubber projectile penetrated through the double Chamois layer, 43 mm into the Gelatin at a muzzle velocity of 269 m/s, but this was reduced at the 10 m distance (**Fig. 11**).

Fig. 11 Rubber projectile penetration through 1.1 mm Chamois (LHS) and into Gelatin Block

Discussion

For more representative evaluations, pertaining to KELTLP ammunition effects on human bodies, a human skin and soft tissue substitute is a requirement. A human skin substitute in front of a 10% Gelatin block (soft tissue representation) should be employed in KELTLP ballistic testing analysis. The skin substitute replicates the tensile resistance offered by human skin prior to projectile penetration of the soft tissue area.

Ballistic Gelatin: A ratio of 1:8 (Gelatin:water) will likely yield the desired density and viscosity according to a SAPS Plattekloof Forensic source. They also use the calibrated clay block method of analysing projectile impacts. This facility use radar to verify their ballistics and stated that the BB Air Rifles velocity must be checked as it decreases from the first shot due to heat build-up (friction).

Gelatin can be difficult to prepare properly, and uncalibrated Gelatin will give incorrect results. For example, if too much heat is used during its preparation, it will become weak and excessively flexible, producing erratic experimental results [9].

Disadvantages of Ballistic Gelatin are the following:

- It is labour-intensive to prepare, store, transport and maintain during testing.
- The organic Gelatin must be carefully prepared to obtain the proper density and viscosity and stored at a low temperature of 4 °C for ~40 hours.
- Must be shot while the Gelatin is still cold.
- The Gelatin must be calibrated to ensure reliable results
- The Gelatin deteriorates quickly, is temperature sensitive and can be messy to work with.
- Disposal may also prove to be a problem if made and used on the CSIR premises.

Various parameters were suggested for future investigations to assist in determining the optimum formulation for the Ballistic Gelatin test block composition (density and viscosity). If the BGB passes calibration, that is primary and the method, secondary.

McPherson indicates that overpenetration is not uncommon due to batch differences and suggests that the following can be undertaken to reduce penetration to within the accepted depth: [9]

- Lower Gelatin temperature from 4 to 3 ^{o}C.
- Prepare the Gelatin concentration at 11% (or more), instead of 10%. 15% concentration will reduce penetration by approximately 10 mm.

It was found that increased curing time (up to a maximum of three weeks) provided penetration results closest to the required standard [9].

The sourcing of a company to manufacture the Ballistic Gelatin Blocks to a set recipe has not been successful.

An alternative option is to procure the necessary industrial mixer to allow 30 to 50 litres of Gelatin to be mixed in one go to prevent inconsistencies creeping into the manufacture if small batches are produced at the CSIR, Landward Sciences. Refrigeration and additional equipment shall also have to be procured.

Skin surrogate: Pigskin due to the challenges of OHS and ethics as used by the SAPS Forensic laboratories is not an ideal option. Though it is useful to note that tests performed on pigs, resulted in the data where the penetration of the steel spherical projectile was within 3% of the calibrated ballistic Gelatin. [8].

The skin surrogate threshold is ~24 J/cm^2, the penetrations quoted by Prof Bir for car impact trauma (Table 2) where more severe than the energy density figure (~24 J/cm^2) for human skin. The skin surrogate requires only one layer of either natural Chamois or car inner tube. Natural Chamois is becoming scarce and a material such as the car inner tube is easily obtainable and simple to use. In the DRDC paper [12], it was stated that the closed-cell foam layer does not contribute to the required skin resistance.

Kinetic Energy LTL Projectiles: Users of KELTLPs have no control over manufacturer's production methods viz. changes to the projectile's mechanical properties or propellant charge will influence subsequent terminal ballistic behaviour of the projectile on a human being. If the manufacturer modifies certain characteristics of its projectile or cartridge, the effect on the reproducibility in tests or in operational use could be 'problematic'.

Force sensor: a "Rigid Wall", force sensor is an alternative method of testing the KELTL projectiles. This apparatus is a 'cleaner' method of evaluating KELTL projectile products. If the force sensor registers a force exceeding 10 kN, at which the strain rate of human skin is exceeded, the KELTLP product fails. It must be noted that the 10 N threshold is the *mean*, and this should be perhaps increased to a V_0 test i.e., no penetrations allowed. The authors could not get assistance in identifying and assembling a Force Sensor Apparatus.

Surrogate Skin/Ballistic Gelatin: BG test blocks were manufactured at Landward Sciences for evaluation and calibrated with a Daisy BB rifle using a 4.5 mm steel spherical pellet. [*The Gelatin must be calibrated by the user (by firing a 0.177" steel BB into the Gelatin at a velocity of 590 ±15 fps and checking for penetration depth between 2.95 – 3.74 ") immediately before it is used and is rejected if it fails*.]

Conversion to metric: minimum/maximum depth:

Velocity: 575 to 605 fps or 175.26 to 184.40 m/s

Depth: 2.95 – 3.74" or 74.34 to 94.25 mm

Conclusion

The Test Methodology described below should be sufficient for testing KELTP rounds for safe use with shotguns to use against humans in riot situations. Care must be taken in training and use not to shoot at facial areas.

Suggested Test Methodology

To get repeatability for tests the following is suggested:

- Measure velocity for each shot using a chronograph or Doppler Radar Chronograph.
- Do precision tests at 10 m, 20 m, and 30 m.
- Calibration of the Gelatin block to fall within the accepted tolerance.
- Evaluation in a 15% calibrated Gelatin block covered with skin surrogate for confirmation of penetration risk should be pursued.
- Decision on the suitability for the specific KELTLP round.

The ideal situation for the CSIR would have been the collaboration with a certified laboratory which could manufacture the BGBs to meet the required procedure necessary to pass calibration.

References

[1] Koene Bart, Papy Alexandre, Id-Boefker Fatiha, "Kinetic Non-lethal Weapons p 9-24," Netherlands Annual Review of Military Studies, 2008.
[2] UN Peacekeeping PDT Standards, "Less Than Lethal Weapons," UN Peacekeeping PDT Standards for Formed Police Units, 2015.
[3] Wayne State University, Test Methodologies for the Assessment of Less-Lethal Kinetic Energy Rounds, 2011.
[4] NATO Standard AEP-94 Skin Penetration Assessment of Non-Lethal Projectiles, 2013.
[5] Bir, C. A., Resslar, M., & Stewart Wayne, S, Skin penetration surrogate for the evaluation of less lethal kinetic energy munitions. (Forensic Science International Volume 220, Issues 1–3, 2012, Pages 126-129).
[6] Papy, Alexandre; Robbe, Cyril; Nsiamp, Nestor; Oukara, Amar; Goffin, Julien, Definition of a standardized skin penetration surrogate for blunt impacts, IRCOBI Conference 2012.
[7] Robbe, Cyril; Papy, Alexandre; Nsiampa, Nestor, Toward a Reference Non-Lethal Projectile to Validate Blunt Trauma Injury Evaluation Models, 2019.
[8] Nicholas, NC; Welsh, JR, Ballistic Gelatin Literature Review. (Institute for Non-Lethal Defense Technologies Report, Applied Research Laboratory Pennsylvania State University), 2004.
[9] Maiden Nicholas R., Fisk Wesley, Wachsberger Christian, Byard Roger W, Ballistics ordnance gelatine – How different concentrations, temperatures and curing times affect calibration results. Journal of Forensic and Legal Medicine, 34, p 145-150, 2015.
[10] Carr D. J., Stevenson T., Mahoney P. F, The use of gelatine in wound ballistics research. International Journal of Legal Medicine, 132, 1659–1664, 2018.
[11] Koene, L., & Papy, A, Towards a better, science-based, evaluation of kinetic non-lethal weapons, 2011.
[12] Anctil, B, Kinetic Energy Non-Lethal Weapons Testing Methodology: Skin Penetration Assessment, DRDC Valcartier CR; Defence R&D Canada – Valcartier. (Defence Research and Development Canada), 2013.
[13] FBI Test Protocol (Hornady Manufacturing), 2022.
[14] Stopforth, R, Self-Defence Ammunition Comparison between .22, 9 mmP, .40 & .45 Projectiles, R&D Journal of the South African Institution of Mechanical Engineering, 2020.
[15] Koene B, Assessment of skin penetration of KNL projectiles using surrogate methods, Sept 2014.

Data Cleaning using OpenRefine: A Case of Blast Incidents and Explosives Research Data Extraction from Social Media Platforms

[1]Matshidiso Marengwa

[1]*Defence & Security, Council for Scientific and Industrial Research, Pretoria, South Africa*

mmarengwa@csir.co.za / marengwas@gmail.com

Abstract

The increase in explosive and blast incidents has resulted in the need for a method or tool to help monitor and keep track of said incidents to provide insight into the methodologies and devices used by attackers to develop counter-active measures. The prevalence of social media in society has harnessed the generation of data and information which can be applied by organisations to improve functions and processes which in turn helps aid decision-making. With regards to the field of explosives, more institutions and news outlets have opted for the use of social media and other online platforms to share real-time data pertaining to explosives and blast related incidents and events that occur on a global scale. This study presents a method for extracting and capturing data pertinent to the field of explosives research from social media sites and other online platforms through monitoring and highlighting any blast related incidents, events and trends.

The data used in the paper was collected over a period of 10 months and retrieved and extracted using a predetermined form which specified the type of information that should be mined and processed. The data was then cleaned, visualised and presented using various techniques available on the OpenRefine application. This data then provided insight into, but not limited to questions such as: the most prevalent sources, types of blast incidents or events, the types of devices used; casualties etc.

The results of the study helped improve operations within the unit through enabling the identification and improvement of training efforts by shedding light on the effective methodologies and techniques used by explosives ordnance disposal (EOD) groups. The results of the study also helped compile a list of tope perpetrators and users of explosives; potential suppliers and/or collaborators which can be used if the need prevails and the data regarding the countries with the highest incidents helped to shift the focus on which states to keep track of.

Keywords—blast, data extraction, incidents, data, social media, twitter, explosives

Introduction

The prevalence of social media in society has harnessed the generation of data and information which can be applied by organisations to improve functions and processes which in turn, help aid decision-making. Social media is defined as “online platforms that support the creation and exchange of user-generated content” [6]. Social media is sometimes referred to as Web 2.0 or the Social Web, seeing that it encompasses internet-based applications are a direct manifestation of Web 2.0 technologies [6] and [4]. Social media platforms enable the provision of copious amounts of data that can be retrieved and processed to generate and extract useful information and knowledge that can be used for the betterment of “social, political and economic arenas” [4]. Data generated on social media platforms can be used for the following purposes [6] and [4]:

- Conduct of research
- Recruiting study participants
- Undertaking participative citizen science research studies
- Fostering stakeholder involvement
- Association and pattern recognition
- Predictive analytics
- Trend analysis

The increase in explosive and blast incidents has resulted in the need for a method or tool to help monitor and keep track of said incidents to provide insight into the methodologies and devices used by attackers to develop counter-active measures. A viable method to keep track of explosive and blast incidents in real-time is the use of social media as leads in identifying events that occur around the world. These leads will then be used as a gateway which lead to more online content covering the stories mentioned in identified social media posts. This data/information is then collected and analysed to extract key points which will then be used to conceptualise the modus operandi of the perpetrators and the methodologies used by identified group who specialise in explosive ordinance disposal activities.

The objective of this paper is to determine how social media posts and online content can be used to provide insight into global incidents and potential threats through the provision of information that provides details about the identified blast incidents which is then used to provide a context for the occurrence, thus facilitating its categorisation of explosive and blast incidents. This can in the long term, be used to formulate incident patterns that can then be used to determine/forecast the activities of the perpetrators.

Mining Social Media Data for Defence and Security/Related Work

The mining of social media data for various purposes has become a norm in most industries due to the discovery of the potential and value of information and knowledge that can be extracted and applied from said data. With respect to defence and security, the mining of social media data can facilitate the reporting and monitoring of incidents that occur on a global scale. This paper is not based on the automated extraction of information from social media data using a system, but rather the manual extraction of information and knowledge from online content using predetermined forms/categories. It should be noted that there are various tools and methods of mining, manipulating, and processing data that can be applied to facilitate defence and security activities such as [2]:

- Information retrieval
- Information extraction
- Classification
- Association

- Machine learning
- Statistical methodologies

Using social media data to gain insight into occurrences in the defence and security domain is vital as communication and exchanges on social media platforms occur in real-time thus making the data timely [4]. Another methodology that can be used to mine online generated data for defence and security is crowdsourcing which is defined as “a type of participative online activity in which an individual, an institution, a non-profit organisation or a company proposes to a group of individuals of varying knowledge, heterogeneity, and number, via a flexible open call, the voluntary undertaking of a task” [5]. This method has been applied by the United Kingdom’s (UK) Ministry of Defence (MOD) and has been used in the missions defined in the table I.

TABLE I. MISSIONS DEFINED BY THE MOD IN THE 2015 SSDR (ADOPTED FROM [5])

No.	Mission
1	Defend and contribute to the security and resilience of the UK and Overseas Territories
2	Provide a nuclear deterrent
3	Contribute to improved understanding of the world through strategic intelligence and the global defence network
4	Reinforce international security and the collective capacity of our allies, partners and multilateral institutions
5	Support humanitarian assistance and disaster response, and conduct rescue missions
6	Conduct strike operations
7	Conduct operations to restore peace and stability
8	Conduct major combat operations if required, including under NATO Article 5

The data produced from the social media crowdsourcing initiative facilitated the following tasks and activities undertook by the MOD [5]:

- Increasing awareness of crisis (facilitates situational awareness)
- Assisting short-term prediction in a crisis
- Reducing the level of uncertainty
- Increasing knowledge in areas of command responsibility

Other tools and methods used to aid data mining in defence and security are as follows:

- **Wikistrat**: An analytical services consultancy which makes use of crowdsourcing to improve client awareness through the provision of predictions for military operations US Africa Command and the prediction of activities carried out in the Islamic State (IS) through the analysis of social media data [5].
- **Aggregative Contingent Estimation System (ACES)**: Predictive tool which made use of answers provided by participants, pertaining to certain scenarios as a means of assessing the opinions of the crowd.

Research provides insight into the available tools and methodologies that facilitate the mining of data in the defence and security domain. It further sheds light on how said data can be applied to support and facilitate the execution of tasks and activities in the domain through the data produced by clients, citizens, and volunteers [5].

The data mined in this paper will not only be sourced from Twitter, but also from other online platforms which cover content on diverse topics. This will in turn result in the corroboration of data through trading-it-off with other viable sources of information.

Blast Incidents and Social Media

The rate of explosive and blast incidents has increased over the years. This increase is a result of the socio-economic and political factors that have a direct effect on the situations of countries. This in turn results in there being conflict and wars between disparate parties and groups who take on various measures to either gain or instil power over regimes. These is usually achieved through practicing hostile takeovers which usually result in violent attacks that lead to casualties.

The focus on explosive and blast incidents is a result of the Council of Scientific and industrial Research's (CSIR) Landward Sciences (LS) impact area which entails a research group that conducts research on the following topics:

- Effects of explosives and blasts on structures (i.e., vehicles, buildings, infrastructure etc.).
- Effects of explosives and blasts on the human body (i.e., spine).
- The types of improvised explosive devices used in global incidents.
- Methods that can be developed and used to counteract explosive attacks and blasts.

The data retrieved from social media and other online platforms can also be used to feed into other areas of research. For this paper, the focus will be on explosive and blast incidents and other areas of research that can be used to expand and facilitate work done to help mitigate said incidents.

Approach and Methods

This section of the paper will look into the approaches and methods used to reach a coherent and conclusive hypothesis that facilitated achivieng the paper's objective.

Data Collection

The construction of a simple spreadsheet in Microsoft Excel to assist with the monitoring and tracking of explosive and blast incidents was chosen as a feasible method to capture data received from social media and online platforms.

The Excel spreadsheet was structured in a manner that highlighted the type of data that needed to be extracted from the social media leads. Data was collected from posts found on Twitter from April 2019 to January 2020. These posts were then used as leads that lead to more sources on information which covered the stories covered in the Twitter posts. This assisted with the verification of the data collected by promoting the triangulation of sources through identifying at least a minimum of three other sources (excluding the Twitter post) for each post in order to determine its legitimacy.

The text in the Twitter post was analysed and keywords extracted to formulate a search query which then provided results related to the post and other incidents that were not heard of before. These results were then screened through determining the legitimacy of the source and the relevance of the content in comparison to the Twitter post from which it stems. The results were then analysed and processed to extract data that will then be placed in the applicable categories within the Excel spreadsheet using the process depicted in **Fig. 1**.

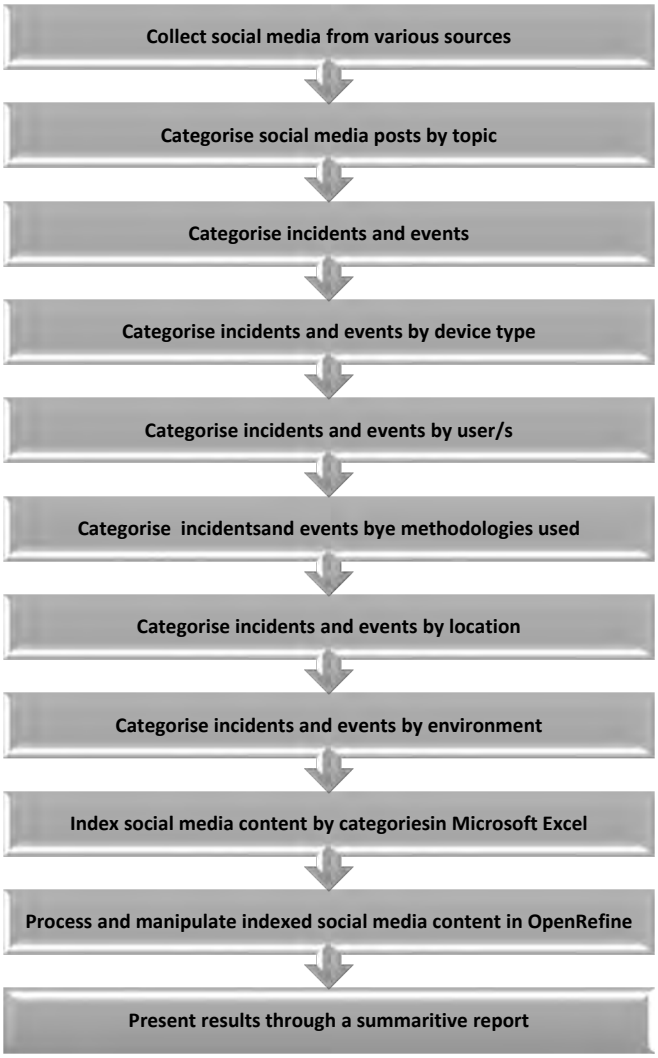

Fig. 1. Process flow (adopted from [5] [3])

The the data extracted from the Twitter posts and other online platforms provided insight into the following:

- Blast incidents occuring around the globe.

- The most prevalent sources of blast related information.
- The types of evet or blast incidents.
- The types of devices used.
- The number of casualties caused by the incidents.
- The perpetrators or user of the explosive devices.
- The types of environments in which the incidents occurred.
- The locations of the incidents.

Other aspects of the data collection phase focussed on the on the following:

- Explosives and fireworkdsafety issues.
- Explosive ordinance disposal (EOD) related information, including the groups/squads and the methodologies used.

Knowledge Extraction

The extraction of knowledgde the data collected was extracted through the use of a thematic analysis method, which entailed “identifying, anaysisng and reporting patterns (themes) within data” [6] **[1]**. The knowledge extracted from the social media and online platform posts was placed in an Excel spreadsheet which contained categories of data that should be extracted from the online content. The categories were as follows:

- Tweet title
- Article title
- Date
- Source
- Event or incident type
- Device type
- User/s
- Number of deaths or injuries
- Location
- Environment
- Device net explosive capacity (NEC)

The extracted data was then placed in the Excel spreadsheet under the correct categories. This data was then analysed and processed using OpenRefine to help clean-up, mine and visualize statistical information which can then be applied to provide insight into the state of explosives research, effects of blast incidents and work being done in the EOD field.

Results

This section of the paper will look into the results received after the analysis of the data collected from Twitter posts and other online content platforms.

Analysis of Social Media Leads

As mentioned earlier in the paper, a majority of the posts received were from Twitter accounts. These post only provided brief descritpitons of the incidents or event covered seeing that Twitter has a limititation on the size of posts which is capped at 280 charatcetrs per tweet (doubled in 2018 from the initial limit of 140 characters per tweet). The number of characters per tweet is an equivalent of about 55 words. This is enough words to provide the following details about the post:

- The title

- The source
- Brief description of the incident or event

First we observe the source of the tweet, then we observe its coherence the tweet to determine its relation to the subject at hand. We then extract the tweet's title, in other instances, the tweets keywords to generate a search query. The hits returned by the chosen search engine are then evaluated to determine whether they cover the information presented in the Twitter post. The following criteria is observed and evaluated in order to determine the relevance of the search engine hits:

- **Title**: To determine whether th syntax is similar to that of the Twitter post and whether it contains keywords from the Twitter post / generated search query. ??
- **Source**: To determine the information's credibility and validity.
- **Date**: To determine the timeliness of the content.
- **Data/Content**: To determine whether the content covered in the post correlates to the title.

The next step entails scraping the top 3 prevalent sources to measure whether they contain information that can be extracted to populate the categories listed in **4.2**.

Analysis of Extracted Information / Knowledge

Blast Incidents

Event or incident type

It was discovered that a majority of the events and incidents captured in the database were related to attacks made on military and government officials, and a majority occurred in public spaces, which resulted in patrons, civilians and pedestrians being injured. This in turn resulted in a total death toll of +-320 and a total of +-900 injuries.

Device types

Fig. 2 depicted below provides a depiction of the most used devices in the reported incidents, with the most prevalent device types being IEDs and car bombs.

Cluster Size	Row Count	Values in Cluster
16	79	• IED (25 rows) • Car bomb (18 rows) • Undisclosed (15 rows) • Mines (3 rows) • Explosive belts (2 rows) • Magnetic bomb (2 rows) • Parcel bomb (2 rows) • Roadside bomb (2 rows) • Suicide bombers (2 rows) • WWII bombs (2 rows) • Cluster bomb (1 rows) • Crude bomb (1 rows) • Drone (1 rows) • Live grenade (1 rows) • Multiple bombs (1 rows) • Unexploded bombs (1 rows)

Fig. 2. Device types

User/s

The data found in the database projected that a majority of the attacks and incidents were caused by militants and terrorists. A majority of the incidents were caused by militants and terrorists made up of the groups listed below.

1. Houthi movement
2. Al-Qaeda linked Al-Shabab group
3. Al-Shabab
4. Naxals
5. Islamic State militants
6. Tehriki Taliban Pakistan (TTP)
7. Jamaah Ansharut Daulah (JAD) militant group
8. Kurdish militants
9. Hamas
10. ISIS
11. Jaish-e-Muhammed (JeM)

Location

Fig. 3 below provides insight into the locations in which a majority of the identified incidents occurred (the first location being the one with most incidents):

1. Afghanistan
2. Pakistan
3. Iraq
4. Syria
5. Somalia
6. Egypt, Libya, Philippines and Russia (tie)

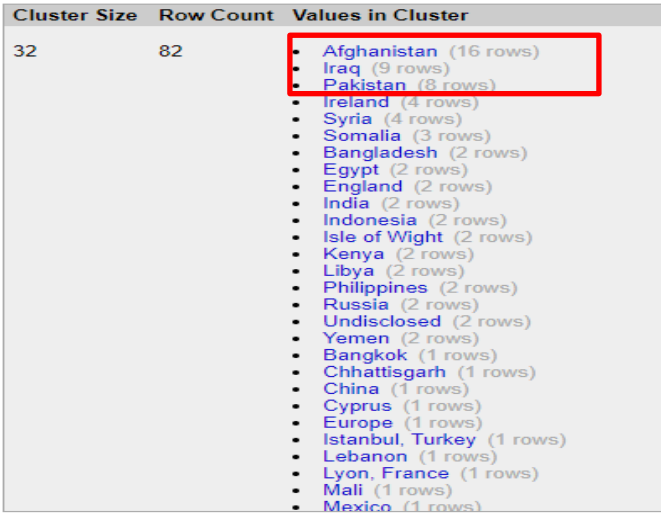

Fig. 3. Location

Therefore, based on the information listed above, a majority of the blast incidents captured in the database occurred in Asia.

Environment

Figure 4 below provides an overview of the environments in which the incidents identified through socila media have taken place, These incidents were then divided into the following categories.

1. Urban
2. Rural
3. Mountainous
4. Sea

Fig. 4. Environment

A majority of incidents occurred in urbans environments (58.9%) hence they resulted in there being a lot of causalities.

Explosive Ordinance Disposal (EOD)

Event type

There are a total of 40 events captured in the database of which a majority of the events were training exercises conducted by EOD groups. All in all, the events were made up of the following as depicted in **Fig. 5** below:

1. Training and Acquisition of EOD Equipment
2. Controlled detonations
3. Evacuations
4. Discovery of unexploded bombs
5. Disarming and disposal of explosive devices
6. Attacks

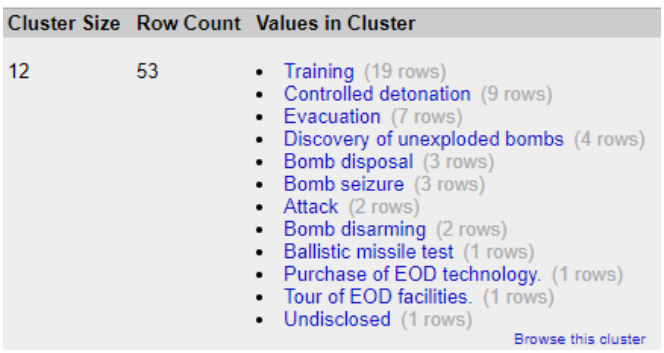

Fig. 5. Event/incident type

Device types

Fig. 6 below provide insight into the majority devices used in the training exercises and those that were detonated and disposed of.

Fig. 6. Device types

- IEDs, mines, missiles and grenades
- Unserviceable munitions and rendering safe munitions that are considered unsafe.
- World War I and II bombs (grenades, mortars and rockets

This category in the database also provided insight into the type of equipment and devices used in the EOD groups training exercises.

- IEDs
- Satellite communications (SATCOM)
- The Mk 18 Mod 2 Kingfish unmanned underwater vehicle (UUV)
- Maritime improvised explosive device (M-IED)

Users and Groups

It was discovered that the following group often partake in joint training exercises.

TABLE I. EOD GROUPS AND PARTICIPANTS

EOD Groups and Participants	
Explosive Ordnance Disposal (EOD) team and 20th Chemical, Biological, Radiological, Nuclear, Explosives (CBRNE)	Navy Explosive Ordnance Disposal (EOD) Group One
Personnel from Explosive Ordnance Disposal Mobile Unit 5, Coastal Riverine Squadron 2, assigned to Coastal Riverine Group 1 Detachment Guam, III Marine Expeditionary Force, 36th Civil Engineering Squadron, and Helicopter Sea Combat Squadron (HSC) 25.	Explosive Ordnance Disposal Mobile Unit (EODMU) 8 deployed from Task Force 68 and Mobile Diving and Salvage Unit (MDSU) 2.
Explosive Ordnance Disposal Mobile Unit (EODMU) 5 and their Japan Maritime Self-Defense Force (JMSDF) EOD counterparts	Elements of Explosive Ordnance Disposal Group One
Distributed Maritime Operations (DMO), Littoral Operations in a Contested Environment (LOCE)	Explosive Ordnance Disposal Mobile Unit (EODMU) 5 and their Japan Maritime Self-Defense Force (JMSDF) EOD counterparts

and the Expeditionary Advanced Base Operations (EABO)	
NATO, Naval Surface Warfare Center Panama City Division (NSWC PCD) and Baltic Operations (BALTOPS) in the Baltic Sea region.	Distributed Maritime Operations (DMO), Littoral Operations in a Contested Environment (LOCE) and the Expeditionary Advanced Base Operations (EABO).
The Ministry of Defence and L3Harris Technologies	5th Battalion Singapore Infantry Regiment and the US army
Royal Australian Navy personnel from Clearance Diving Team One and Four	Regional Command East's Task Force Explosive Ordnance Disposal Soldiers, Kosovo Security Forces and Swiss, Ukrainian and Moldovan EOD teams.
Royal Canadian Navy personnel from Fleet Diving Unit – Pacific	The 341 CES Explosive Ordnance Disposal (EOD) flight and the Department of Energy's (DOE) Accident Response Group (ARG).
The Explosive Ordnance Disposal team at Little Rock Air Force Base	Navy personnel from HMNZS Matataua Maritime Explosive Ordnance Disposal
19th Civil Engineer Squadron EOD	Mines Advisory Group (MAG)
4th Civil Engineer Squadron, 8th Engineer Support Battalion, and 2nd Marine Logistics Group.	Spanish Police
	Pakistan's military
Royal Navy	MacDill's EOD
Israeli Police and Israel Defense Forces	155th Air Refuelling Wing and Nebraska Air National Guard
21st Civil Engineer Squadron's	U.S Army TFOD

Methodologies used

The methodologies applied during EOD related exercises mainly consisted of the deployment of teams to various sites, controlled detonations of explosives, evacuations and raiding bomb-making factories. The most prominent methods discovered in the social media posts were as follows:

1. Controlled detonations using sandbags and digging holes.
2. Evacuations and putting up cordons.
3. Having bilateral exercises to help increase proficiency in mine countermeasure operations, including sweeping; hunting and neutralization using remotely operated vehicles, sonars and sweep gear.
4. Orchestration of IED response scenarios based on current and recurring trends over the past 20 years.
5. Having technical exchange sessions between the DOD and the DOE to focus on nuclear accident response procedures.
6. Orchestrating exercises that practice a wide range of expeditionary competencies to include visit, board, search and seizure (VBSS), land and sea insertion techniques, joint demolition operations, small arms proficiency, counter improvised explosive device (CIED) operations, and anti-terrorism force protection (ATFP) diving operations.
7. Supporting local, state and federal law enforcement agencies with cases for which EOD groups may be better equipped.
8. Having joint discussions with law enforcement on how to properly identify different types of military unexploded ordnances.

9. Having joint demolition training to share knowledge of how each team operates.

10. The testing of joint expeditionary force logistical transfer capabilities in the Arctic environment, including wet logistics over the shore, expeditionary mine countermeasures, mobile diving and salvage, offshore petroleum discharge system operations, and expeditionary infrastructure assessment programs.

11. Providing operational EOD capabilities to enable the locating, identifying, rendering safe, exploiting, recovering, and disposing of all explosive ordnance.

Location

The top 4 locations in which EOD related exercises took place are depicted in **Fig. 7** below.

1. United Stated
2. England
3. Europe
4. Asia

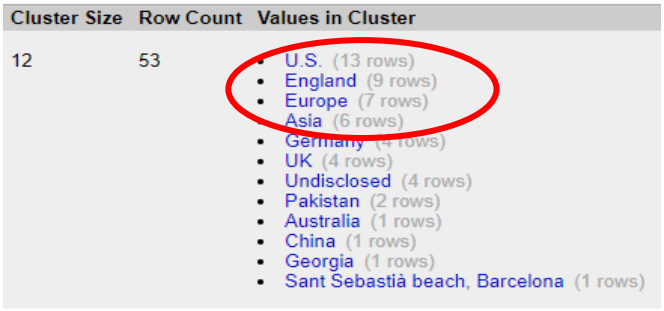

Fig. 7. Location

Based on the information depicted in **Fig. 7**, a majority of the events occurred in the U.S. This will in turn shift the focus of monitoring and evaluation efforts to the US, which might in turn assist with the development of counteractive methods and strategies.

Environment

Fig. 8 below provides a depiction of the environments in which the identified training exercises, explosives disposal and evacuations took place.

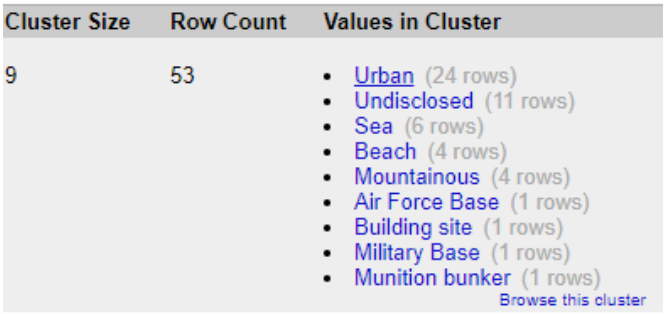

Fig. 8. Environment

The prevalent environment categories were as follows (in descending order):

1. Urban – 45%

2. Undisclosed – 21%

3. Sea/beach – 19%

4. Mountainous – 7.5%

5. Other – 7.5%

Based on the information above, a majority of training exercises that took place were staged in urban environments. This information denotes that groupd should put more training efforts into familiarising themselves with

Recommendations and Future Work

The manual extraction and triangulation of the data from the sources of information was a tedious process, therefore the following recommendations are made:

- The automation of the extraction of applicable data and information to save time and enable the retrieval of larger data sets.
- Expansion of the subject covered in the through adding additional topics that might be of relevance to the research area.
- The automation of the extraction and triangulation of data from the sources of information used in the study.
- Automation of the validation of the authenticity of sources.
- Investigate the use of web scraping and semantic analysis software to automatically extract defined data from online platforms.

Conclusion

It was discovered that the use of social media platforms to retrieve and extract was a useful method as it help discover new streams of information useful for research conducted in the explosives research domain. The data and information extracted provided insight into the various types of devices used, the core users of said devices and instigators of the blast incidents captured in the spreadsheet. Another aspect of the processed data information shed insight into the methodologies, tools and technologies that can be used to help counter blast incidents and attacks.

References

[1] Braun, V., & Clarke, V. (2006). Using thematic analysis in psychology. Qualitative Research in Psychology, 3(2), 77-101.
[2] de Boer, M. H., Bakker, B. J., Boertjes, E., Wilmer, M., Raaijmakers, S., & van der Kleij, R. (2019). Text Mining in Cybersecurity: Exploring Threats and Opportunities. Multimodal Technologies and Interaction, 3(3), 62.
[3] Feng, J., Barbosa, L. D. A., & Torres, V. (2016). U.S. Patent No. 9,262,517. Washington, DC: U.S. Patent and Trademark Office.
[4] Namugera, F., Wesonga, R., & Jehopio, P. (2019). Text mining and determinants of sentiments: Twitter social media usage by traditional media houses in Uganda. Computational Social Networks, 6(1), 3.
[5] Papapesios, N., Ellul, C., Shakir, A., & Hart, G. (2019). Exploring the use of crowdsourced geographic information in defence: challenges and opportunities. Journal of Geographical Systems, 21(1), 133-160.
[6] Taylor, J., & Pagliari, C. (2018). Mining social media data: How are research sponsors and researchers addressing the ethical challenges? Research Ethics, 14(2), 1-39.

PROUDLY SOUTH AFRICAN

SABO

Diamond Sponsors

PROUDLY SOUTH AFRICAN

SABO

South African Ballistic Organization (SABO)

ARMSCOR
Armaments Corporation of South Africa SOC Ltd

South Africa's defence industry is recognised as being among the most technologically advanced in the world. At the forefront is Armscor - The Armaments Corporation of South Africa SOC Limited, the acquisition agency for the South African Department of Defence (DOD), and other state organs and entities. The organisation manages the strategic capabilities of the DOD, producing research and vanguard technological solutions through its facilities and capabilities functions.

ALKANTPAN

Alkantpan Test Range is an all-purpose ballistics test range situated at Copperton, Prieska in the Northern Cape region of South Africa. With a notable 30 year history of success, Alkantpan is equipped for the testing of all kinds of weaponry ranging in caliber from 5.56mm to 155mm and larger. An ISO 9001 and ISO 14001 accredited facility, this 85000ha facility provides customized ordnance testing and related services in artillery, mortars, armour, rockets, short range missiles, insensitive munitions, sequential environmental testing, unmanned aerial vehicles, amongst others to local and international clients. Other strategic services offered include offering measurements assessments, facilities hire (firing sites, ammunition assembly, demolition terrain, conferencing, accommodation, etc.) and other value-added services such as project management and specialized logistics.

Armour Development

The Armour Development facility has more than 40 years' experience in conducting research and development and the testing of armour protection systems and technologies, for the DOD and the entire defence industry. The Armour Development team has extensive knowledge of ballistics, materials and armour systems. Our success is attributed to the years of experience in the testing of protection systems to develop effective solutions that will provide protection against various threat types:

- Light caliber weapons: up to and including .338 caliber, penetrators from lead ball to tungsten carbide penetrators.
- Medium caliber weapons: up to and including 35 mm armour piercing ammunition.
- Heavy caliber weapons: up to and including 125 mm armour piercing, fin stabilized discarding sabot (APFSDS) ammunition with tungsten long rod penetrators.
- Shaped charge HEAT systems from 40 mm hand held grenade launchers to 180 mm anti-tank mono and tandem missile configurations.
- Fragmentation weapons: hand grenades up to artillery shells.

FLAMENGRO

Flamengro is a multi-disciplinary team of engineers and scientists geared to solving engineering and software related problems in the South African and global defence environment. The mandate of Flamengro is the development, maintenance, and expansion of computational mechanics modelling capability in the DOD environment. Flamengro has four main capability areas: Computational Mechanics: Modelling and Simulation (CFD & FEA), Test and Measurement, Software Development and Small Scale Manufacturing.

Armscor, your strategic partner of choice for defence and security solutions.

info@armscor.co.za

www.armscor.co.za

PROUDLY SOUTH AFRICAN

SABO

Horne Technologies

HORNE Technologies, operating since 2010, represents a number of high-technology manufacturing companies in South Africa. These include FAULHABER – precision drive systems used in optical, missile, laboratory, robotic and general industrial systems; TELOPS – leaders in scientific high-speed infra red and hyperspectral imaging; Vision Research – premier high-speed cameras, leading in back side illuminated sensors; Specialised Imaging – specialists in test range optical recording systems, with frame rates up to 1 billion fps.

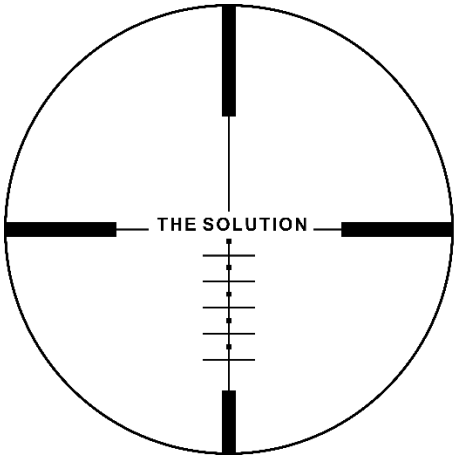

HORNE
TECHNOLOGIES
Suppliers of expert solutions and specialist equipment
www.hornet.cc

Gold Sponsors

QFINSOFT

Qfinsoft (Pty) Ltd was founded in 1999 and represents the combined expertise of a group of engineers with years of practical and consulting experience in computer aided engineering. These technical capabilities have led to the development of several commercial products and engineering software packages. Through Qfinsoft's international network, we have partnered with world-leading CAE companies to represent them in South Africa. With these partnerships we distribute, train and support local users in the use of these software products. Through the consulting efforts, Qfinsoft has also built up contacts with an extensive network of expertise both in academia and industry worldwide. Qfinsoft became known in the industry for its technical excellence and high quality of technical support to our customers.

DCD Protected Mobility

DCD Protected Mobility is a world-leader in **design, manufacture, integration** and support of special-purpose tactical wheeled vehicles, delivering innovative and sustainable solutions. DCD Protected Mobility is a fully accredited, socially responsible, international systems house, providing sustainable products and solutions for the defence and transport sectors. CD manufactures the Husky Vehicle Mounted Mine Detection System and a range of Springbuck Armoured Personnel Carriers (APC).

For more information, visit our website www.dcd.co.za

Bronze Sponsors

SIMTEQ Engineering makes product developing and manufacturing companies profitable and competitive by taking costly trial-and-error design and manufacturing processes of products into the virtual world. With our team of expert engineers and the best simulation and analysis technology, we make it simple to solve and prevent manufacturing and in-service problems of parts, assemblies and systems. We:

- Sell the right technical solutions
- Train users
- Provide technical support
- Offer knowledge transfer consulting and services
- Advise senior and postgraduate students

SIMTEQ ENGINEERING
Your Partner in Simulation Technology

CONFERENCE:

PROCEEDINGS OF THE
SOUTH AFRICAN BALLISTICS ORGANISATION
SYMPOSIUM 2023

ISBN: 978-0-6397-6256-2